This document is downloaded from DR-NTU (https://dr.ntu.edu.sg)
Nanyang Technological University, Singapore.

Reliability study on polymer/inorganic interface in microelectronic packaging

Zhang, Yanlie

2006

Zhang, Y. (2006). Reliability study on polymer/inorganic interface in microelectronic packaging. Doctoral thesis, Nanyang Technological University, Singapore.

https://hdl.handle.net/10356/36114

https://doi.org/10.32657/10356/36114

Downloaded on 09 Apr 2024 10:42:30 SGT

ATTENTION: The Singapore Copyright Act applies to the use of this document. Nanyang Technological University Library

a455913

Reliability Study of Polymer/Inorganic Interface in Microelectronic Packaging

Zhang Yanlie

NANYANG TECHNOLOGICAL UNIVERSITY
08 MAY 2007
LIBRARY

School of Mechanical and Aerospace Engineering

A thesis submitted to the Nanyang Technological University
in FULFILMENT of the requirement for the degree of
Doctor of Philosophy

2006

ATTENTION: The Singapore Copyright Act applies to the use of this document. Nanyang Technological University Library

Abstract

Flip chip technology has been increasingly used in electronics packaging and considerable effort has been made in the recent years to increase the reliability of the solder joints. It has been well established that underfill can be introduced to improve lifetime of solder joints in flip chip structures. However, due to considerable coefficient of thermal expansion (CTE) mismatch between the underfill and its adjacent materials such as silicon wafer and FR-4 composite, delamination at the interface of the adjacent layers becomes a new reliability problem. The CTE mismatch and manufacturing defects between underfill and its adjacent materials may induce severe interfacial delamination during temperature variation or in the presence of moisture. The present project, therefore, aimed to study the delamination behaviour using either temperature cycling test or hygrothermal loading.

Multifunctional micro-moiré interferometry (M^3I) system was utilized to study the interfacial response of flip chip assembly under an accelerated thermal cycling (ATC) test in the temperature range of –40 °C to 125 °C. This in-situ measurement provided good interpretation of interfacial behavior of delaminated flip chip assembly. Finite element analysis (FEA) was carried out with consideration of the viscoelastic properties of underfill material. The simulation results were found to be in good agreement with the experimental results. It was found that interfacial toughness is not only related to CTE mismatch but also a function of stiffness mismatch between chip/underfill.

ATTENTION: The Singapore Copyright Act applies to the use of this document. Nanyang Technological University Library

Abstract

Interfacial reliability of flip chip on board (FCOB) exposed at 85 °C/85%RH was studied using the M^3I system. A thermal aging study was simultaneously performed to understand the effect of aging time on the deformation behaviour. The results showed that thermal aging relieved the stresses induced by hygrothermal swelling mismatch between the dissimilar materials involved. This clearly indicates the beneficial effect of creep deformation in the moisture conditioning.

Since the reliability study on interfacial fracture will not be completed without a discussion on fracture strength, the characterization of the interfacial adhesion was carried out under loading angles varying from 20° to 90° over a wide temperature range from 25°C to 125°C and moisture conditioning at 85 °C/85%RH, to study the effects of loading angle, temperature and moisture on the interfacial fracture toughness. An in-situ/real-time micro-digital image speckle correlation (μ-DiSC) system was established to determine the fracture toughness of underfill/chip interface. An interfacial fracture mechanics based finite element (FE) model was implemented to examine the findings of μ-DiSC technique, under different loading configurations. The results obtained from the simulation are found to be in good agreement with those measured by μ-DiSC system, indicating that the system can be used as an accurate and effective experimental tool for electronic packages. The morphologies of fracture surfaces were studied using the scanning electron microscope (SEM). The fractographs show strong correlation between temperature, moisture-induced reaction, and fracture mode mixity.

ATTENTION: The Singapore Copyright Act applies to the use of this document. Nanyang Technological University Library

Acknowledgement

It has been a real privilege to do research under the supervision of Professor Zhou Wei over the last 3 years. He is the rare person who has enormous enthusiasm for science, a sense of fun, academic savvy, and technical prowess all rolled into one. I learned a lot, and I really enjoyed the last three years. Zhou inspired me and believed in my abilities, and for that I am very grateful.

Dr. Shi Xunqing from Singapore Institute of Manufacturing Technology patiently taught me the principles of fracture mechanics and mentored my research. I always enjoyed talking to both Dr. Shi and Professor Zhou, because when I showed them some results, they gave plenty of scientist's thoughts and said "good and carry on". Nothing could be more encouraging to a graduate student.

I would also like to thank my precursors for building up the detailed material databases for my further research, although I have not had chance to meet them. The entire group deserves recognition for being the best co-workers I am expecting. This diverse group of talented people from all over the world was always helpful and supportive.

Dr. Zhang Xueren worked with me for about six months, but in that time he made a significant contribution by providing suggestion in finite element simulation and interface facture mechanics.

Mr. Sun Yaofeng showed me his knowledge on image speckle correlation and gave me precious suggestions on the speckle pattern preparation and the strategies for the correlation. These people are the unsung heroes of the thesis - without them, I do not know how any research would get done.

ATTENTION: The Singapore Copyright Act applies to the use of this document. Nanyang Technological University Library

A special heartfelt thanks goes out to all my friends who over the years have encouraged me, laughed with me, and dragged me out of the lab. Ms. Wang Chunmei, Ms. Ngoh Shwu Lan and Ms. Shen Jinye, the fun-loving women kept me encouraged and buoyant everyday. My girlfriend and partner, Bai Jie, has encouraged and helped me on all fronts over last year. I am grateful for her love and devotion and her sense of humor that keeps me in stitches.

My parents and my big family have always been so supportive of my endeavors throughout the years. I am grateful for their unconditional love and encouragement.

ATTENTION: The Singapore Copyright Act applies to the use of this document. Nanyang Technological University Library

Publications

Journal Paper Accepted or in Peer Review

Y.L. Zhang, X.Q. Shi and W. Zhou, "*Reliability Study of Underfill/Chip Interface with Multifunctional Micro-Moiré Interferometry System*," accepted for publication in Microelectronics Reliability, 2005, in press.

Y.L. Zhang, X.Q. Shi and W. Zhou, "*Determination of Fracture Toughness of Underfill/Chip Interface with Digital Image Speckle Correlation Technique*," accepted for publication in IEEE Transaction on Component, Packaging and Manufacturing Technology, 2005, in press.

Y.L. Zhang, X.Q. Shi and W. Zhou, "*Effect of Hygrothermal Aging on Interfacial Reliability of Flip Chip on Board (FCOB) Assembly,*" Submitted to IEEE Transaction on Component, Packaging and Manufacturing Technology.

X.Q. Shi and Y.L. Zhang, "*Characterization of Interface Fracture Toughness of Chip/Underfill/Chip Sandwiched System Subjected to Mixed Mode Loading with Digital Image Correlation Technique*," Submitted to Material Science.

Conference Paper

Y.L. Zhang, X.Q. Shi and W. Zhou, (2004), "*Effect of Hygrothermal Aging on Interfacial Reliability of Flip Chip on Board (FCOB) Assembly*," Proceedings of 6th Electronics Packaging Technology Conference, pp. 404—409.

Y.L. Zhang, X.Q. Shi and W. Zhou, (2004), "*Determination of Fracture Toughness of Underfill/Chip Interface with Digital Image Speckle Correlation Technique*," Proceedings of Electronic Components and Technology 2004, Vol. 1, pp. 140-147.

ATTENTION: The Singapore Copyright Act applies to the use of this document. Nanyang Technological University Library

Table of Contents

ATTENTION: The Singapore Copyright Act applies to the use of this document. Nanyang Technological University Library

ATTENTION: The Singapore Copyright Act applies to the use of this document. Nanyang Technological University Library

ATTENTION: The Singapore Copyright Act applies to the use of this document. Nanyang Technological University Library

List of Figures

ATTENTION: The Singapore Copyright Act applies to the use of this document. Nanyang Technological University Library

ATTENTION: The Singapore Copyright Act applies to the use of this document. Nanyang Technological University Library

ATTENTION: The Singapore Copyright Act applies to the use of this document. Nanyang Technological University Library

ATTENTION: The Singapore Copyright Act applies to the use of this document. Nanyang Technological University Library

List of Tables

ATTENTION: The Singapore Copyright Act applies to the use of this document. Nanyang Technological University Library

Chapter 1 Introduction

Electronic packaging serves as an important link between the silicon and the electronic system. A variety of electronic packaging technologies have been developed to achieve the aims of lower cost, better reliability and higher density/performance. Flip chip technology, also referred to as direct chip attach (DCA) technology, is potentially attractive for a large variety of microelectronics packaging applications, because it provides fast clock frequency and large package pin counts.

In order to perpetuate this trend and be able to meet future market growth predictions, technologies associated with the flip chip package are currently being improved with plans for further developments in the future. Developments include improvements in the C4 interconnect technology, the underfill technique, and the substrate technology. Higher interconnect density is a driving force for research and development of the flip chip package. To meet this need, research is being done to increase reliability issues of the C4 bump and underfill technique.

The original flip chip did not contain underfill and corner solder joint failure due to CTE mismatch between the chip and substrate was the main concern. Great effort was made to improve the flip chip design. The introduction of underfill (Nakano et al. 1987) encapsulated between the chip and the PCB has considerably enhanced the solder fatigue life. The epoxy-based underfill reduces the global thermal expansion mismatch between the silicon chip and the low-cost organic substrate. Since the chip, underfill and substrate deform together as a unit, the relative deformation between the chip and the substrate is minimized and the

ATTENTION: The Singapore Copyright Act applies to the use of this document. Nanyang Technological University Library

corresponding shear deformation of the solder joint is small (Baggerman et al. 1996).

Although the use of the underfill encapsulant eliminates, to a large extent, the problem of low-cycle solder fatigue, a number of reliability issues remain. The underfill layer shifts the local shear strain from the solder balls to the underfill/die and the underfill/substrate interfaces, causing delamination of these interfaces (Ho et al. 2004). Once delamination occurs, crack will propagate along the interfaces and quickly sever the solder joints, leading to the eventual failure of the whole package.

Another problem is that the underfill, which is epoxy-based, is susceptible to moisture. Moisture may cause hydroxylation and swelling of epoxy and thus degrade the adhesive strength of the underfill. Especially, when the temperature is high (e.g., during reflow process), moisture in the underfill will vaporize and turn into high-pressure steam, which could be sufficient to cause delamination within the package, or even worse, an internal or external crack in the plastic package. Cracks in the plastic package would allow easy moisture penetration, inducing transport of ionic contaminants to the die surface and increasing the potential for early device failure. Even at the relatively low temperatures, e.g., 85 °C, the moisture swelling and plasticization will greatly change the material properties as well as residual stress in sandwich specimen, which can consequently menace package reliability issues.

In this thesis, with the aid of photomechanics measurement techniques and finite element method, the reliability of Si/underfill interface of flip chip assembly under both thermal cycling and hygrothermal aging conditions were investigated. The interfacial behavior under both thermal cycling and hygrothermal aging

ATTENTION: The Singapore Copyright Act applies to the use of this document. Nanyang Technological University Library

conditions are strongly dependent on various factors, such as thermal properties & mechanical properties of polymeric materials, moisture expansion, moisture degradation and hygrothermal induced moisture concentration variation. All of them are non-linear and dependent on any others. Therefore, in this thesis, various experimental methods were carried out to formulize the effects of temperature and moisture, including degradation of interface adhesion (during interfacial fracture toughness measurement), change of material properties and consequent stresses introduced by expansion mismatch, on interfacial toughness and interfacial fracture toughness so as to provide guidance on a protocol for testing to save sample size of experiment.

Firstly, the responses of the delaminated module under two environmental loading conditions were determined using moiré interferometry developed in the project. Secondly, the failure assessment diagrams with respect to different temperature and moisture conditions were obtained using advanced micro digital image speckle correlation system. It should be pointed out that the entire interfacial reliability evaluation system was built in this project and the system has been demonstrated to be very useful in characterizing the properties of various interfaces with arbitrary materials combinations in different microelectronic packages.

The thesis is outlined as follows:

Chapter 2: Literature Review. The technology of flip chip packaging is introduced, followed by description of the interfacial reliability issues under the thermal and hygrothermal loading conditions. Interfacial fracture mechanics and relevant measurement technologies are also reviewed.

ATTENTION: The Singapore Copyright Act applies to the use of this document. Nanyang Technological University Library

Chapter 3: Experimental Details and Instrumentations. The configuration and preparation procedures of two types of specimens, photomechanics measurement techniques and testing programs are described in detail.

Chapter 4: Interface Behavior of Chip/Underfill under ATC Loading. The solutions of interfacial fracture mechanics are described. The validity of the interfacial fracture mechanics is discussed. The deformation and fracture behavior of the flip chip assembly under thermal cycling from –40 °C to 125 °C is measured using the moiré interferometry developed. The finite element model with viscoelastic property of the underfill material embedded is established to examine the experimental results.

Chapter 5: Interface Behavior of Chip/Underfill under Hygrothermal Aging. The deformation and fracture behavior of the flip chip assembly under hygrothermal aging at 85 °C/85%RH is measured using the moiré interferometry. The creep behavior of the assembly is determined to separate the time-temperature effect from the underfill swelling effect in long-term aging.

Chapter 6: Characterization of Interfacial Fracture Toughness of Si/Underfill. Brail-nut specimen is used to characterize the interface fracture toughness under the temperature loading and after the hygrothermal aging. The fracture morphologies throughout the test are studied with respect to different loading angles and environmental loading conditions.

Chapter 7: Conclusions and Recommendations for Further Research.

ATTENTION: The Singapore Copyright Act applies to the use of this document. Nanyang Technological University Library

Chapter 2 Literature Review

Nowadays the requirements for faster performance and higher Input/Output (I/O) signals in integrated circuits (IC) are commercially increasing in smaller and more complex package interconnect structures. Therefore, many packaging types and technologies, such as ball grid array (BGA), plastic ball grid array (PBGA), thin small outline package (TSOP), flip chip on board (FCOB), wire bonding, are being applied on electronic packaging for the objective of area saving, weight saving and money saving. In all of these innovative electronic packaging methods, FCOB is a kind of solder ball array packaging technology with latent capacity of growing since it can work in a higher package pin counts with high clock frequency. In other words, it is smaller, lighter and cheaper than many others.

In this chapter, the FCOB and its reliability issues are reviewed and the objectives of the research project are illustrated. Structure of this chapter is shown in Fig. 2.1.

2.1 Flip Chip Technology

Flip chip is defined as mounting an IC chip to a substrate or printed circuit board (PCB) with Input/Output bumps directly. Compared with the other packaging technologies, flip chip technology provides shorter possible leads, lower inductance, higher frequency, better noise control, higher density, greater I/O, smaller device footprints and lower profiles.

ATTENTION: The Singapore Copyright Act applies to the use of this document. Nanyang Technological University Library

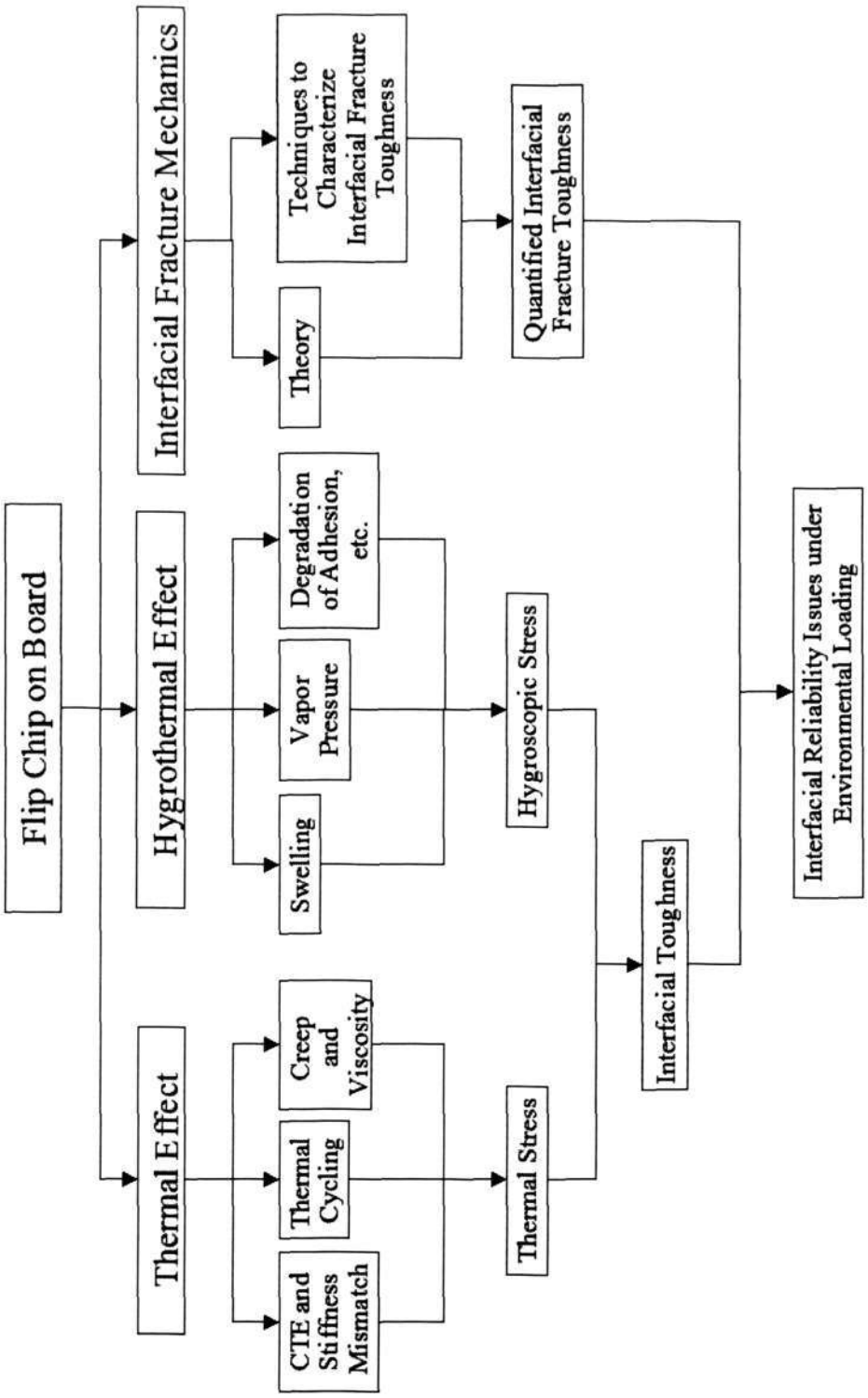

Fig. 2.1 Overview of thermal and moisture induced problems

ATTENTION: The Singapore Copyright Act applies to the use of this document. Nanyang Technological University Library

IBM developed one of the earliest flip chip technologies in 1964, as a possible replacement of face-up wire-bonding technology. After that, many forms of flip chip were put forward. Recently, since 1990, IBM has been assembling solder-bumped flip chips on organic PCB, whose results showed that solder-bumped flip chip assembly technology is applicable for high-cost substrates, e.g., ceramics, as well as low-cost PCB, e.g., FR-4. The schematic drawing of solder-bumped flip chip is shown in Fig. 2.2.

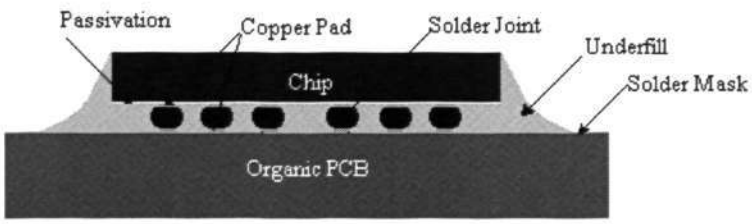

Fig. 2.2 Solder-bumped flip chip on low-cost PCB with underfill encapsulated

It is estimated that the number of flip chip units increased by 40 percent during 1998 to a total of 899 million units, as shown in Fig. 2.3 (Bartoszyk et al. 2000). It seems that Bartoszyk et al underestimated the amount of produced flip chip components in the past few years. The rising demands and innovative technologies in cell phone, mini storage devices etc. promote the yield of flip chip components in a very high-speed manner.

ATTENTION: The Singapore Copyright Act applies to the use of this document. Nanyang Technological University Library

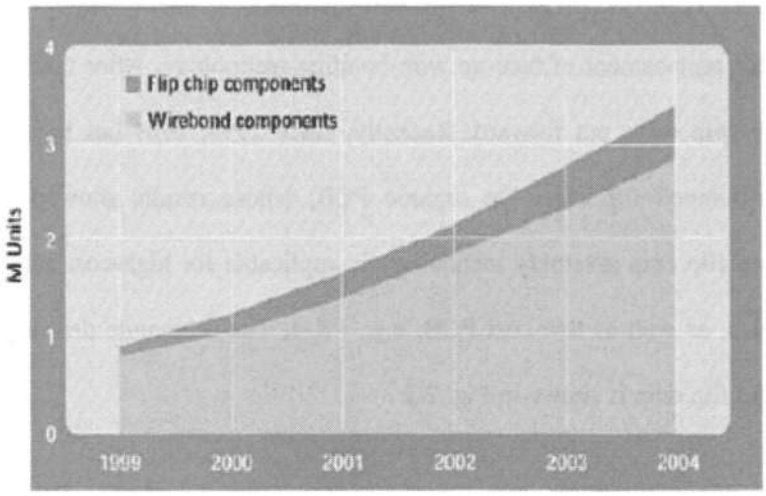

Fig. 2.3 Projected growth of flip chip and wire bond packages (Bartoszyk et al. 2000)

However, during production process and service, manufacturers discover that there is large thermal expansion (CTE) mismatch existing in the layers between silicon chip (about $3\times ppm/^{o}C$) and organic PCB (about $20\times ppm/^{o}C$). The consequent uneven deformation causes considerable shear strain in solder interconnections and thus initiates or opens the crack in the solder joint or the delamination at the interface between solder joint and metal pad (Rzepka et al. 1998). As an effective solution, an introduction of rigid epoxy-based underfill, which fills the gap between the chip and substrate, can greatly improve the long-term reliability of flip chip interconnection structure by several orders of magnitude (Doi et al. 1996). Because of capillary action, underfill can be dispensed into the gap between chip and PCB naturally. Madenci et al. (1998) investigated the effect of underfill and underfill delamination on the thermal stress in flip chip solder joints with the aid of FEA simulation. Their results indicated that the rapid failing of flip chip modulus due to delamination can be effectively

ATTENTION: The Singapore Copyright Act applies to the use of this document. Nanyang Technological University Library

prevented with underfill and the lifetime could be estimated according to the failure prediction model.

Practically, after curing, underfill material with smaller CTE, higher Young's modulus and higher glass transition temperature does mechanically prolong the solder joint fatigue life since it reduces the effect of the global thermal expansion mismatch between the silicon chip and the low-cost organic PCB or substrate (Gektin et al. 1997). This mechanical coupling also reduces the strain in the solder connections by additional load transferring through shear stress and thus enhancing the thermal mechanical reliability of flip chip assembly (Madenci et al. 1998). In the meanwhile, the application of underfill can protect the solder joints and chip from moisture, ionic contamination, radiation and hostile operating environments such as thermal mechanical, shock and vibration (Lau et al. 2000).

However, the epoxy material has larger CTE than the CTE of solder material, which may introduce additional stress between the solder joint and the underfill. Therefore, to equalize the CTE of the underfill with that of the solder joints, silica fillers are used to modify the CTE of the epoxy-based adhesives. Various levels of residual stresses are consequently achieved, and the cost is considerably reduced since these fillers are generally cheaper than epoxy materials (Suryanarayana et al. 1993, Dai et al. 2000). In some cases, rubber particles are added to enhance the bulk fracture toughness of the underfill. Organosilanes are frequently used to improve the adhesion of resin matrix to the silica filler particles as well as to the inorganic substrates.

Such improvements have significantly minimized the possibility of joint failure. However, delamination in flip chip architecture and crack in underfill have been observed as a new reliability issue during the manufacturing operation or

ATTENTION: The Singapore Copyright Act applies to the use of this document. Nanyang Technological University Library

service phases. In the next section, the interfacial reliability issues are to be illustrated and motivations about this research project are to be extended.

2.2 Challenges in Interfacial Reliability Issues

Defects, occurring in the form of die cleaving, adhesive cracking and interfacial delamination, are ubiquitous in layered package structures. Among all of them, interfacial delamination is the worst threat to reliability improvement. During the manufacturing process, low adhesion due to incompatible interfaces, under-cured underfill, and void defects caused by trapped moisture can lead to interface delamination in the flip chip assembly (Wu et al. 1996). It is difficult to avoid such defect even in well-controlled fabrication processes (Hu et al. 1995).

Many factors affect the interfacial reliability of flip chip package. These factors include assembly process (reflow soldering, under-filling and curing), the mechanical properties of underfill (temperature-dependent moduli and viscoelasticity), adhesion strength in the interfaces, and the viscoplastic deformation of solder joints, etc. (Borgesen et al. 2000). The most common failure mechanisms of flip chip assembly are (Sham and Kim 2003):

(1) Underfill delamination at the interface between underfill and its adherends, as illustrated in Fig. 2.4(a) and Fig. 2.4(b);

(2) Cohesive crack in underfill bulk underfill material, as illustrated in Fig. 2.4(c), which leads to interfacial delamination or mixed mode of interfacial and cohesive fracture in flip chip packages;

(3) The stress/strain responses of solder joints and initiation and propagation of a creep-fatigue crack.

ATTENTION: The Singapore Copyright Act applies to the use of this document. Nanyang Technological University Library

In this study, of particular interest is the reliability of underfill/Si interface, since the delamination of this interface encountering the largest CTE mismatch, is the salient cause for failure of FCOB assemblies during reliability testing.

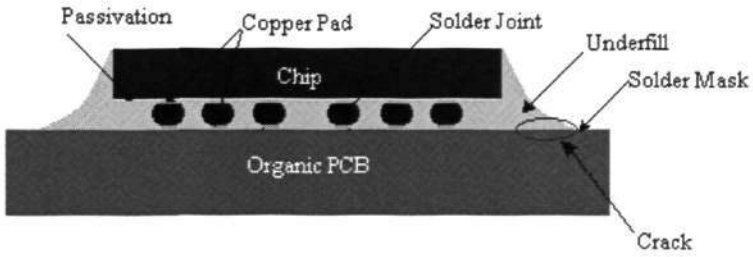

(a) Delamination at the interface between solder mask and underfill

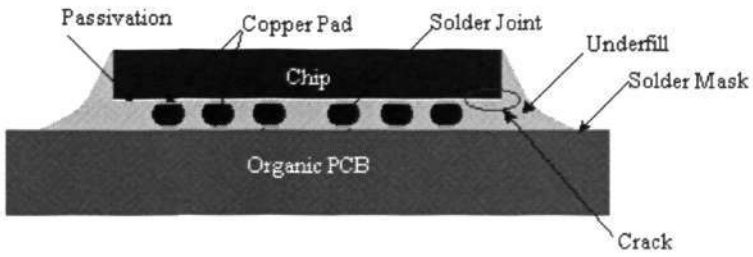

(b) Delamination at the interface between die and underfill

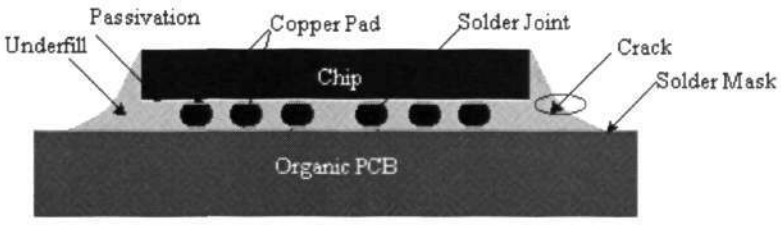

(c) Crack in underfill fillet

Fig. 2.4 Three types of underfill failures (Bartoszyk et al. 2000)

ATTENTION: The Singapore Copyright Act applies to the use of this document. Nanyang Technological University Library

2.2.1 Thermal Effect on Interfacial Failure

The root of thermally induced interfacial delamination is from the CTE mismatch and stiffness mismatch between the adjacent materials. The stresses generate inside the assembly module due to mismatch in deformations, such as shearing and bending. These stresses are to be magnified during thermal cycling, especially during high temperature and large difference-in-temperature cycling. The resulting fatigue failure opens the crack at the corner of the assembly or the initial defect generated during manufacturing operations. Moreover, for a device operating under high temperature for a long period, time-temperature related creep behavior has a considerable effect on the stress status within the package.

Therefore, three aspects, i.e. CTE/stiffness mismatch, thermal cycling and creep, are to be reviewed in order to gather information about thermomechanical studies so far.

2.2.1.1 CTE/Stiffness Mismatch

Generally, failure with delamination at the interface between underfill and adherent layers together with cracking of the adjacent materials often occurs and shows ordeal for present flip chip technology (Hohlfelder et al. 2001). There are various causes leading to delamination, including low adhesion due to incompatible interfaces, and loss of adhesion due to contamination and void formation caused by trapped moisture (Wu et al. 1996). It is believed that the shear stress caused by CTE mismatch dominates the delamination process (Jackson & Carnevali 1991). It was also shown that the cracks in real solder joints are exactly at the location of the computed maximum tensile stress, while the shear stress is

ATTENTION: The Singapore Copyright Act applies to the use of this document. Nanyang Technological University Library

quite uniform in the joints (Rzepka et al. 1998). Hence, the interfacial peel stress also played an important role in interfacial fracture (Jiang et al. 1997, Madenci et al. 1998).

On the other hand, stiffness (e.g. Young's modulus) of underfill and interposer has a critical effect on improving the reliability of flip chip on board (FCOB) under thermal cycling (Okura et al. 2000). For instance, when a kind of underfill with low modulus is used, the underfill simply shrinks and opens cracks at the delamination site. However, in modulus with hard underfill the rapid failure of package does not seem to happen since it protects the solder joint in compression. (Rzepka et al. 1998) It was also reported that the underfill with smaller CTE, higher Young's modulus and higher glass transition temperature improved the fatigue life of solder joint significantly (Gektin et al. 1997). The rigid underfill mechanically couples the chip and substrate and reduces the difference in the deformation of the chip and the substrate under thermal cycling. It was reported that the thermal fatigue life of the underfilled flip chip package could increase as much as 20 times more than those without underfill (Chen et al. 2001).

For most underfilled flip chip assemblies, delamination in the interface between chip and underfill occurs prior to fatigue failure of the solder joints, resulting in the failure of solder joints (Madenci et al. 1998). This failure is caused by high thermal expansion mismatch and epoxy curing strains generated in the packages during manufacturing operation (e.g. cooling and aging) and service stages (e.g. thermal cycling). The resulting stresses stay in the region of solder joint and interconnected underfill region, doing harm to the reliability of interface integrity (Rzepka et al. 1998). Therefore, it is of importance to expand the study to understand the thermal fatigue behavior during thermal cycling.

ATTENTION: The Singapore Copyright Act applies to the use of this document. Nanyang Technological University Library

2.2.1.2 Thermal Cycling

The delamination or cracking of the layered package is linked with the increase in thermal resistance suffered with thermal cycling. The larger the CTE mismatch, the faster the increase in thermal resistance during thermal cycling (Tuhus & Bjorneklett 1993). Prior to the fatigue failure of solder joint, the delamination of underfill adjacent interface was observed (Madenci et al. 1998).

Once the underfill delamination occurs, it will result in significant reduction of the thermal fatigue life of solder joints (Su et al. 1999). Therefore, as long as the interface delamination behavior or strain (stress) status under thermal cycling is thoroughly understood, the fatigue life of the assembly becomes predictable according to various models for thermomechanical stress analysis and fatigue failure of materials. It was experimentally observed that higher cycling temperature has a more damaging effect than lower one when keeping the ΔT constant and the reduction of fatigue life occurred with an increase of heating/cooling rates during thermal cycling (Ghaffarian 2000).

Dissipated energy or plastic work during cyclic loading is an important and fundamental measure to define the progressive changes leading to the deterioration (or growth) in a material under cyclic thermomechanical loading. Based on this consideration, various models have been proposed to predict the fatigue life and reliability of packages. The review of models and the disturbed state concept for thermomechanical analysis in electronic packaging are listed in Table 2.1, which has pointed out the principle to form the FEM meshes and the ways to predict life of various electronic packages (Desai & Whitenack 2001).

During all of these methods, Coffin-Mansion and fracture mechanics methods are commonly used. Fan et al. (2001) investigated underfill delamination

ATTENTION: The Singapore Copyright Act applies to the use of this document. Nanyang Technological University Library

and cracking in flip chip modules under thermal cyclic loading with the aid of characterization of stress singularity nature. Their results showed that the criterion for delamination initiation could correctly predict the interface that is prone to such defect. Moreover, the opening stress intensity factor along the interface (or peeling stress) plays an important role in causing interface failure.

Consequently, for the purpose of predicting the fatigue life of flip chip assembly, it is of importance to experimentally as well as theoretically understand the interface delamination behavior under thermal cycling. As long as the fracture behavior is clarified, it is easy to use fracture mechanics model to calculate the thermomechanical status with consideration of proper material properties. This will be specified in section 2.3.

ATTENTION: The Singapore Copyright Act applies to the use of this document. Nanyang Technological University Library

Table 2.1 Comparison of approaches for thermomechanical analysis (Desai & Whitenack 2001)

Approach	Parameters E*	Parameters M*	Testing Requirement E	Testing Requirement M	Capabilities	Limitations
1. Load Drop	ϕ	Elastic, Elastoplastic, Viscoplastic, etc.	Cyclic Softening	Quasistatic and/or cyclic	Fatigue life and cycles (N_f)	• Based essentially on one-dimensional behaviour • May not allow for multi-dimensional effects • Allows effect of stress only
2. Coffin-Mansion	C m	Elastic, Elastoplastic, Viscoplastic, etc.	Cyclic Softening	Quasistatic, cyclic and/or creep	Fatigue life and cycles (N_f)	• Based essentially on one-dimensional behaviour • May not allow for multi-dimensional effects • Allows effect of strains only
3. Fracture Mechanics	-	- Elastic, Elastoplastic, Viscoplastic, etc. - Stress intensity/Fracture	Quasistatic cyclic and/or creep	- Crack growth and length, and fatigue life (N_f) - Multidimensional	• *A priori* assumption of crack location and dimensions may not be realistic • May not allow adequately for influence of zones in the neighborhood of cracks • Often, based on linear elastic material behaviour
4. Energy (w)	-	Elastic, Elastoplastic, Viscoplastic, etc.	Quasistatic, cyclic and/or creep	Growth of volume (area) fraction with critical energy to identify microcrack-ing and fracture - Fatigue life - Multidimensional	• Calculations required for energy accumulation ~in elements! during cyclic incremental analysis • Computational effort for all cycles
5. Damage ~v!	-	Elastic, Elastoplastic, Viscoplastic, etc.	Quasistatic, cyclic and/or creep	- Growth of volume (area) fraction with critical damage values - Fatigue life - Multidimensional	• Classical approach suffers from spurious mesh dependence and nonuniqueness • Does not include microcrack interaction • Enrichments required for mesh independent and unique solutions • Computational effort for all cycles
6. Micromechanics		Elastic, Elastoplastic, Viscoplastic, etc.	Quasistatic, cyclic and/or creep	- Growth of microcracking and fracture - Fatigue life - Multidimensional	• Difficult to define constitutive equations at the micro ~particle! level • May not allow adequately for coupling in complex material systems • Computational effort for all cycles
7(a). Disturbance (D)		Elastic, Elastoplastic, Viscoplastic, etc.	Quasistatic, cyclic and/or creep	- Growth of volume (area) fraction with critical disturbance to identify microcracking and fracture - Fatigue life - Multidimensional - Microcrack interaction and coupling included - No spurious mesh dependence - Unified and holistic	• Computational effort for all cycles
7(b) Accelerated-Approximate Analysis	b	Elastic, Elastoplastic, Viscoplastic, etc.	Quasistatic, cyclic and/or creep	- Growth of volume (area) fraction with critical disturbance to identify microcracking and fracture-Fatigue life - Multidimensional - Microcrac interaction and coupling included - No spurious mesh dependence - Unified and holistic - Lower computational effort than for 7(a)	• Approximate and would require verification

E=Empirical ; M=Multidimensional Methods

ATTENTION: The Singapore Copyright Act applies to the use of this document. Nanyang Technological University Library

2.2.1.3 Creep

Since thermal cycling normally lasts long period of time, there is another concern, that is, time-temperature-dependent creep behavior of the underfill material. Both the mechanical properties and thermal properties of underfill materials close to their glass transition temperature range are sensitive to time as well as temperature and show viscoelastic nature (creep and stress relaxation) (Kenner et al. 1997). In addition, since the flip chip packages normally operate under the temperature ranging from –65 °C to 150°C, the viscoelastic mechanical properties of the underfill should be considered in order to study the thermal cycle reliability of flip chip package with underfill (Qian et al. 1999). It was shown that the temperature-independent and temperature-dependent elastic model of underfill underestimated the plastic strain in solder joint and accordingly overestimated the thermal fatigue lifetime of solder joint compared with the viscoelastic model of the underfill (Chen et al. 2001). Wang et al. 1998 investigated the creep behavior of flip chip package by both FEM modeling and real time moiré interferometry, whose results showed that the viscoelastic properties of the underfill and the viscoplastic properties of solder joint modeled by finite element analysis can more realistically describe the creep deformation of the flip-chip package during the test. In addition, they observed that the creep behavior had a strong effect on the stresses at the edges and the corners of all interfaces, which indicated that time-temperature dependent materials properties affected the interfacial reliability significantly.

Since the temperature cycling undergoes high temperature and relatively long time, it is important to know the different interfacial behavior, taking the viscoelasticity of underfill into consideration rather than elastic properties. It is

ATTENTION: The Singapore Copyright Act applies to the use of this document. Nanyang Technological University Library

well known that the Maxwell model as well as the Kelvin model can sufficiently describe linear viscoelastic property of underfill. The temperature and time dependent properties can be obtained by fitting the parameters in the models. Both tensile test (Shi et al. 2002) and dynamic prediction (Rao et al. 2000) were used to generate relaxation moduli and time.

However, to the author's best knowledge, at the present, the viscosity response of underfill in flip chip application is less involved in the failure analysis even though such knowledge is definitely important to lifetime prediction of flip chip package. Only up-to-now, the investigation of underfill materials on temperature and strain rate effects were carried out to found the viscoelastic mechanical model of the underfill to embed it into FEM simulation (Shi et al. 2002, Kuo et al. 2004).

Therefore, in this research project, FCOB with a pre-crack at the Si/underfill interface was subjected to thermal cycling loading with the displacement fields measured by moiré interferometry. The effects of CTE/stiffness mismatch with time effect were studied under thermal cycling. On the other hand, finite element analysis with built-in viscoelastic model of underfill material was carried out to examine the findings of moiré experimental results. The results show that time effect is important in the assessment of assembly reliability. The results of thermal effect on reliability issue of Si/underill interface is shown in Chapter 4.

ATTENTION: The Singapore Copyright Act applies to the use of this document. Nanyang Technological University Library

2.2.2 Hygrothermal Effect on Interfacial Failure

Since underfill is a kind of epoxy-based composite, which is vulnerable to humidity attack, the introduction of underfill material induces a new failure mode in solder interconnections under the constant temperature and humidity level. The moisture effect on the underfilled FCOB package can be classified into two aspects: on the global level, the presence of moisture induces differential hygroscopic swelling and accordingly hygroscopic stresses; on the local level, the presence of moisture reduces interfacial adhesion strength leading to delamination, and induces vapor pressure during solder reflow resulting in "popcorn" cracking (Wong et al. 2002a). Moreover, the hazardous moisture immigrating into epoxy-based material alters the thermal stress through modifying both the mechanical and thermal properties (Akay et al. 1997); alters electric properties such as dielectric constant (Gonon et al. 2001); and catalyzes corrosion and electro-migration (Wong et al. 2002a).

Hygroscopic stresses in FCOB may cause delamination and subsequent system failure due to underfill swelling (Oesterholt 1997, Lin & Tay 1997, Wong et al. 1999, Li et al. 2002, Wong et al. 2002b, Tounsi et al. 2002), plasticization (Guedes et al. 2000, Varelidis et al. 2000, Li & Sue 2002) and mode of failure alteration (Lawrence et al. 2001). The grouped molecules called bounded and unbounded water molecules determine the absorption behavior and adhesion strength. The former water molecule can probably cause most of the swelling, which is defined as an increase in the inter-segmental hydrogen bond length due to disruption of the intra-chain hydrogen bonding between polar groups in the network. On the other hand, plasticization is another factor that would probably affect the material properties. The hydrolysed moisture especially single hydrogen

ATTENTION: The Singapore Copyright Act applies to the use of this document. Nanyang Technological University Library

and/or dispersion bond will deteriorate the polymer, which will lower the modulus of resin (Uschitsky & Suhir 2001).

2.2.2.1 Swelling and Moisture Diffusion

Swelling is thought to be the result of an increase in the inter-segmental hydrogen bonding length. If hydrogen bonds form in epoxy resin due to moisture absorption, polar state existing water will disrupt the intra-chain hydrogen bonding between polar groups in the network (Kwei 1966). This phenomenon was explained by two kinds of water molecule in the matrix, i.e. bound water and unbound water. The former, which causes most of the swelling, is immobilized by the polar groups in the matrix; while the latter, which causes no or little of the swelling, is contained in the epoxy free volume (Adamson 1980).

Hygroscopic swelling of underfill has been found to be responsible for the transverse tensile cracking of solder interconnections under hygrothermal loading (Wong et al. 2002b). Tay & Lin (1999) proposed the mixture mode of temperature, moisture and fracture mode composition according to fracture mechanics. They also proposed the temperature and moisture superposition method to calculate the J integral by the consideration of thermal expansion and moisture swelling effects, which may present the strain energy release rate G as $G = E^{'} K^2$, where $E^{'} = \sum_{i=1}^{2} \frac{1-\nu_i}{4G_i}$ (plane strain) and $E^{'} = \sum_{i=1}^{2} \frac{1}{4G_i(1+\nu_i)}$ (plane stress), K is stress intensity factors $K = K_I + iK_{II}$ (Tay & Lin 1999). Such theory was supported elsewhere (Tounsi et al. 2002). In this dissertation, the superposition method was

ATTENTION: The Singapore Copyright Act applies to the use of this document. Nanyang Technological University Library

accordingly used to understand the effect of hygrothermal aging on FCOB interface reliability, as to be illustrated in Chapter 5.

In order to understand the moisture effect on the deformation and fracture behavior of flip chip package, FE simulation is applied to understand the hygroscopic stresses induced by moisture swelling. With known moisture distribution of plastic package by experimentally acquiring the parameters based on diffusion modeling and CME of polymeric material, hygrothermal stresses in the flip chip package can be simulated using hygro-mechanical analogy. The coefficient of moisture expansion (CME) of the underfill material can be characterized using combined TGA–TMA technology (Wong et al. 2002b).

Apart from the CME characterization, moisture diffusion behavior is studied in order to understand the moisture distribution in the package. Once the CME and moisture diffusion status are understood, the hygroscopic stresses is ready to be calculated to be $\varepsilon = \beta C$, where ε is the strain caused by the moisture induced swelling, β is the CME of the polymeric material and C is the moisture concentration in the material. Some of the polymers may show two stages of moisture diffusion i.e. Fuckian and non-Fuckian diffusion during hygrothermal aging (Bao et al. 2001). This is because in polymer the cross-linking segments the cross-linking points, preventing dense molecular packing. As a result, cross-linked regions have a higher free volume, and so they can accommodate more water (Gonon et al. 2001). The effect of moisture after a given period of preconditioning cannot be fully reversed by the same period of prebaking or desorption (Akay et al. 1997, Varelidis et al. 1998, Varelidis et al. 2000, Gonon et al. 2001, Loh et al. 2002). The hydrolysis reaction (Loh et al. 2002) due to moisture diffusion interferes with the ester bonds of resin, breaking the polymeric chain (Varelidis et

ATTENTION: The Singapore Copyright Act applies to the use of this document. Nanyang Technological University Library

al. 1998). Wong and Rajoo (2003) gave a comprehensive presentation of the characterization techniques for moisture absorption and diffusion properties with consideration of the effects of aspect ratio and Non–Fickian absorption.

2.2.2.2 Plasticization

Plasticization occurs when hydrolysis interferes with the ester bonds of the resin, breaking the polymeric chain, i.e., water molecules intercept the inter- and intra-molecular hydrogen bonding provided by the hydroxyl groups. It lowers the room temperature tensile strength and modulus (Lawrence et al. 2001). A simple ester hydrolysis reaction can be presented as follows (Gurumurthy et al.2001):

$$R-\overset{\overset{O}{\|}}{C}-O-R+H_2O(g)=R-\overset{\overset{O}{\|}}{C}-O-H+R'-O-H$$

Ideally, one molecule of water hydrolyzes the $-\overset{\overset{O}{\|}}{C}-O-$ functional group in the ester (*R-COO-R'*) to form acid (*R-COOH*) and alcohol (*R'-OH*) hydrolysis products. The breakage of the original chains can significantly lower the material strength since *O-C* bonding has been replaced by *OH-OH* bonding.

Note that at certain low degree of moisture absorption, the moisture swelling relieves the residual stresses residing from cooling down from the curing temperature and temporarily increase the resistance to epoxy & interface cracking (Haener et al. 1967, Lee et al. 1978). In the macro level, the effect of moisture is exhibited on material properties, such as moduli, CTE and glass transition temperature T_g. Yi & Hilton (1995) showed hygrothermal effects on viscoelastic responses of laminated composites, which reported that normal residual stress

ATTENTION: The Singapore Copyright Act applies to the use of this document. Nanyang Technological University Library

relaxes much more rapidly than shear stress loading. Guedes et al. (2000) introduced viscoelasticity on the properties of material when exposed to humidity ambient and showed good agreement between experiment and theoretical model. Baschek et al. (1999) extended the material properties to low and high temperature rather than room temperature and showed interesting results at low temperature with moisture, as shown in Fig. 2.5, where tanδ was the loss factor, whose peak represented the glass transition temperature T_g, G was the shear modulus. It can be seen that both the modulus and T_g decreased with the increase of moisture content. The decrease was specifically obvious when the temperature increased, which indicated that hygrothermal attack has more harmful effects on material degradation (Park et al. 1997).

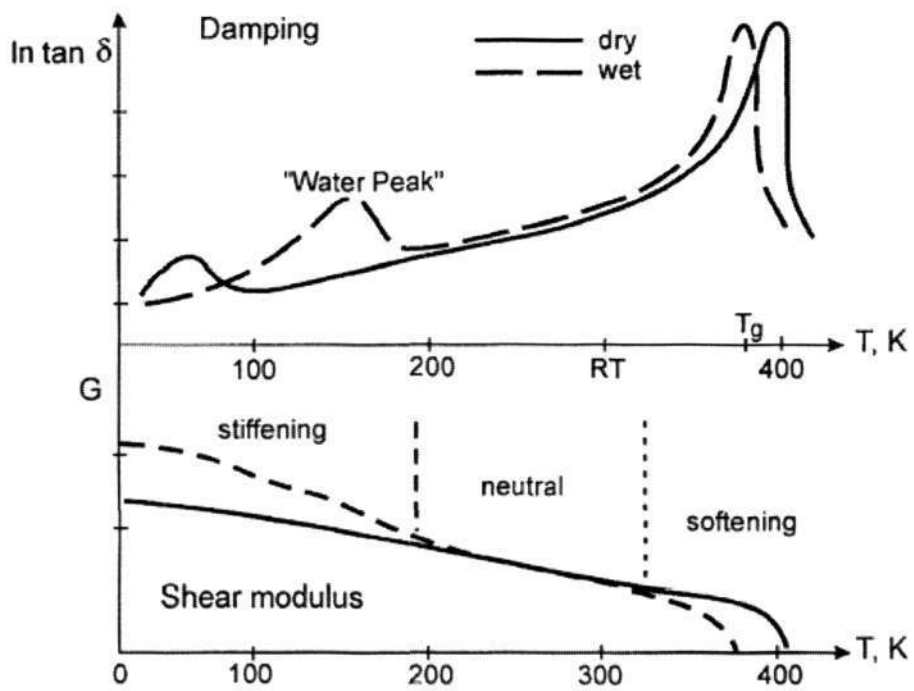

Fig. 2.5 Schematic presentation of loss factor and shear modulus for dry and wet specimens (Baschek et al. 1999)

ATTENTION: The Singapore Copyright Act applies to the use of this document. Nanyang Technological University Library

2.2.2.3 Vapor Pressure

When temperature goes high, the moisture evaporates into steam, which introduces another effect resulting from steam with high pressure. This kind of failure was reported in many articles (Pearson et al. 1995, Nguyen et al. 1995, Galloway & Miles 1996, Lim et al. 1998, Lau & Lee 2000a). Particularly, when steam caused delamination develops to crack and steam escapes to outside, a crisp sound comes into being due to the steam pressure release. This kind of failure is named as "popcorn" (Lim et al. 1998, Lau & Lee 2000a).

Many researchers have attempted to address this critical and yet challenging mission of vapor pressure modeling (Kitano et al. 1988, Tay and Lin 1996, Alpern et al. 2000). Recently, wetness technology is applied to study the packages with multiplayer delamination interfaces induced by swelling as well as vapor pressure (Wong et al. 2002c). It is observed that the lower modulus of underfill material leads to lower vapor pressure and accordingly lower structure rigidity. Experiment and simulation show that at a high temperature for solder reflow, the moisture concentrated in the moisture-susceptible material is vaporized, resulting in the vapor pressure threatening the interfacial adhesion of interconnect structure (Fukuzawa 1985). Further, it is proposed that the moisture content and concentration are critical factors to influence the reflow behavior (Lin 1988, Kitano et al. 1988). The resulting interfacial delamination occurs at various interconnected sites with the combination of CTE mismatch with steam pressure generated during reflow process (Lau and Lee 2000a). It has been detected that both the fracture energy release rate and modulus data are related to the moisture content rather than the exposure time (Loh et al. 2002).

ATTENTION: The Singapore Copyright Act applies to the use of this document. Nanyang Technological University Library

If delamination or crack initiates, it will result in a tunnel for electro-migration and corrosion, especially permitting moisture to penetrate into the package to form potential crack during the process of solder reflow due to vapor pressure. Consequently, the interlayer strength may degrade and moisture penetrates along the path of damaged solder joint, especially along the solder joint at the corner of the chip, which undergoes the largest shear stress Therefore, the deterioration of moisture on polymer interface adhesion was also essentially studied since plastic IC package subjected to moisture is vulnerable to delamination or cracking during solder reflow or even at relatively low temperature.

2.2.2.4 Decrease of Interfacial Adhesion

The adhesion strength significantly degrades in humidity environment (Yi et al. 1997). The water assisted stress corrosion crack growth kinetics along an underfill/passivation surface was studied and modeled by Gurumurthy et al. 2001. Ferguson & Qu (2002) found that moisture preconditioning strongly influenced the interfacial fracture toughness of the underfill/solder mask interface, decreasing the interfacial adhesion by approximately one-half after 725h of exposure at 85 °C/85%RH. Kawagoe et al. (2001) tested interfacial fracture resistance of resin/glass bi-layer after subjected to cyclic absorption-desorption and continuous absorption, whose results showed significant toughness diminution in the early stage of moisture absorption. Kinloch (1987) reported that moisture-assisted crack growth along polymer and glass interfaces under monotonic loading is due to displacement type reaction where water modules displace the polymer chain in

ATTENTION: The Singapore Copyright Act applies to the use of this document. Nanyang Technological University Library

Van-der Waals bonding of the polymer adhesive to the glass surface. Nguyen et al. (1997) applied different moisture levels to measure correspondent interfacial fracture toughness by testing bending of laminated beams and shearing of blocks. Gurumurthy et al. (2001) developed Wiederhorn model to predict the hygrothermal fatigue crack growth rates along the underfill/chip passivation (polyimide) interface. Loh et al. (2002) and Wylde & Spelt (1998) used open-faced, which can accelerate the moisture absorption and ensured uniformity of moisture diffusive content in plate polymer.

Many researchers have made tremendous efforts to understand the interface reliability issues of FCOB assembly using FE software to simulate the effects of moisture immigration in the plastic flip chip package (Wong et al. 2002a, Wong et al. 2002b). However, in the author's best knowledge, limited experimental work has been carried out to understand the realistic response of delaminated package loaded in humidity environment. This limitation causes uncertainty to verify results simulated by FE. How can swelling significantly influence the fracture characteristic parameters, such as stress intensity factor (SIF), phase angle and strain energy release rate? What is the real displacement status in flip chip structure? If such improvement and knowledge can be obtained, it will have advantages for the future development on flip chip technology. This thesis proposed experimental study of interfacial response of delaminated flip chip package under hygrothermal loading based on moiré technology, which is suitable to detect the in-plane contour deformation under quasi-static thermal or hygrothermal condition. With digital image correlation measurement, the effect of moisture on interfacial fracture toughness was subsequently addressed to evaluate

ATTENTION: The Singapore Copyright Act applies to the use of this document. Nanyang Technological University Library

the interfacial reliability under moisture loading. The effect of hygrothermal aging on the interface of Si/underfill is discussed in Chapter 5 and Chapter 6.

2.3 Interfacial Fracture Mechanics

Since the interfacial reliability is one of the dominant failure modes for flip chip package, quantitative characterization of underfill adhesion to passivation layers, to solder mask and so on, is especially critical for flip chip applications both in terms of underfill material development and reliability design and analysis. The conventional method to evaluate the reliability issue is to manufacture statistically considerable amount of assemblies, subject them to environmental loading, and do failure analysis. This methodology is time-consuming and expensive. Sometimes, it is complicated due to the geometry of the assembly and specification of the device.

Currently, strength analysis and fracture mechanics analysis are accepted as the methods to quantify the interfacial adhesion, which are faster and more promising for industry. In practice, fracture mechanics using "interfacial fracture toughness" is more accurate, quantitative and reliable measure of interfacial adhesion (Kuhl & Qu 2000). The purpose of interfacial fracture mechanics is to define a measurable and usable material property, toughness, to parameterize fracture resistance of interfaces and improve the reliability and serving life of assembly (Wang & Suo 1990). From a mechanical point of view, interfacial fracture is confined as the interface regardless of local stress mode provided that the interface is relatively weak.

ATTENTION: The Singapore Copyright Act applies to the use of this document. Nanyang Technological University Library

Defined as the interface's resistance to decohesion, interfacial fracture toughness is typically evaluated by the strain-energy release rate (G) or stress intensity factor (SIF) (K). Basically, fundamental theory and experimental method have been proposed. Rice (1988) used elastic fracture mechanics concepts for interfacial cracks and mainly emphasized on the small-scale contact zone at the crack tip.

Table 2.2 Methodologies for the determination of interfacial toughness

Serial No.	Testing Methodologies	Authors	Year of Publication
1	Symmetric and asymmetric cantilever beam sandwich specimen	Cao and Evens	1989
2	Notched four-point flexure specimen	Charalambides et al.; Cao and Evens	1989
3	Brazil-nut-sandwich specimen	Wang and Suo	1990
4	Biaxially loaded bimaterial strip	Liechti and Chai	1991
5	Symmetric/asymmetric three/four points bend specimen	O'Dowd et al.	1992
6	Brazilian disks	O'Dowd et al.	1992
7	Bimaterial and sandwich blister specimen	Liechti and Liang	1992
8	Thin layer sandwich specimen	Suo and Hutchinson; Thurson and Zehnder	1993
9	Asymmetric double cantilever beam test	Sundararaman and Davidson	1995
10	Single leg bending test	Sundararaman and Davidson	1995
11	Asymmetric end-notched flexure test	Sundararaman and Davidson	1995

Since the separated mode fracture parameters like K_I and K_{II} do not exist in a bimaterial system except for a special material combinations with $\beta = 0$ (Rice

ATTENTION: The Singapore Copyright Act applies to the use of this document. Nanyang Technological University Library

1988, Suo & Hutchinson 1989, Wang & Suo 1990, Hutchinson & Suo 1992), it is difficult to represent the whole singular field at the crack tip by using one or few parameters. To solve this complexity, Suo and Hutchinson (1989) showed ways to measure interface crack toughness by applying sandwich test specimen, who used homogeneous solution as an approximated replacement of the actual interface stress intensity factors. Both the comparison and varieties of test methods for determining fracture toughness as a function of mode mixity have been proposed. The details are listed in

Table **2.2**. Hutchinson and Suo (1992) also proposed a review of interfacial fracture mechanics including theories and experimental methods. Recently, Fan et al. (2001) defined the concept of the opening and shearing mode "(SIF)" and proposed a criteria to predict crack propagation for flip chip configuration.

The introduction of general concepts as well as the development of testing methods enables the investigation of interfacial fracture in electronic packaging under thermal cycling, thermal creep, thermal shock, moisture aging and monotonic/alternative mechanical loading etc. To calibrate the delamination criteria, strain release energy rate from J-integral or stress intensity factor (SIF) is applied to establish self-stretching flip chip solder joint crack under thermal fatigue crack propagation and to predict thermal fatigue life in solder joint (Lau 1993). Kook et al. (1998) studied polymer/inorganic interfacial adhesion behavior under monotonic or cyclic loading, which showed that fracture resistance was strongly dependent on the interface morphology and the thickness of the polymer layer. Nishimura et al. (1992) stated three-point bending tests of two-layer end-notched flexure (ENF), which measured interfacial adhesion strength by applying load onto both directions to get arithmetic average value (Fig. 2.6), to eliminate residual

ATTENTION: The Singapore Copyright Act applies to the use of this document. Nanyang Technological University Library

stress influence on fracture toughness. Yao et al. (1999) tested the silane additive's effect on the underfill and substrate interfacial toughness. Lau and Lee (2000b) showed temperature-dependent stress and plastic strain at the corner solder joint of flip chip with different crack length, and proposed that crack tip opening displacement method (CTOD) as well as virtual crack closure technique (VCCT) are suitable for evolution of fracture parameters. Jiao et al. (1998) indicated that the effect of thermal residual stress must be taken into consideration in the calculation of critical strain release rate to obtain the true interfacial fracture energy. Dutta, et al. (2002) developed a new single joint-shear (SJS) test to investigate the impact of the constraint imposed by the underfill on a solder joint, which the strain response of a eutectic Pb-Sn solder joint is influenced significantly by the underfill properties.

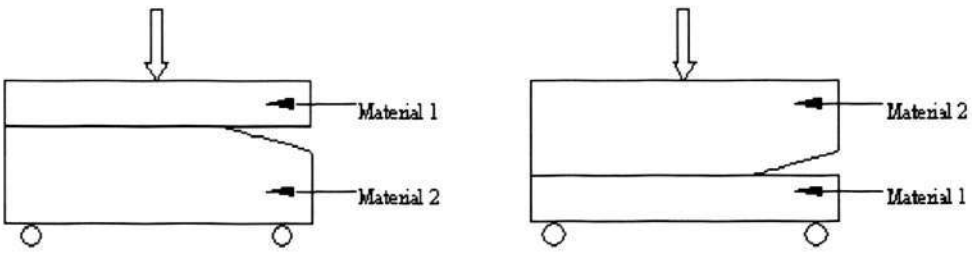

Fig. 2.6 Schematic diagram for three-point bending experiment (Nishimura et al. 1992)

To sum up, both the understanding of interfacial toughness and the characterization of interfacial fracture toughness under thermal or hygrothermal conditioning are of significant importance to improve the interfacial reliability of flip chip assembly. If toughness and fracture toughness is comparable, it is easy to

ATTENTION: The Singapore Copyright Act applies to the use of this document. Nanyang Technological University Library

evaluate the interface and choose the appropriate underfill/structure to improve the resistance to delamination.

In this project, a moiré interferometer was developed and used to measure the interfacial toughness under the thermal cycling and hygrothermal aging. An innovated speckle correlation technique and Brazil nut fixture was proposed to characterize the interfacial fracture toughness under both thermal and hygrothermal loadings. An interfacial fracture mechanics parameter called crack tip opening displacement (CTOD) was applied to quantify the interface response under two environmental loadings. Basic formulas in interfacial fracture mechanics are further reviewed in Chapter 4, with special attention paid to their validity. The details of moiré interferometry technique and speckle correlation technique are to be introduced in the next chapter. The review of CTOD method is to be specified in the beginning of chapter 4. The results presented in Chapter 4, Chapter 5 and Chapter 6 enable the assessment of environmental interface reliabilities of delaminated flip chip assembly by comparing interfacial toughness with interfacial fracture toughness between Si/Underfill.

ATTENTION: The Singapore Copyright Act applies to the use of this document. Nanyang Technological University Library

Chapter 3 Experimental Details and Instrumentations

This chapter presents:

(1) thermal and mechanical properties of assembly materials;

(2) procedures of specimen preparation;

for the reliability studies of FCOB assembly under thermal cycling loading and hygrothermal loading conditions. Generally, the specimens are classified into two groups, as illustrated in Fig. 3.1.

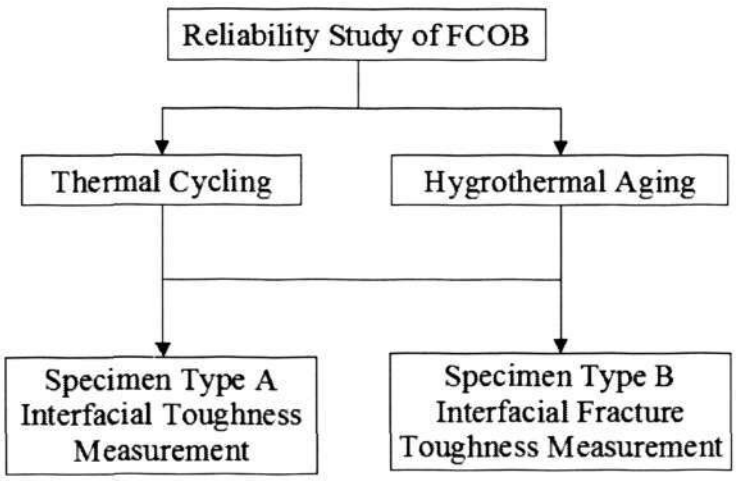

Fig. 3.1 Classification of specimens for reliability evaluation

- Specimens type A: sandwiched specimens used to measure interfacial toughness based on moiré interferometry. The results are presented in Chapters 4 and 5.

ATTENTION: The Singapore Copyright Act applies to the use of this document. Nanyang Technological University Library

- Specimens type B: Brazil-Nut (BN) specimens used to measure interfacial fracture toughness using digital image correlation system. The results are presented in Chapter 6.

In addition, sections 3.3 and 3.4 provide the details of two photomechanics measurement techniques, namely moiré interferometry technique and digital image correlation technique, for real-time displacement measurement.

3.1 Materials

In this section, the materials used in the study are specified. The structures of the specimens and their preparations are illustrated in section 3.2. The specimens are made of the following materials:

(1) Silicon wafer with SiO_2 passivation (of 10^{-4} *mm* in thickness) and Si_3N_4 passivation (of 2×10^{-4} *mm* in thickness). The total thickness of Si wafer is 0.5 *mm*.

(2) Type 3563 silica filled epoxy composites supplied by Loctite®, which is widely used in flip chip packages as underfill material. The filler content is 40% with the average particle sizes ranging from 1 μm to 2 μm.

(3) FR-4 composites with solder mask passivation. No holes or delamination exist in such materials. The thickness is 0.8 *mm*.

In order to study the effect of thermal cyclic loading on the delaminated flip chip assembly, additional finite element analysis (FEA) modelling was employed to examine the findings of experimental results. Both the interface

ATTENTION: The Singapore Copyright Act applies to the use of this document. Nanyang Technological University Library

fracture mechanics and FEA simulation require accurate thermal and mechanical materials properties, as the databases, to obtain good solutions.

The constituent materials properties of the sandwich structure analysed are shown in Table 3.1 (Shi et al. 2002b), where silicon chip and FR-4 were modelled as temperature-dependent in order to have good estimates from finite element analysis for proper comparison with experimental results.

Table 3.1 Material properties for sandwich structure except underfill (Shi et al. 2002b)

		Young's Modulus (GPa)	CTE (*ppm*/°C)	Poisson's Ratio
Silicon Chip		132.46-0.00954T	2.113+0.00235T	0.28
FR-4	In-plane	24.422-0.0226T	17.6	0.11
	Out-of-plane	10.562-0.00957T	24	0.39

Since the epoxy-based underfill exhibits viscous nature, especially when the temperature is around or above T_g, time-temperature-dependent properties of underfill material can significantly affect the responses of flip chip assembly structure (Wang et al. 1998). The underfill is realistically characterized to be linear viscoelastic based on the various viscoelastic models. The viscoelastic Maxwell model was established in previous works (Shi et al. 2002a, Zhang et al. 2002). In these works, the tensile testing data with different strain rates (Shi et al. 2002a) were processed and arranged corresponding to algorithmic details provided by ANSYS (Zhang et al. 2002). It is found that the tangent modulus or the differential of the stress-strain curve from constant strain rate test is equal to the relaxation modulus determined from stress relaxation test. The plot of σ/α versus ε/α is no

ATTENTION: The Singapore Copyright Act applies to the use of this document. Nanyang Technological University Library

longer dependent on the strain rate for linear viscoelasticity (Zhang et al. 2002). The basic equation is expressed as:

$$E(t) = E_0 + \sum_{i=1}^{I} E_i e^{-t/\tau_{Ri}} = E_T(t) \tag{3.1}$$

where $E(t)$ is the relaxation modulus, I is the number of the Maxwell elements, τ_{Ri} is the relaxation time related to the ith Maxwell element, $E_T(t)$ is tangent modulus, defined as $E_T(t) = d\sigma(t)/d\varepsilon(t)$, which is non-strain-rate related.

The parameters for linear viscoelastic properties of the underfill material can be subsequently deduced by data fitting from the tensile test of thin-film underfill (Shi et al. 2002a). Based on the Maxwell model, the time-dependent shear modulus was given by:

$$G(\xi) = G(\infty) + \sum_{i=1}^{I} G_i e^{(-\xi/\lambda_i)} \tag{3.2}$$

where $G(\infty)$ was the equilibrium shear modulus; $G_i = C_i(G(0) - G(\infty))$ was the modulus at different time, C_i is constant associated with the instantaneous response and $G(0)$ is initial modulus; λ_i is relaxation time constants of each Maxwell element; ξ is the reduced or pseudo time defined as

$$\xi = \int_0^t \Phi \, dt' \tag{3.3}$$

where Φ = shift factor=e^A, $A = \frac{H}{R}\left(\frac{1}{T_{ref}} - \frac{x}{T(t')} - \frac{(1-x)}{T_f(t')}\right)$, $\frac{H}{R}$ is activation energy divided by the ideal gas constant, T_{ref}, $T(t')$ and $T_f(t')$ are reference temperature, temperature at time t and fictive temperature at time t' respectively. The stress can be related at any time by the convolution integral:

ATTENTION: The Singapore Copyright Act applies to the use of this document. Nanyang Technological University Library

$$\sigma(t) = \int_{-0}^{t} G(\xi - \xi') \frac{d\varepsilon(t')}{dt'} dt' \tag{3.4}$$

where σ is stress and ε is total strain including thermal strain. The parameters mentioned above are listed in Table 3.2.

Table 3.2 Viscoelastic parameters for underfill material (Zhang et al. 2002)

Parameters		Value	Parameter	Value
H/R		15644	C_1	0.264
CTE (ppm/ °C)	Below T_g	T-Dependent	C_2	0.2
	Above T_g	110	C_3	0.536
$G_{xy}(0)$ (MPa)		1691.7	λ_1	0.198
$G_{xy}(\infty)$ (MPa)		23.3	λ_2	451
K(0) (MPa)		4500	λ_3	30435
K(∞) (MPa)		62		

3.2 Specimen Preparation

To simplify the study, the solder joints are not included in both specimens type A and B, since solder joints play a small role in the warpage of the underfilled flip chip assembly while the underfill epoxy plays a dominant role (Zhang et al. 1998). They also observed that the delamination at the interfaces such as Si/underfill, underfill/FR-4 occurs prior to fatigue fracture of the solder joints. The total time to function loss is dominated by stable crack propagation along interface between the underfill meniscus and the edge of the chip rather than by crack growth within the solder joints (Madenci et al. 1998).

ATTENTION: The Singapore Copyright Act applies to the use of this document. Nanyang Technological University Library

3.2.1 Specimen Type A

In order to understand the deformation and fracture behaviour of flip-chip package under either thermal loading or hygrothermal loading conditions, sandwich specimens type A with pre-crack, were prepared for moiré interferometry testing. Subsequently, the specimen with pre-crack was used to access the interfacial toughness under an environmental loading.

A flip chip assembly, as shown in Fig. 3.2(a), was simulated. It is noted that, since the cross section of the assembly was to be studied, half of the assembly was tested due to the symmetric reason. Consequently, the flip chip assembly used in this study (see Fig. 3.2(b)) consisted of three materials, namely, silicon chip, underfill and FR-4.

A specially designed mould, as shown in Fig. 3.3, was employed to prepare the assembly with the desired dimensions, i.e. 8 *mm(L)*×5 *mm(W)* ×1.8 *mm(H)*. The thickness of underfill was determined to be 0.5 *mm*. In addition, the choice of the underfill thickness optimised for critical adhesion does not result in enhanced resistance to progressive debonding under the temperature cycling load, which was carried out in this study (Kook et al. 1998). In order to measure the interface toughness, a piece of silicone rubber film with a thickness of 20 μm adhering to the chip passivation was used to prevent the adhesion of the underfill material during curing. The crack length was chosen to be a=2.7 *mm*, based on interfacial linear elastic fracture mechanics (Hutchinson and Suo 1992). After the curing of the underfill, a pre-crack was made at the chip/underfill interface with length a=2.7 *mm*, and the ligament ahead of the crack tip w=5.3 *mm*, satisfying $a, w > H + h + t$, where H, h, and t are the thickness of FR-4, silicon wafer and underfill respectively.

ATTENTION: The Singapore Copyright Act applies to the use of this document. Nanyang Technological University Library

The selection of these dimensions was to neglect edge effects on loading. Under these situations, a steady state solution was valid and the dependence of the energy release rate or SIFs on the crack length can be eliminated (Hutchinson and Suo 1992).

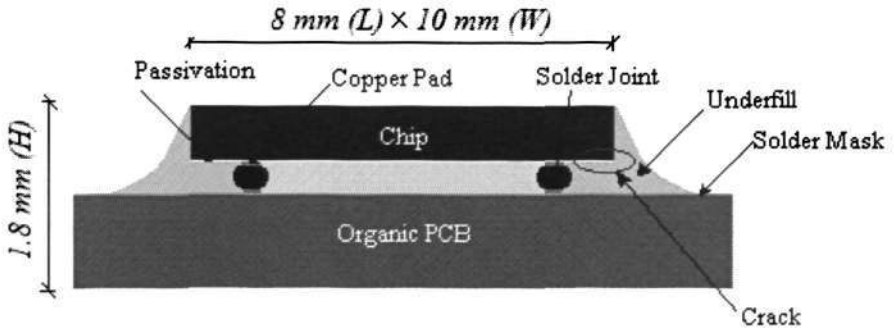

(a)

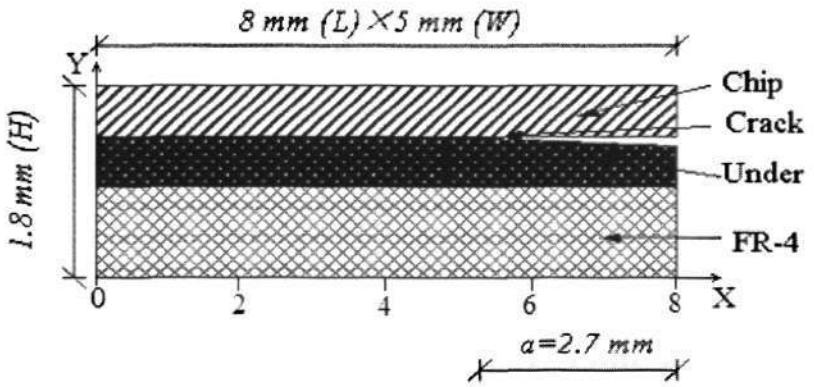

(b)

Fig. 3.2 Schematic diagram of the assembly to be studied: (a) flip chip assembly, (b) simplified flip chip assembly

ATTENTION: The Singapore Copyright Act applies to the use of this document. Nanyang Technological University Library

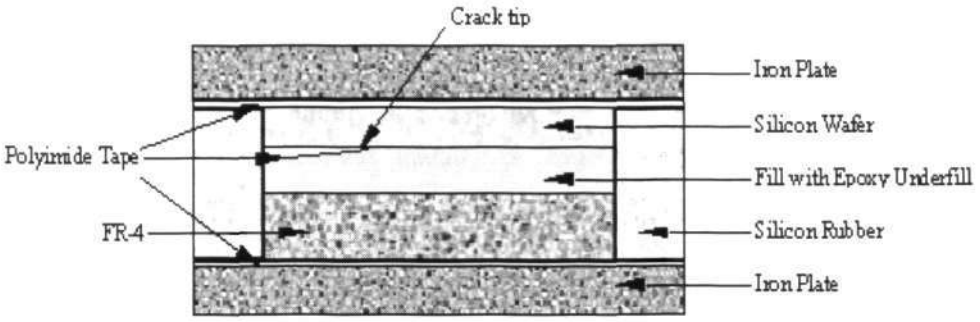

Fig. 3.3 Schematic diagram of the mould for the preparation of sandwich specimen

Polyimide tape was first replicated on the iron plate to prevent unexpected adherence to the iron plate by the underfill material. Subsequently, the mould without underfill was heated to 95 °C. Under this temperature, the uncured underfill has low viscosity and thus is easier to dispense. The uncured underfill, which was stored in a syringe at –40 °C, was warmed under the dry keeper (30%RH) to the room temperature. A dispenser and a curing oven were employed to prepare the sandwich specimen. By following flip-chip packaging process, an optimised curing condition was defined to be 165 °C for 8 *min* (Shi, Wang & Pickering 2003). Due to capillary action, underfill was dispensed into the gap between the chip and FR-4. When the specimen was partially cured, the rubber was quickly removed from the specimen and a sharp crack was fabricated, as shown in Fig. 3.4. After moulding, each specimen was carefully polished with a fine SiC paper to remove excessive underfill and to obtain the desired dimensions.

ATTENTION: The Singapore Copyright Act applies to the use of this document. Nanyang Technological University Library

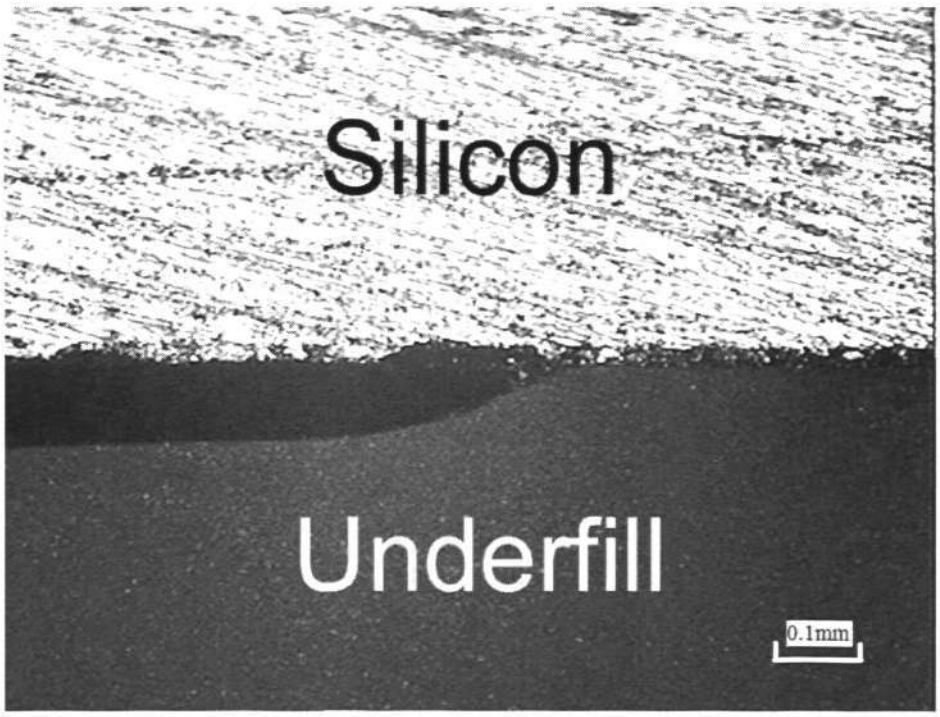

Fig. 3.4 Microscopic picture of crack tip region between Chip/underfill

Since specimen type A was designed to study the deformation and the interface toughness of the delaminated flip chip assembly using moiré interferometry, the grating replication on the specimen cross-sectional surface was necessary to generate the moiré fringe pattern.

A high frequency cross-lined diffraction grating replicated on the surface of specimen is the key element in moiré interferometry application. The deformed specimen grating and reference grating fixed in the testing vehicle can interact to produce the moiré fringe pattern. To achieve the moiré fringe pattern, two grating, namely, master grating and reference grating, were necessary to get interferogram. The objective grating (master grating) made of aluminium film was firstly moulded on the substrate. To replicate master grating on the surface of the

ATTENTION: The Singapore Copyright Act applies to the use of this document. Nanyang Technological University Library

specimen, a pool of room temperature curing epoxy (F114, Tracon™) was poured on the mould and squeezed into a thin film by pressing the specimen against the mould. As the excessive liquid adhesive was squeezed out, it was cleaned away from all specimen boundaries with cotton swabs, which could be slightly dampened with alcohol (Post et al. 1994). The epoxy curing lasted about 18 hours at room temperature. Therefore, the epoxy for grating replication was cured at the room temperature, which was considered as start point in the experiment. After polymerization of epoxy, the mould was pried off with small force with a reflective diffraction grating replicated on the surface of the specimen. The schematic diagram for grating replication is shown in Fig. 3.5.

ATTENTION: The Singapore Copyright Act applies to the use of this document. Nanyang Technological University Library

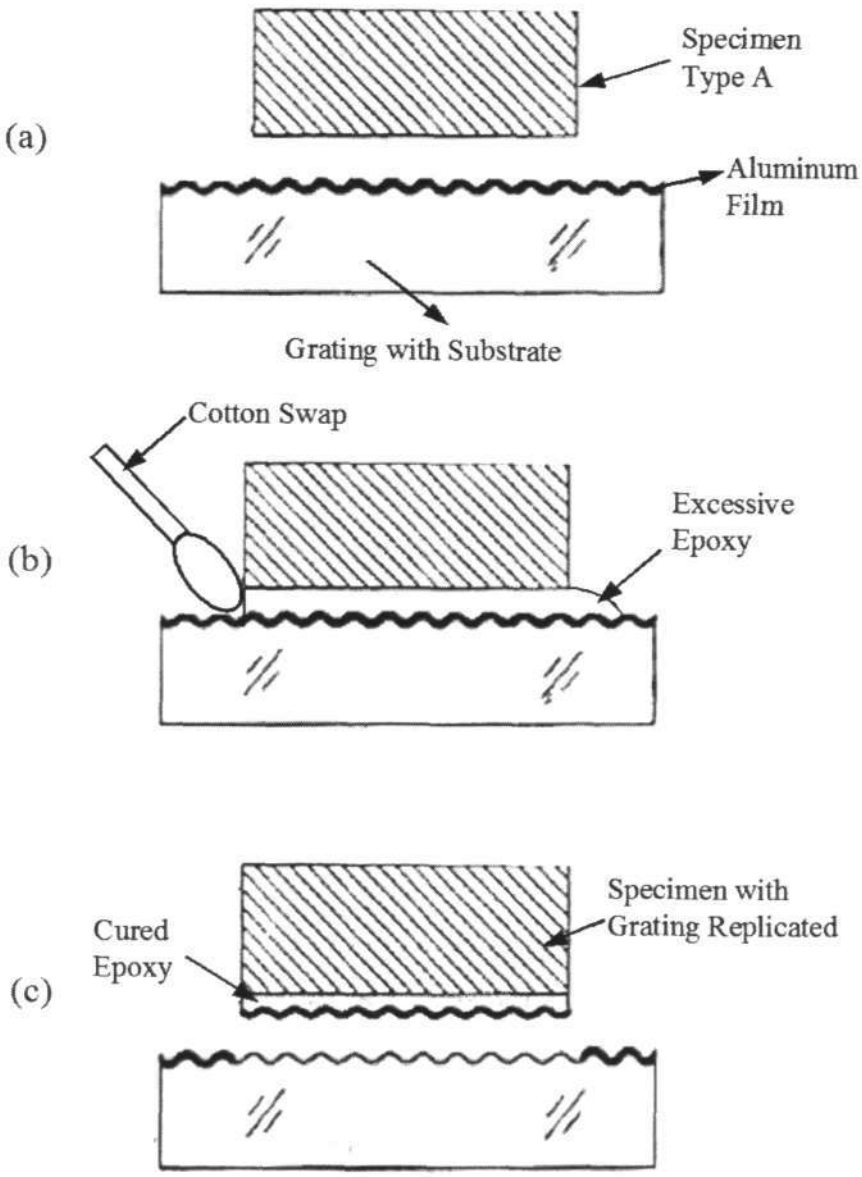

Fig. 3.5 Steps in replicating the grating on the specimen surface: (a) specimen type A and grating; (b) adhesion with specimen type A and grating with epoxy, cotton swab is to remove excessive epoxy; (c) replication of the grating to the surface of the specimen type A. (Post et al. 1994)

ATTENTION: The Singapore Copyright Act applies to the use of this document. Nanyang Technological University Library

3.2.2 Specimen Type B

3.2.2.1 Sandwiched Brazil-Nut Loading Fixture

Interface fracture mechanics has been increasingly applied to study the reliability issues in microelectronic packages. Interfacial fracture toughness is usually used as a fracture criterion to evaluate the reliability of polymer/inorganic interface. Different characterization methodologies have been developed to determine the fracture toughness of polymer/inorganic interface.

However, electronic packages are multiplayer material systems and often suffer from complex environmental loadings, the interfacial fracture mode mixity of polymer/inorganic interface in the packages is governed by both local material mismatch and global complex loading. Therefore, sandwiched brazil-nut (SBN) specimen, as shown in Fig. 3.6, was used to characterize the fracture toughness with wide range of loading angles (Atkinson et al.z 1982, Wang & Suo 1990). The advantage of SBN fixture is that it can load the specimen with various angles, and therefore a number of mode mixities can be obtained, which is meaningful to interface affairs. The common BN fixture was fabricated as the substrate of sandwich specimen. However, in this study, due to the difficulty of fabricating Si SBN fixture, modified fixtures, which are made of aluminium, were specially designed with slotting at the centre of fixture, as shown in Fig. 3.6.

ATTENTION: The Singapore Copyright Act applies to the use of this document. Nanyang Technological University Library

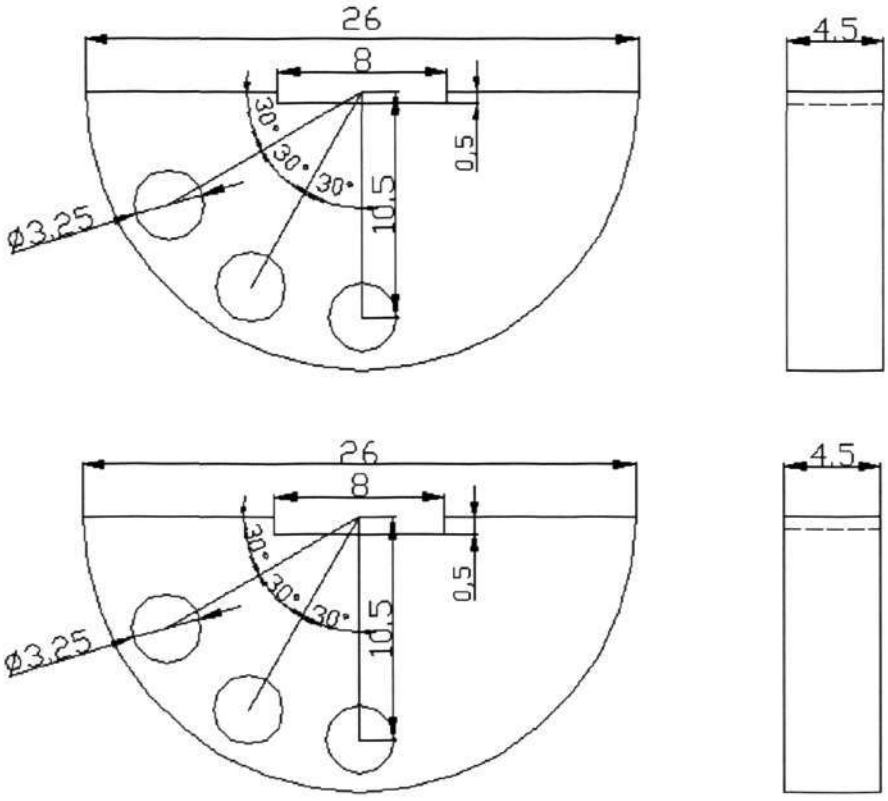

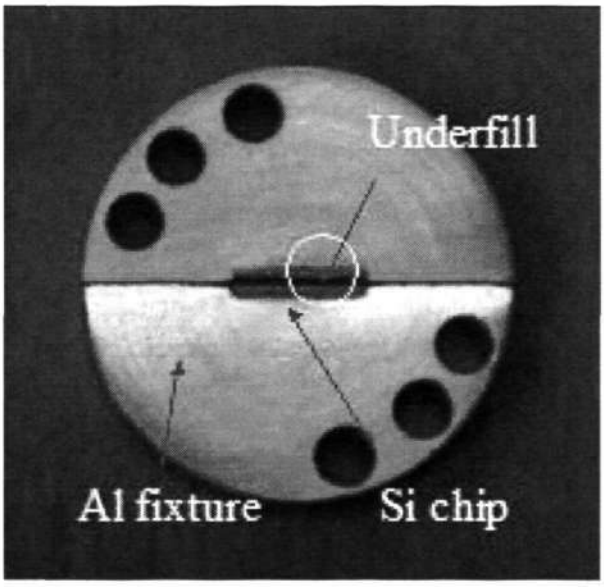

Fig. 3.6 Specially designed SBN fixture (dimensions in *mm*)

ATTENTION: The Singapore Copyright Act applies to the use of this document. Nanyang Technological University Library

The core of the specimens used in the measurement of interfacial fracture toughness consisted of two layers of Si wafer sandwiching a thin layer of underfill material (0.5 *mm*), as shown in Fig. 3.7. The crack length was $a = 4\,mm$, and the ligament ahead of the crack tip was $w = 4mm$, satisfying $a, w > 2H + h$, where H, and t were the thickness of silicon chip and underfill respectively. The selection of these dimensions is to neglect edge effects on loading (Hutchinson and Suo 1992). Under these situations, a steady state solution was valid and any dependence of the energy release rate on the crack length was eliminated.

TRA-BOND® F202 was used as adhesive to bond the core part onto the fixtures. The initial test showed that the bonding strength between Si and Al is far higher than that between Si and underfill. Apart from the nature of bonding strength, due to the introduction of pre-crack in the experiment, the adhesion of chip/fixture is much stronger than that of chip/underfill. Therefore, it can be concluded that the deformation of F202 layer during the loading is negligible compared to the deformation of sandwich specimen. After bonding, a sandwich is ready to be made by bonding two halves with underfill material. The process of dispensation and curing of the underfill were the same as that for specimen type A. After moulding, each specimen was carefully polished with a dine SiC paper to remove excessive underfill and to obtain the desired dimensions.

ATTENTION: The Singapore Copyright Act applies to the use of this document. Nanyang Technological University Library

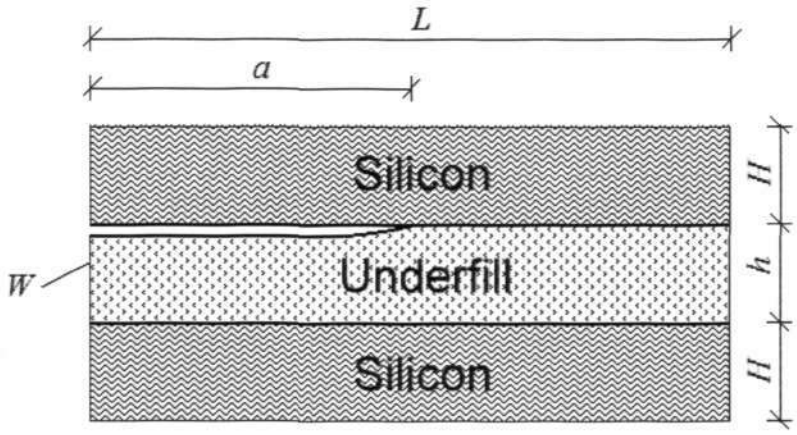

Fig. 3.7 Schematic diagram of the core of SBN specimen

3.2.2.2 Speckle Pattern Generation

In order to implement image analysis using the digital image correlation method, speckle patterns were obtained by firstly painting the specimen surface with black paint, and secondly sputtering with gold particles to create images with high contrast of grey level. The speckle size and distribution were therefore determined by controlling sputtering time, sputtering distance and current. Each specimen type B was observed under the optical microscope, and the average speckle size was determined based on magnification of microscope and pixel sizes of particles in the recorded image. The average particle size was measured to be 5.6 μm. Typical speckle pattern at the crack tip is presented in Fig. 3.8.

ATTENTION: The Singapore Copyright Act applies to the use of this document. Nanyang Technological University Library

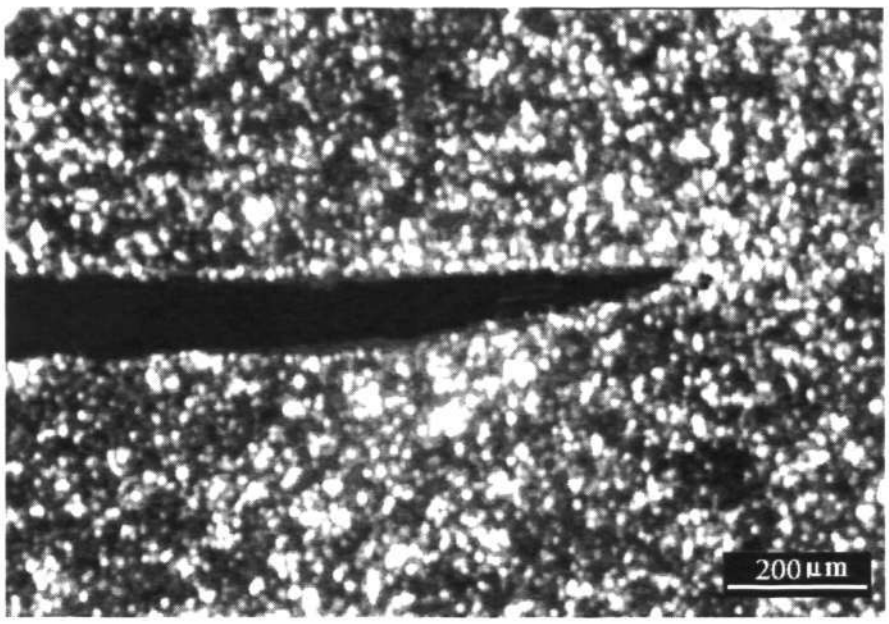

(a) Before deformation

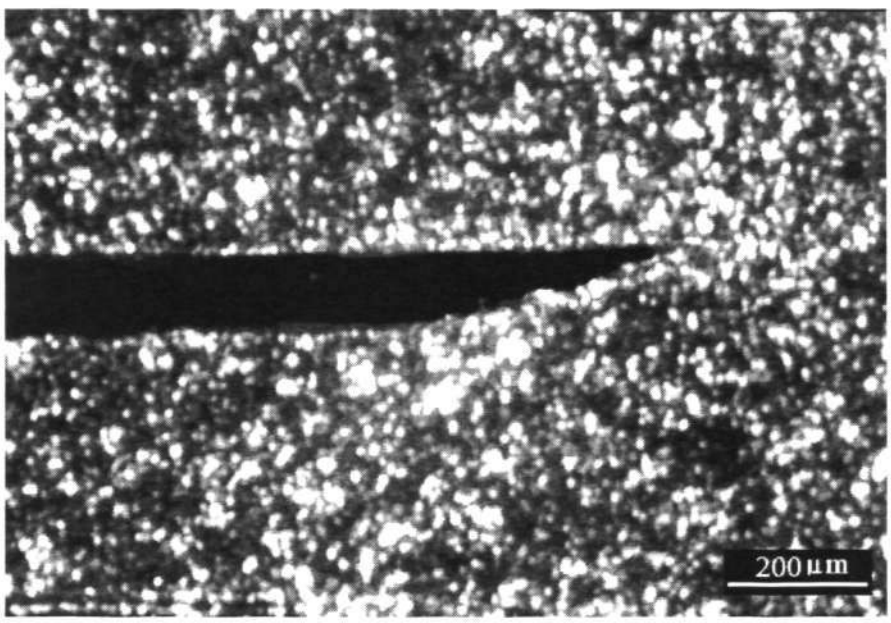

(b) After deformation

Fig. 3.8 Typical speckle pattern obtained from the test

ATTENTION: The Singapore Copyright Act applies to the use of this document. Nanyang Technological University Library

3.3 Moiré Interferometry

Although finite element analysis has been extensively used to estimate stresses and strains in design and testing of microelectronics devices, simplifications and uncertainties in stress analysis and fatigue life prediction remain inevitable due to complex loading and boundary condition in reality (Derveaux & Mawer 1995). Therefore, advanced experimental techniques, especially photomechanics methods including moiré, shadow moiré, Twyman/Green interferometry and far infrared Fizeau interferometry (Han 2003), are being demanded to provide accurate measurement for deformation/stress analysis under thermal cycling for microelectronic packages (Han & Guo 1995, Cho et al. 2002). Recently, moiré technique has been extensively used to measure determine the coefficient of hygroscopic swelling of commercially available mold compounds (Stellrecht et al. 2004). Experimental evaluation is expected to give realistic solutions of stresses and strains since they are not based on assumptions made to facilitate numerical analysis. With a decrease of assembly size, high resolution and sensitivity experimental techniques are required. Real-time observation is, at the meanwhile, of importance to investigate the deformation trend with respect to time. Cho et al. (2004) studied the whole-field moiré patterns of the assembly during an accelerated thermal cycling condition, indicating a significant nonlinear behavior due to complete relaxation of stresses in plastic assembly.

In this dissertation, moiré interferometry was used to observe the real-time deformation of FCOB assembly specimen type A under either thermal cycling loading or hygrothermal loading. The results are presented in Chapters 4 and 5.

ATTENTION: The Singapore Copyright Act applies to the use of this document. Nanyang Technological University Library

3.3.1 Background

Increasing demands for an understanding of interfacial fracture require high spatial resolution and displacement sensitivity experimental method. Moiré interferometry, providing non-contact in-plane measurements, has been designed to meet this requirement (Han & Guo 1996a, Zhu et al. 1998, Guo & Liu 1998). This method is ideal for FEA verification and hybrid analysis (Han et al. 1996b). The hybrid method, such as FEA-moiré method, can provide great potential for micro-mechanical analysis in electronic packaging area.

As seen in Fig. 3.9, two coherent He-Ne laser beams illuminate the specimen grating from the gradients α and –α, generating interference between each other and creating virtual reference grating in the zone of their intersection. The virtual grating acts as the reference grating, whose frequency is given as:

$$f = \left(\frac{2}{\lambda}\right)\sin\alpha \tag{3.5}$$

where λ is the wavelength of the light source (633 *nm* for He-Ne laser).

Due to the interference, the virtual reference grating and the grating replicated on the specimen interact with each other to generate moiré fringe pattern. This pattern can be observed and recorded by a CCD camera with microscope. The moiré fringe pattern in U displacement field is defined by interaction of the x direction of the specimen grating lines with reference grating. While it is similar for the moiré fringe pattern in V displacement field, which is formed by interaction of the y direction of the specimen grating lines with reference grating (Post et al. 1994).

The displacements then can be determined from the fringe patterns as Eq. (3.6a) and Eq. (3.6b)

ATTENTION: The Singapore Copyright Act applies to the use of this document. Nanyang Technological University Library

$$U = \frac{1}{f} N_x \tag{3.6a}$$

$$V = \frac{1}{f} N_y \tag{3.6b}$$

where f is the frequency of virtual reference grating, and N_x and N_y are fringe orders in the U and V field respectively. In practice, a virtual reference grating with a frequency of 2400 *lines/mm* was used, which provided a basic sensitivity of $2.4\,fringe/\mu m$ displacement. The corresponding contour interval in the moiré fringe patterns was 417 *nm/fringe order*. The normal strain ε_x and ε_y, and the shear strain τ_{xy} are determined by the small-strain relationships, as listed in Eq. (3.7):

$$\varepsilon_x = \frac{\partial U}{\partial x} = \frac{1}{f}\left[\frac{\partial N_x}{\partial x}\right] \tag{3.7a}$$

$$\varepsilon_y = \frac{\partial V}{\partial y} = \frac{1}{f}\left[\frac{\partial N_y}{\partial y}\right] \tag{3.7b}$$

$$\gamma_{xy} = \frac{\partial U}{\partial y} + \frac{\partial V}{\partial x} = \frac{1}{f}\left[\frac{\partial N_x}{\partial y} + \frac{\partial N_y}{\partial x}\right] \tag{3.7c}$$

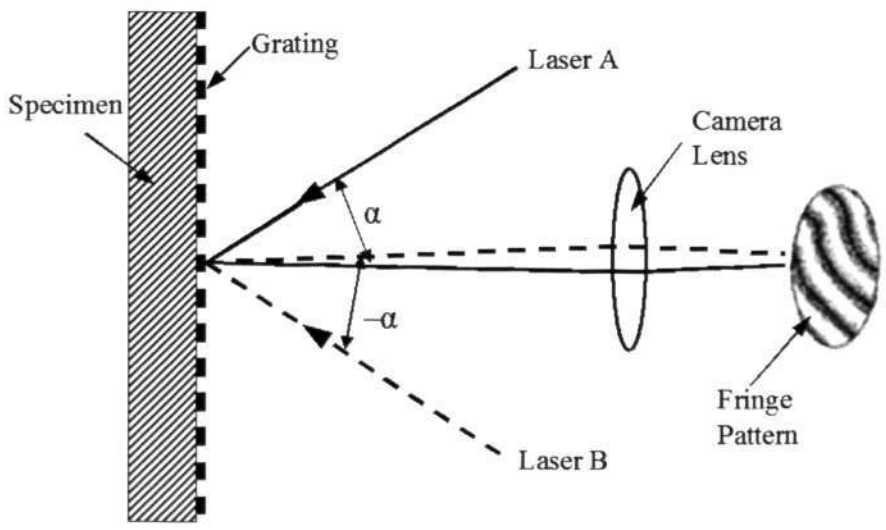

Fig. 3.9 The principle of moiré interferometry

ATTENTION: The Singapore Copyright Act applies to the use of this document. Nanyang Technological University Library

3.3.2 Moiré Interferometer

Moiré interferometry (MI) has been used in microelectronic packaging area to measure thermal deformation, to characterize material properties and to evaluate structure design of electronic components. However, conventional MI technique could not be applied for the determination of the in-situ deformation of microelectronics packages in thermal cycling, humidity environment and under mechanical loading. By combining MI technique with phase shifting, micro–force application, thermoelectric heating/cooling, ultrasonic humidity actuation and microscopic imaging techniques, an integrated multi-functional micro-moiré interferometry (M^3I) system was developed by Singapore Institute of Manufacturing Technology (SIM Tech), as presented in Fig. 3.10.

Overall, the system consists of six main parts: an optical table (11); XYZ motorized translation stage (7); a microscope with high-resolution CCD camera (3); a miniaturized thermal cycling or humidity chamber (8) and a computer (1). The thermal cycling chamber (8) was equipped with resistance heaters and thermoelectric coolers, while the humidity chamber was equipped with resistance heaters and ultrasonic humidity excitation. Temperature/humidity controller was designed to activate the chambers in order to produce the required temperature and humidity level in the chamber. XYZ stage (7) was designed to move the chamber to the desired position, where the microscope could observe the image of the specimen. A CCD camera (3) was connected to a microscope to acquire images of the specimen under any loading conditions. The images were transferred to computer for recordings.

Moiré interferometry is an in-situ non-contact and nondestructive measurement technique with relatively high testing accuracy for displacement field

ATTENTION: The Singapore Copyright Act applies to the use of this document. Nanyang Technological University Library

and interfacial toughness measurement. However, the specific surface preparation, computation time and incapacity of large deformation measurement (e.g. destructive test) limit the application of moiré technique to interfacial fracture toughness measurement, since the replicated grating is susceptible to be destroyed under large deformation condition. Therefore, DIC technique was chosen to measure interfacial fracture toughness for Si/underfill interface.

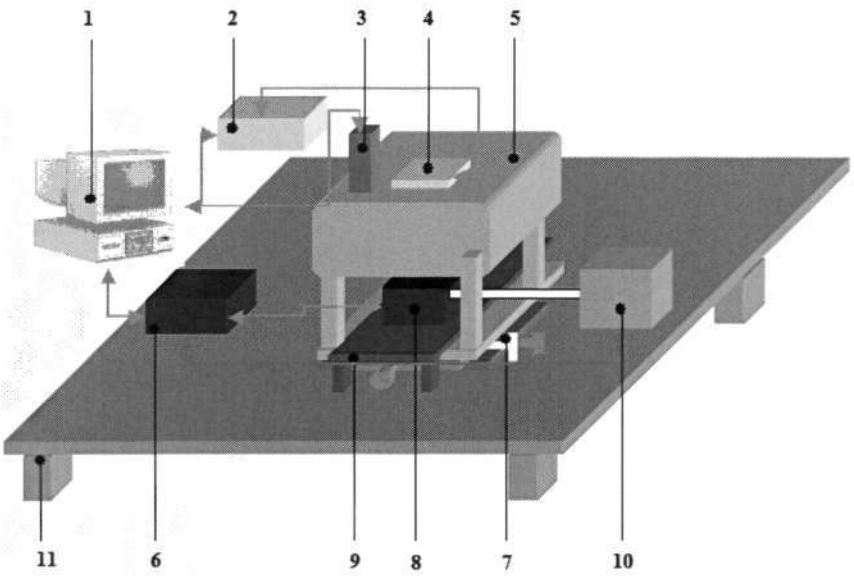

Fig. 3.10 Schematic diagram of M^3I system. 1: computer; 2: driver of phase shifter; 3: microscopic imaging device; 4: phase shifter; 5: moiré interferometer; 6: temperature and humidity level controller; 7: six-axis adjustment; 8: miniature thermal cycling chamber (or humidity chamber); 9: chamber support; 10: ultrasonic humidity excitation; 11: optical table

ATTENTION: The Singapore Copyright Act applies to the use of this document. Nanyang Technological University Library

3.4 Digital Image Correlation (DIC) System

In the past decade, varieties of experimental photomechanics techniques were developed in different laboratories for the management of the deformation and stress and the validation of the theoretical and numerical models, including shadow moiré (SM), projection moiré (PM), moiré interferometry (MI), holographic interferometry (HI), speckle interferometry (SI), electronic speckle pattern interferometry (ESPI), and digital image speckle correlation (DISC). Among these techniques, digital image speckle correlation shows its potential to be a key experimental measurement technique for the development of reliability design methodology, especially in the application of the two-dimensional image-correlation method to thin-sheet mixed-mode I/II fracture studies, local crack-closure measurements (Sutton et al. 2000). It has the following advantages as compared to other experimental photomechanics techniques (Shi et al. 2004):

1) Simple optics based non-contact and nondestructive measurement technique (to MI, HI, and ESPI);
2) Wide range of measurement sensitivity and resolution for macro- and micro-scale deformation measurement (to all);
3) It does not require interferometric laser source or anti-vibration optical table and thus suitable for both laboratory and field applications (to MI, HI, SI, and ESPI);
4) No need for speckle pattern storing, photoelectrical signal conversion, speckle averaging, or signal correlation processing and it can be used to conduct real-time measurement (to SI and ESPI);

ATTENTION: The Singapore Copyright Act applies to the use of this document. Nanyang Technological University Library

5) As a computer-aided-measurement technique, it can be easily automated (to MI, HI, SI, and ESPI).

However, DIC technique has its limitation since the technique is in the development stage and some technical issues, such as tremendous computational time and discrete deformation distribution, etc., have not been well solved in the conventional correlation algorithms. During the study, it was found the polymeric cross-section of FR-4 / underfill was not suitable to create high contrast image. Therefore, specific surface treatment was required. In addition, since the accelerated temperature cycling test and hygrothermal test were carried out in a hermetic miniaturized chamber, the image wobble due to convection of heated air or moisture introduces poor image correlation quality (e.g. change of image contrast and surface contamination) compared with moiré interferometry. However, moiré interferometry is not capable to measure large deformation, such as deformation under destructive test.

Therefore, in this dissertation, moiré interferometry was used to test interfacial toughness under thermal and hygrothermal loading, while DIC technique was used to characterize the interfacial fracture mechanics of FCOB assembly specimen type B either under thermal mechanical loading or after hygrothermal aging. The results are presented in Chapter 6.

3.4.1 Correlation Algorithm

Speckle effect appears when the surface of a specimen is illuminated by a light source (either white light or laser beam). The point on the surface scatter the light with difference light intensity, generating randomly distributed light and shade spots in the front space of the object surface. When a specimen is subjected

ATTENTION: The Singapore Copyright Act applies to the use of this document. Nanyang Technological University Library

to loading, the speckle spots on the specimen surface deforms with the specimen. Accordingly, the speckle effect can be used to measure the displacement of the specimen (Bruck et al. 1989).

Digital image speckle correlation is a technique, which works by tracking the gray value pattern in small local neighbourhoods commonly referred to as subsets (Fig. 3.11), to obtain the displacement and strain components, such as U, V, $\partial U/\partial x$, $\partial V/\partial y$, $\partial U/\partial y$, $\partial V/\partial x$, and searches for the maximum correlation coefficient C (Shi, et al. 2003)

$$C(U,V)=\frac{\sum_{i=1}^{m}\sum_{j=1}^{n}\left[f(x_i,y_j)-\bar{f}\right]\bullet\left[g(x_i',y_j')-\bar{g}\right]}{\sqrt{\sum_{i=1}^{m}\sum_{j=1}^{n}\left[f(x_i,y_j)-\bar{f}\right]^2}\bullet\sqrt{\sum_{i=1}^{m}\sum_{j=1}^{n}\left[g(x_i',y_j')-\bar{g}\right]^2}} \tag{3.8}$$

where U and V are the displacement components in the x and y directions, respectively; $f(x_i,y_j)$ and $g(x_i',y_j')$ are the gray-levels at points (x_i,y_j) and (x_i',y_j') on the sub-images before and after loading, respectively; $\bar{f}$ and $\bar{g}$ are the mean values of gray levels at (x_i,y_i) and (x_i',y_i') on the sub-images before and after loading. A simple presentation of the principles of digital image correlation is shown in Fig. 3.11. The deformation components are then determined from the coordinates of points (x_i,y_j) and (x_i',y_j').

Because of the operational characteristics of video cameras and digitization circuits, the gray-level obtained is discrete in nature. It means that no gray-level information is available between pixels. In order to reach higher accuracy, the bicubic spline interpolation method was employed in this study to smooth the surface of the gray-level distribution and further to determine the values of gray-level at any position in the images:

ATTENTION: The Singapore Copyright Act applies to the use of this document. Nanyang Technological University Library

$$G(x^*, y^*) = \sum_{i=0}^{3} \sum_{j=0}^{3} \alpha_{ij} (x^*)^i (y^*)^j \tag{3.9}$$

where α_{ij} is the gray-level at point (x_i, y_j), and x^* and y^* are the distances along x-axis and y-axis from the point (x_i, y_j). The benchmark was done in the previous work (Shi et al. 2003). An axial displacement with linear increment and a quadratic displacement distribution was applied onto the same speckle pattern the algorithm with finite element (FE) smoothing can predict the displacements accurately and therefore obtained an accurate strain distribution. The experimental results showed that the algorithm with FE smoothing is able to achieve an accuracy of 0.02 pixels (Shi et al. 2004).

In this dissertation, the two-dimensional image correlation method was applied to planar specimens that experience small out-of-plane displacements during loading. The CCD camera is placed perpendicular to the specimen surface and calibration only requires the determination of a scale factor.

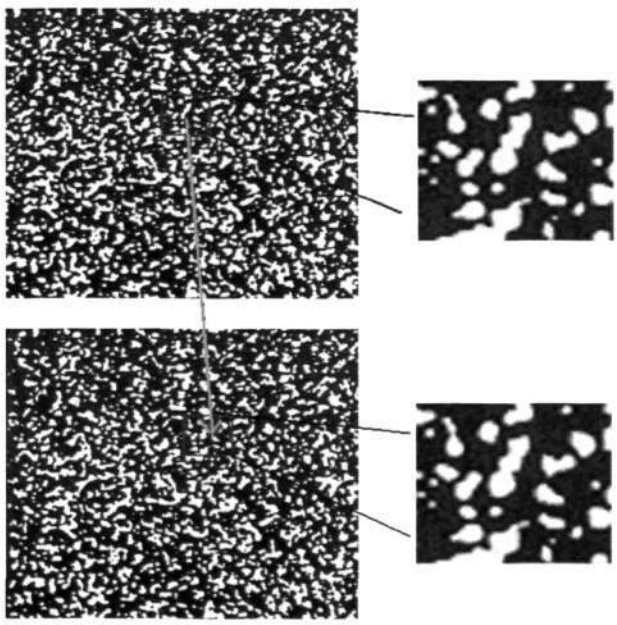

Fig. 3.11 Principle of digital image correlation

ATTENTION: The Singapore Copyright Act applies to the use of this document. Nanyang Technological University Library

3.4.2 Micro-Digital Image Speckle Correlation (μ-DiSC) System

A non-contact and non-destructive measurement system, called micro-digital image speckle correlation (μ-DiSC) system, was designed and constructed for measurement of interfacial fracture toughness under thermal mechanical loading. The overall arrangement of the experiment setup is shown in Fig. 3.12.

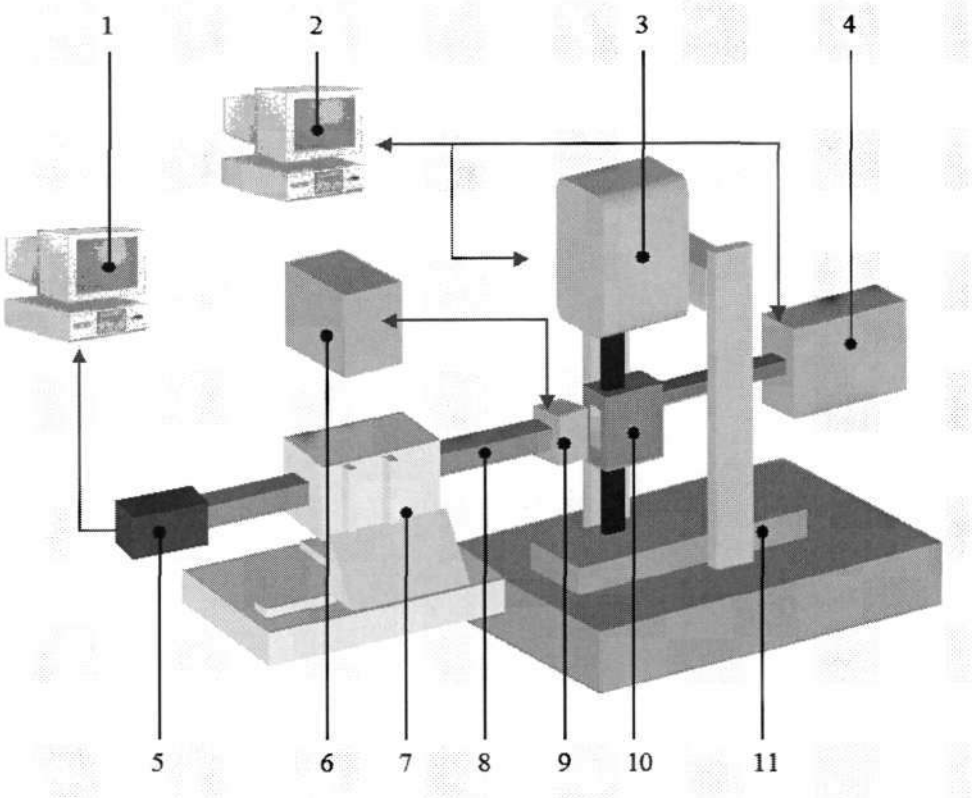

(a) 1: computer; 2: computer; 3: INSTRON micro tensile tester; 4: heater; 5: CCD camera; 6: light source; 7: six-axis adjustment; 8: microscope; 9: illuminator; 10: attemperator; 11. pedestal

ATTENTION: The Singapore Copyright Act applies to the use of this document. Nanyang Technological University Library

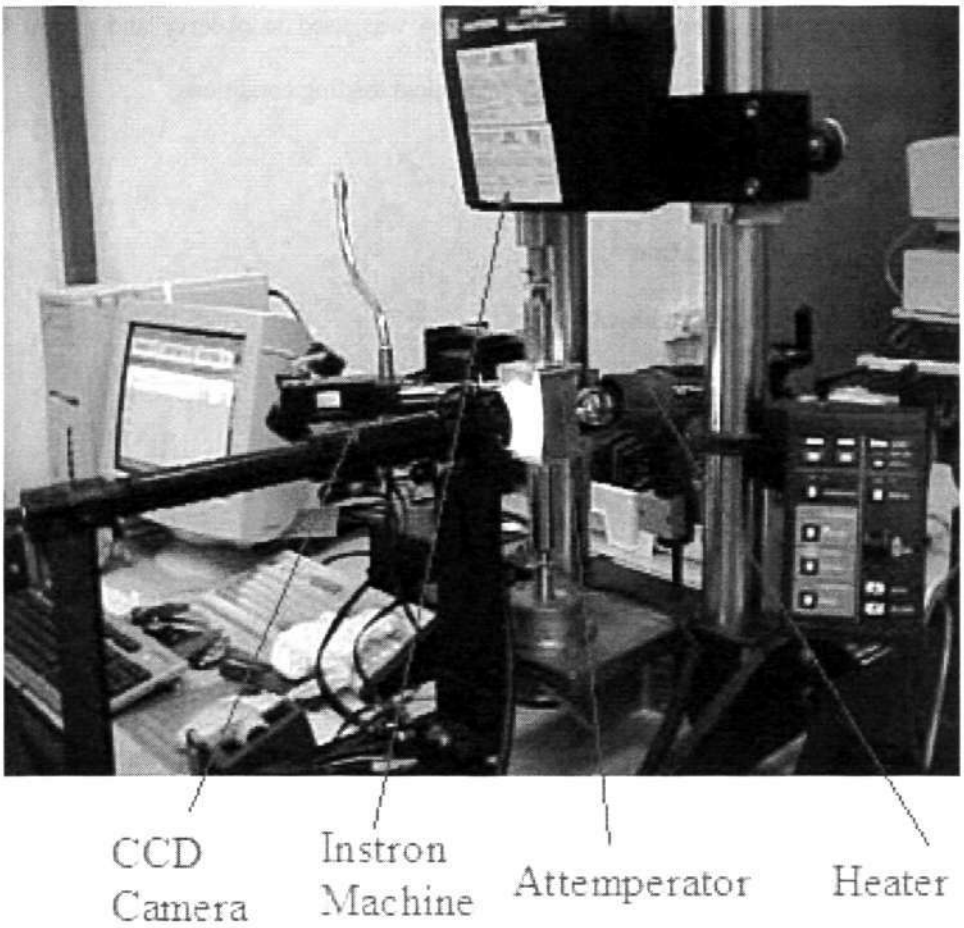

(b)

Fig. 3.12 Integrated digital image speckle correlation system for fracture toughness measurement. (a) schematic diagram of μ-DiSC system; (b) photograph of μ-DiSC system

An Instron® micro tester was employed to apply the mechanical force for the characterization of interfacial fracture toughness. A heater and an attemperator were mounted on the Instron® machine to achieve the desired temperature of the tested specimen. A ring white light source was mounted to the microscope to illuminate the sample and acquire good contrast of speckle patterns. A computer

ATTENTION: The Singapore Copyright Act applies to the use of this document. Nanyang Technological University Library

connected to high-resolution CCD camera was used to observe and record the images of the sample under thermomechanical loading conditions.

3.5 Testing Program

3.5.1 Thermal Mechanical Study

3.5.1.1 Thermal Static Test

The specimen type A without pre-crack was first examined to understand the most dangerous point in the flip chip assembly subjected to temperature loading. The temperature was determined to be 100 °C. The specimen type A was heated in a miniaturized thermal chamber. The deformation under the temperature loading was measured and recorder using M^3I system. As a result, the potential failure site in the specimen was judged according to the moiré fringe pattern and the strains calculated based on Eq. (3.6) and Eq. (3.7). The determined site was consequently studied to understand the fracture response in an accelerated thermal test with a crack artificially prepared.

3.5.1.2 Accelerated Thermal Test (ATC)

The specimen type A with pre-crack was put into a miniaturized thermal cycling chamber with temperature controller. The deformations throughout the whole thermal cycle were measured and recorded using M^3I system. The requirement of in-situ measurement was, therefore, achieved to investigate the deformation behavior of delaminated flip chip assembly under a single temperature cycling. The temperature range of ATC loading was determined to be –40 °C to

ATTENTION: The Singapore Copyright Act applies to the use of this document. Nanyang Technological University Library

125 °C. Additionally, the dwell time (for thermal aging), which was kept at both temperature extremes, was set to 12 minutes. The cycle was circulated within 65 minutes in order to follow the same paces in real ATC test. The fringe patterns were recorded at the specific temperature steps, e.g., –40 °C, –25 °C, 0 °C, 25 °C, 50 °C, 75 °C, 100 °C and 125 °C. The schematic diagram for the thermal cycling testing is illustrated in Fig. 3.13. The platform plotted in the figure showed time for recording fringe pattern images. The moiré fringe patterns were consequently recorded according to the ATC test profiles, from which the deformations of assembly as well as CTODs around the crack tip could be read. The interfacial toughness and mode mixity using interface fracture mechanics were obtained accordingly. The results are shown in Chapter 4.

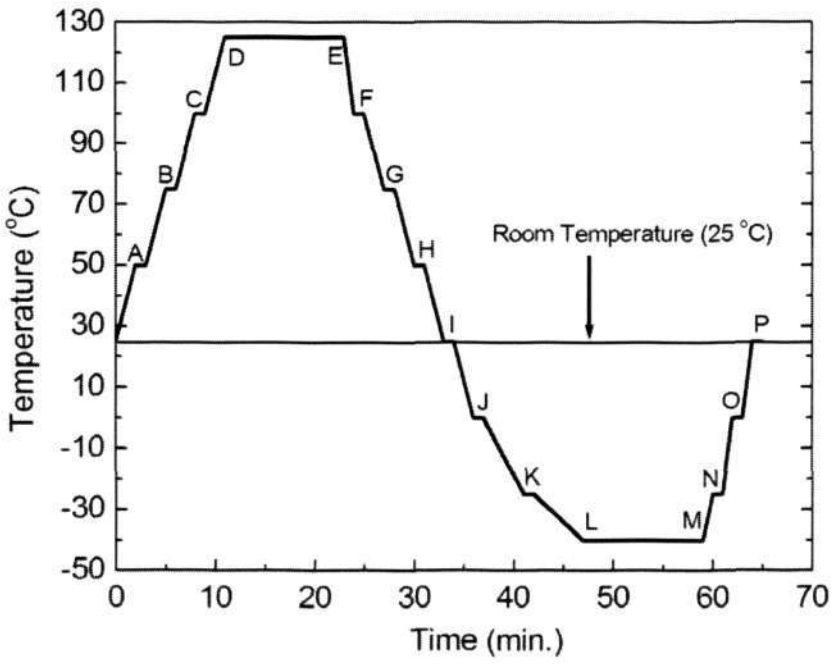

Fig. 3.13 Schematic illustration of temperature profile used in experiment

ATTENTION: The Singapore Copyright Act applies to the use of this document. Nanyang Technological University Library

3.5.1.3 Interfacial Fracture Toughness Measurement Using μ-DiSC

The specimen type B with the μ-DiSC system was used to determine the interfacial fracture toughness of the interface between Si/underfill under thermal loading. The characterization of interfacial fracture toughness between Si/underfill was conducted on Instron® micro-tensile machine with a mini-aluminium attemperator surrounded. The purpose of this attemperator is to minimize the effect of convection when the heat blower continued heating the SBN fixture. The tests were carried out with a constant loading rate 0.006mm/min. The testing program is given in Table 3.3. A high resolution CCD camera with 640×480 pixels was used to capture speckle patterns at different load levels for each testing temperature. After the digital speckle images were obtained, the correlation software was employed to determine the displacement fields around the crack-tip. Finally, the SIFs were calculated with interfacial fracture mechanics. The results are shown in Chapter 6.

Table 3.3 Schedule for measurement of interfacial fracture toughness (sample size is 3 specimen per loading angle)

Temperature (°C)	Loading angle (°)
25	90, 75, 60, 45, 30, 20
75	90, 75, 60, 45, 30, 20
125	90, 75, 60, 45, 30, 20

ATTENTION: The Singapore Copyright Act applies to the use of this document. Nanyang Technological University Library

3.5.2 Hygrothermal Aging Effect

3.5.2.1 Hygrothermal and Thermal Aging

With M^3I system, the specimen type A was put into the miniaturized moisture chamber with the hygrothermal loading conditioned at 85°C/85%RH for 168 hours. This condition was chosen according to JEDEC (Joint Electron Device Engineering Council) standard, moisture sensitive level 1, which represents unlimited lifetime with the hygrothermal condition $\leq 30^{o}C/85\%RH$. The moiré fringe patterns were captured at the times of 0, 1, 3, 7, 11, 24, 48, 96 and 168 hour.

Since hygrothermal aging test lasted around one week, which is a long-time duration, the thermal aging study was simultaneously implemented to study the time effect on delaminated FCOB assembly. The thermal aging test was carried out on the same specimen type A and the moiré fringe patterns were acquired at the same time intervals. The aging temperature was 85 °C. The moisture level under the thermal aging test was determined to be 18%, which was expected to cause negligible moisture absorption in the assembly. The results of this test are shown in Chapter 5.

3.5.2.2 Determination of Interfacial Fracture Toughness After Hygrothermal Aging

The specimen type B was aged under the 85 °C/85%RH in hygrothermal chamber for 168 hours beforehand. The samples were taken out thereafter, and the fracture tests were conducted with INSTRON® micro-tensile machine attached to μ-DiSC system at the room temperature. A high resolution CCD camera was used

ATTENTION: The Singapore Copyright Act applies to the use of this document. Nanyang Technological University Library

to capture speckle patterns at different load levels. With the load-time curve, the speckle pattern at the load level where the interface crack propagated could be obtained. This pattern and the initial speckle pattern were used as the un-deformed and deformed images. With the correlation software, the displacement fields around the crack-tip could be determined. Since the data were determined for the critical load, they were defined as the interface fracture toughness with respect to different loading angles, i.e. 90°, 75°, 60°, 45°, 30°, 20°, after the hygrothermal aging. For each loading angle, three samples were measured. The measured results are shown in Chapter 6.

ATTENTION: The Singapore Copyright Act applies to the use of this document. Nanyang Technological University Library

Chapter 4 Interface Behavior of Chip/Underfill under ATC Loading

4.1 Introduction

Due to the complex nature of flip chip assembly and complicated environmental loading, considerable limitations and difficulties exist in studying the interface delamination problem in flip chip packages using traditional strength theory. The most common method used in industry is accelerated temperature cycling (ATC) test, which not only takes long time and considerable resources, but also gives little insight into the failure mechanisms and thus less help in the package design.

Accordingly, research emphasis has been shifted strongly to damage and fracture mechanics, which offers a fundamental approach to the delamination problems. Briefly, two categories of research work have been carried out. On the one hand, different numerical and experimental methodologies have been developed to characterize the fracture toughness of polymer/inorganic interface (Yan & Agarwal 1998, Pang et al. 2002). The parameter of fracture toughness is employed as a criterion for the interface design. On the other hand, numerical simulations (Madenci et al. 1998, Rzepka et al. 1998) and in-situ measurement (Han & Guo 1995, Guo & Liu 1998, Wang et al. 1998, Zhang et al. 2004) have been performed to investigate the reliability of flip chip assembly subject to different mechanical and environmental loadings. However, less experimental investigation has been conducted on the delamination reliability of

ATTENTION: The Singapore Copyright Act applies to the use of this document. Nanyang Technological University Library

polymer/inorganic interface, especially under real ATC loading due to a lack of in-situ/real-time optical measurement system.

In this chapter, a kind of interfacial fracture mechanics parameter called crack tip opening displacement (CTOD) is being reviewed. The validity of this CTOD method is carefully examined. This method is also used later in Chapters 5 and 6.

Subsequently, an integrated multi-functional micro-moiré interferometry (M^3I) system was developed to measure the deformation of flip chip assembly under the ATC loading. Firstly, in order to verify the possibility of delamination on the underfill and its adherends, the sandwich specimen without pre-crack was tested under thermal cycling. The moiré fringe pattern and calculation results indicated that the failure site of flip chip assembly was the interface between the underfill and silicon chip. Afterwards, specimen type A (see Chapter 3 for details of the specimen) was used to measure the delaminated flip chip assembly under cyclic temperature loading. Interfacial fracture mechanics was employed to analyze the crack-tip displacement field and subsequently study the interfacial behavior of the delaminated chip/underfill interface.

Furthermore, in order to examine the findings of the M^3I system, an interfacial fracture mechanics based FEA model was developed to determine the effective interfacial toughness of the assembly under the same temperature loading profile used in the moiré interferometry. The simulation results were found to be in good agreement with the experimental results. Both results showed that interfacial toughness is not only relative to CTE mismatch but also a function of stiffness mismatch between chip/underfill.

ATTENTION: The Singapore Copyright Act applies to the use of this document. Nanyang Technological University Library

4.2 Interfacial Fracture Mechanics

Interfacial fracture mechanics (IFM) is applied to characterize the elastic fracture or small-scale yield interfacial fracture between dissimilar materials. Due to dissimilar deformation of a bimaterial system, crack tip at interface experiences both normal and shear stresses. For the interface crack shown in the Fig. 4.1, Dundurs elastic mismatch parameters α and β are functions of the elastic properties of the component materials defined as (Dundurs 1969)

$$\alpha = \frac{\mu_1(\kappa_2+1)-\mu_2(\kappa_1+1)}{\mu_1(\kappa_2+1)+\mu_2(\kappa_1+1)} \tag{4.1a}$$

$$\beta = \frac{\mu_1(\kappa_2-1)-\mu_2(\kappa_1-1)}{\mu_1(\kappa_2+1)+\mu_2(\kappa_1+1)} \tag{4.1b}$$

where μ_i is the shear modulus; subscripts 1 and 2 donate specified materials 1 and 2 respectively, which represented silicon chip and underfill material respectively in this article; and κ is given by

$$\kappa_i = (3-4\nu_i)/(1+\nu_i) \qquad \text{for plane stress} \tag{4.2a}$$

$$\kappa_i = 3-4\nu_i \qquad \text{for plane strain} \tag{4.2b}$$

where ν_i is the Poisson's ratio of the materials. Nondimensional constant ε is related to the Dundurs parameters α and β, through

$$\varepsilon = \frac{1}{2\pi} In\left(\frac{1-\beta}{1+\beta}\right) \tag{4.3}$$

ATTENTION: The Singapore Copyright Act applies to the use of this document. Nanyang Technological University Library

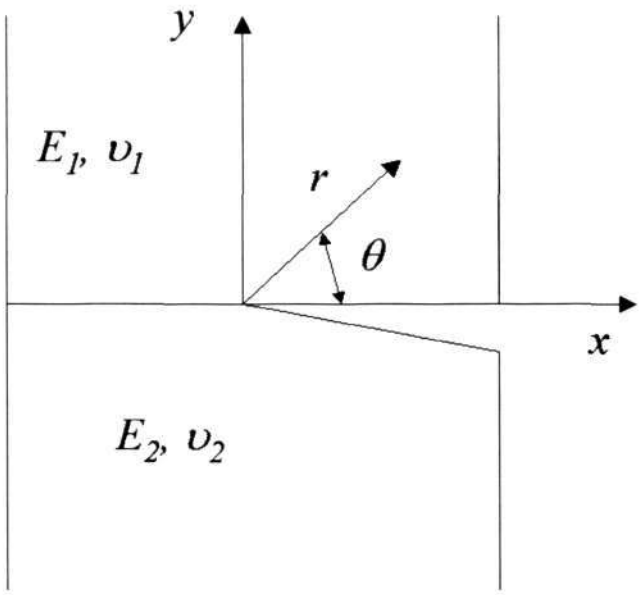

Fig. 4.1 Interface crack problem

In these equations, α is a measurement of the stiffness dissimilarity between the two kinds of materials. In this thesis, silicon wafer was selected as material 1 and underfill was chosen as material 2. Since Si (E=132 GPa) is stiffer than underfill (E=3.75 GPa), α is great than 0 according to Eq. (4.1a). ε and β are the parameters representing the oscillating nature of stress and strain field near the crack tip as r approaches the tip through Eq. (4.5) (Williams 1959, Rice 1988).

The relative crack displacement $\delta = \delta_y + i\delta_x$ at a distance of r behind the crack tip (or equivalently in polar coordinates written as $\delta \left| e^{i\phi} \right.$, as shown in Fig. 4.2, is (Rice 1988)

$$\delta = \delta_y + i\delta_x = \frac{8}{(1+2i\varepsilon)\cosh(\pi\varepsilon)} \sqrt{\frac{r}{2\pi}} \frac{K'}{E^*} \left(\frac{r}{L}\right)^{i\varepsilon} \tag{4.4}$$

with $i^2 = -1$ and

ATTENTION: The Singapore Copyright Act applies to the use of this document. Nanyang Technological University Library

$$r^{i\varepsilon} \equiv e^{i\varepsilon Inr} \equiv \cos(\varepsilon Inr) + i\sin(\varepsilon Inr) \tag{4.5}$$

where δ_x and δ_y are the crack-tip opening displacements (CTODs) in the X and Y direction, respectively; E^* is the effective Young's modulus given by

$$\frac{2}{E^*} = \frac{1}{\overline{E_1}} + \frac{1}{\overline{E_2}} \tag{4.6}$$

with $\overline{E_i} = E_i/(1-\nu_i)$ for the plane strain and $\overline{E_i} = E_i$ for plane stress. In this thesis, $\overline{E_i} = E_i/(1-\nu_i)$ is represented as a function of temperature, i.e. $\overline{E_i}(T) = E_i(T)/(1-\nu_i)$. K' is the nominal complex interfacial stress intensity factor (SIF) from a distance r away from the crack tip, which is defined as

$$K' = K_1' + iK_2' \tag{4.7}$$

where K_1' and K_2' are the nominal mode I and mode II SIFs respectively. Since the interfacial toughness (K or G) is defined only at the crack-tip, it is independent of the coordinate (r, θ), the "interfacial toughness" determined at the distance emanating from the crack-tip is not the interfacial toughness. The nominal K_1' and K_2' are the supplementary parameters that are used to determine the interfacial toughness at the crack-tip by using extrapolation method (Owen & Fawkes 1983).

It can be seen that the CTOD method is established by considering K_1' and K_2' to be characteristic parameters in different specimens with the same bimaterial interface. However, when $\beta \neq 0$, the decoupling of normal and shear stress at the interface and the dominant singularity of the displacements behind the crack tip require some modification. Due to unusual singularity, K_1' and K_2' in interfacial fracture problem cannot determine the fracture mode in the same sense as in the fracture mechanics for homogenous material. This feature together with the

ATTENTION: The Singapore Copyright Act applies to the use of this document. Nanyang Technological University Library

possibility of interpenetration of crack flanks causes conceptual difficulties in the application of interfacial fracture mechanics. So a remedy with the introduction of a fixed length L (Rice 1988) was used to combine $KL^{i\varepsilon}$ as the basic parameter, which has the dimension of conventional SIF.

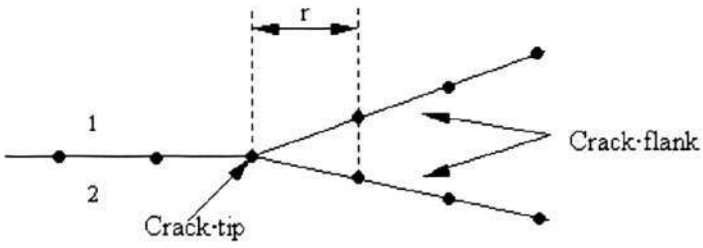

(a) Before loading

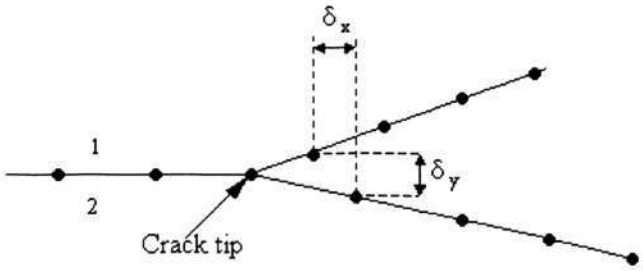

(b) After loading

Fig. 4.2 Schematic diagram for the crack tip opening displacement (CTOD

The selection of L is somewhat arbitrary, since the ratio of the shear traction to normal traction varies very slowly with the distance r to the tip when $\beta \neq 0$ (Hutchinson and Suo 1992). In this study, $L=2.7\ mm$ was chosen to base on the in-plane length of the specimen geometry, which is useful for discussing the mixed mode character of a bimaterial crack solution, independent of individual material fracture behavior (Hutchinson and Suo 1992).

ATTENTION: The Singapore Copyright Act applies to the use of this document. Nanyang Technological University Library

By solving Eq. (4.4), the individual nominal SIF is obtained

$$\begin{cases} K_1^{'} = \{A\cos[\varepsilon In(r/L)] + B\sin[\varepsilon In(r/L)]\}/D \\ K_2^{'} = \{B\cos[\varepsilon In(r/L)] - A\sin[\varepsilon In(r/L)]\}/D \end{cases} \tag{4.8}$$

where

$$\begin{cases} A = \delta_y - 2\varepsilon\delta_x \\ B = \delta_x + 2\varepsilon\delta_y \\ D = \dfrac{8}{E^* \cosh(\pi\varepsilon)}\sqrt{\dfrac{r}{2\pi}} \end{cases} \tag{4.9}$$

It can be observed that the exact solutions of $K_1^{'}$ and $K_2^{'}$ at the crack tip are supposed to be acquired through extrapolation method according to nominal SIFs as a function of distance r away from crack tip (Owen and Fawkes 1983). From Eq. (4.8) and Eq. (4.9), it can be observed that the displacement fields near the crack tip are proportional to $r^{-1/2}$. The details are to be discussed later regarding different results.

After the extrapolation, the interfacial toughness at the crack tip is readily determined. The effective stress intensity factor K_{eff}, is related to the mode I and mode II stress intensity factors by (Williams 1959)

$$K_{eff} = \sqrt{K_1^2 + K_2^2} \tag{4.10}$$

where K_1 and K_2 are the SIFs at the crack tip. The phase angle is accordingly defined as

$$\psi = \tan^{-1}\left(\frac{\mathrm{Im}(KL^{i\varepsilon})}{\mathrm{Re}(KL^{i\varepsilon})}\right)_{\beta\neq 0} \tag{4.11}$$

Based on interfacial fracture mechanics, it is explicit that the interfacial toughness as well as phase angle can be determined as long as one could obtain the

ATTENTION: The Singapore Copyright Act applies to the use of this document. Nanyang Technological University Library

CTODs δ_x and δ_y behind the crack with respect to a distance r away from crack tip.

4.3 Validity of Interfacial Fracture Mechanics

The interfacial fracture mechanics are based on the assumption of small deformation and small plastic zone around crack tip. At some conditions, e.g. at some temperatures (75, 100, 125 °C) around T_g of the underfill, it might introduce the invalidity of application of interfacial fracture mechanics. This is due to large viscoelasticity of the underfill material.

In order to examine the assumption made for interfacial fracture mechanics, i.e. there is no plastic deformation and ductile crack propagation occurring at the crack tip, scanning electron microscope (SEM) was employed to observe the surface morphology around the crack-tip for monotonic underfill material, as shown in Fig. 4.3. The details were previously reported (Shi, Wang and Pickering 2003). It is noted from SEM picture that the plastic zone is very small and satisfying the small-scale yield criterion, i.e.

$$r_p \square\ a/10 \tag{4.12}$$

where r_p is the radius of the plastic zone and a is the length of the crack.

In addition, referring to Shi, Wang and Pickering (2003), it is noticed that the interfacial toughness of underfill under high temperature is far lower than the fracture toughness of underfill film material. It is therefore reasonable to assume that the interfacial fracture mechanics is applicable for high temperatures.

ATTENTION: The Singapore Copyright Act applies to the use of this document. Nanyang Technological University Library

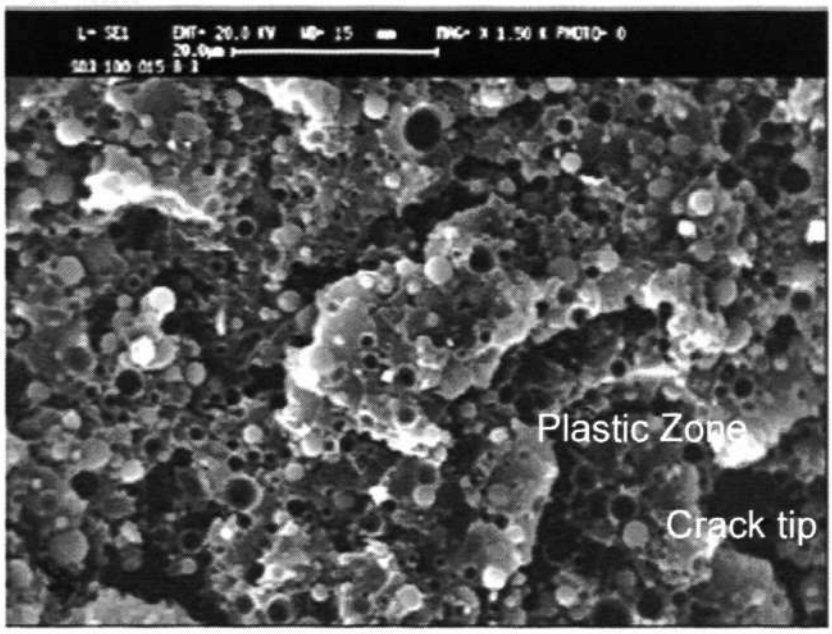

Fig. 4.3 Typical micrographs to show the deformation characteristic of the filed epoxy film obtained by SEM at the crack-tip for the specimen tested at 100 °C (Shi, Wang & Pickering 2003)

4.4 Numerical Simulation

In this study, the specimen type A was used. The experimental details on the specimen preparation and the test programs were illustrated in Chapter 3, sections 3.2.1, 3.5.1.1 and 3.5.1.2, respectively.

For the purpose of verification, in the study of the effect of thermal cyclic loading on the delaminated flip chip assembly, additional FEA modelling was applied to examine the findings of the M^3I system. The FEA model was established to determine the deformation of the assembly with the same materials, dimensions and temperature loading profile tested on specimen type A in the moiré experiment. Therefore, this section presented the details about finite element analysis for the delaminated assembly under thermal cyclic loading.

ATTENTION: The Singapore Copyright Act applies to the use of this document. Nanyang Technological University Library

Some assumptions are made in the simulation:

1) Underfill is modeled as viscoelastic material, which is time and temperature dependent.
2) The adhesion is perfect without micro defects and damage between underfill and its adjacent materials except for pre-crack region.
3) The reliability evaluation is solely based on potential crack propagation rather than both crack initiation and propagation.

4.4.1 Material Properties

The materials properties of silicon chip, FR-4 and underfill were presented in Chapter 3, section 3.1. In order to achieve accurate solutions in the simulation, the materials properties were simulated as real as possible. The silicon chip and FR-4 were modelled as temperature-dependent, while underfill was described to be viscoelastic material. The data were listed in Table 3.1 and Table 3.2.

4.4.2 Finite Element Modeling

Commercial FE software, ANSYS version 6.1, was employed and a 3D finite element model was built to simulate the package under the ATC test. Although conventional 2D model was being widely used in mechanical simulation, it is believed that 3D model is capable of simulating the assembly deformation more accurately since it takes out-of-plane deformation into consideration. The assembly was modelled with the same dimensions depicted in Fig. 3.2 (b). 3D Visco89 elements were used to simulate the assembly with imperfect underfill, as shown in Fig. 4.4(a). A zoomed-in area around the crack tip is shown in Fig. 4.4(b).

ATTENTION: The Singapore Copyright Act applies to the use of this document. Nanyang Technological University Library

FR-4 and silicon chip were modelled as 3D 20-node hexahedron solid95 elements with temperature-dependent properties. Totally, the 3D model had 22335 elements and 96800 nodes.

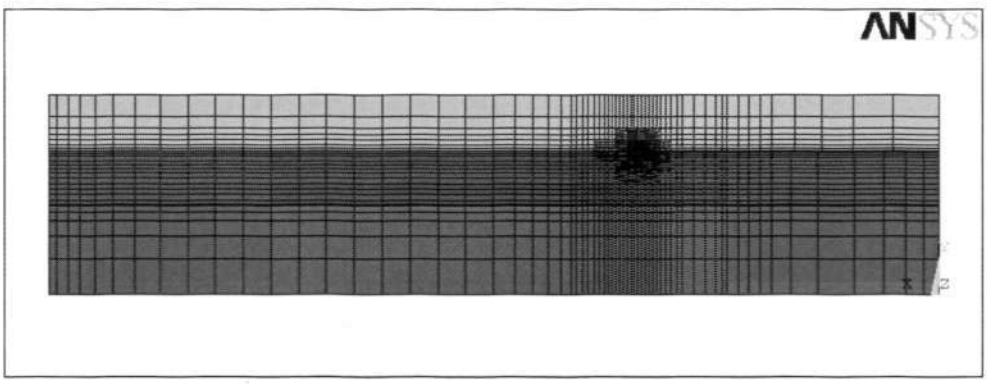

(a) 3D mesh of sandwich specimen

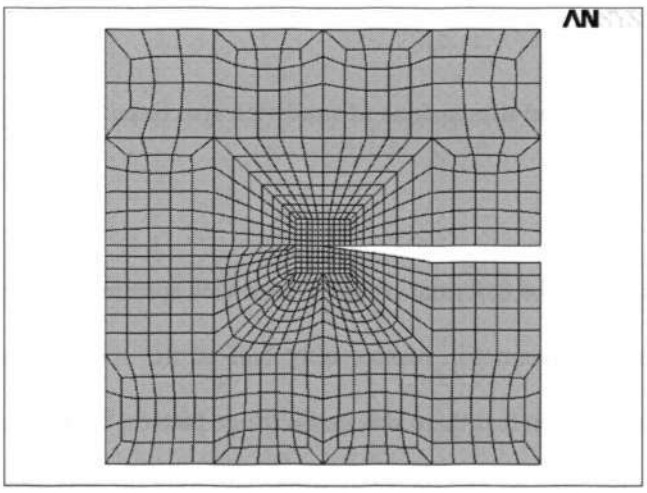

(b) Mesh zoomed-in at crack front

Fig. 4.4 Finite element model

ATTENTION: The Singapore Copyright Act applies to the use of this document. Nanyang Technological University Library

4.5 Thermal Cycling Test on Specimen without Pre-Crack

The specimens were prepared by the following flip chip packaging procedures illustrated in section 3.2.1. The difference between specimen type A was that there was no tape between Si chip and underfill. Therefore, there was no pre-crack after the curing of underfill material. The geometry and dimension of the specimen are given in Fig. 4.5.

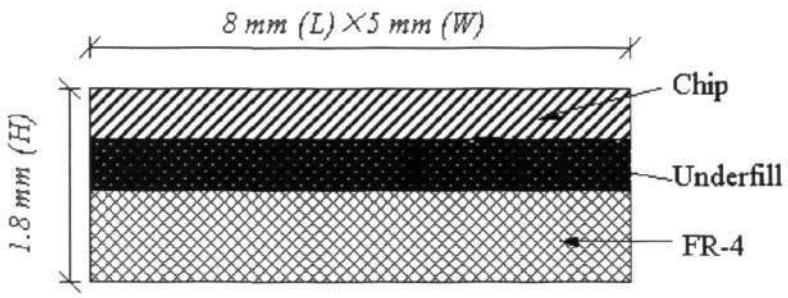

Fig. 4.5 Geometry and dimensions of sandwich specimen without pre-crack

Fig. 4.6 shows the deformation of the sandwich specimen under the thermal cycling. Due to the symmetric reason, only half of the specimen was plotted. Obviously, it can be seen that there was dense fringe pattern, i.e. large deformation, in the interface between Si and underfill, especially near the free edge. Based on Eq. (3.6) and Eq. (3.7), the corresponding shear strain (γ_{xy}) and normal strain (ε_y) along Si-underfill and FR-4-underfill interfaces are shown in Fig. 4.7 (a) and (b). The temperature was 100 °C. It can be seen that ε_y increased gradually toward the free edge of the specimen. However, γ_{xy} increased significantly along the

ATTENTION: The Singapore Copyright Act applies to the use of this document. Nanyang Technological University Library

interface, the maximum value occurred close to the free edge of the specimen. The areas, where fringe patterns were dense, were prone to nucleate interfacial cracks. The nucleate cracks are possible to grow and subsequently result in interfacial delamination. Simultaneously, the results proved that the potential failure site would be mostly located along underfill adjacent interfaces. From Fig. 4.7, it is note that the strain along Si-underfill had greater value than that along FR-4-underfill because of larger CTE mismatch between Si (about 2.8 *ppm/°C*) and underfill (about 30 *ppm/°C*). It was also noted that the shear strain in the Si/underfill interface was larger than that in the FR-4/underfill interface. Therefore, for the shear dominant deformation, the Si/underfill interface had greater possibility of delamination during thermal cycling. Based on this observation, the following study was concentrated on the interface between Si and underfill.

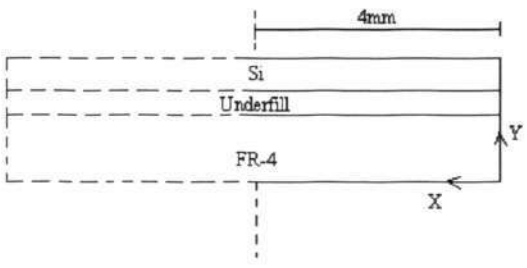

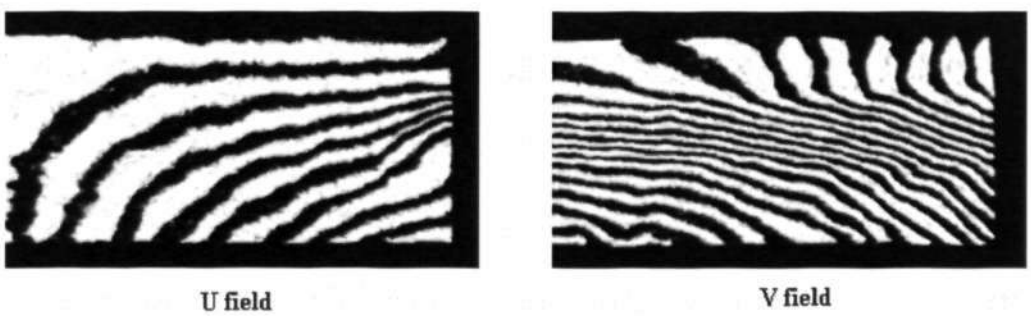

U field **V field**

(a) Heated up to 100 °C

ATTENTION: The Singapore Copyright Act applies to the use of this document. Nanyang Technological University Library

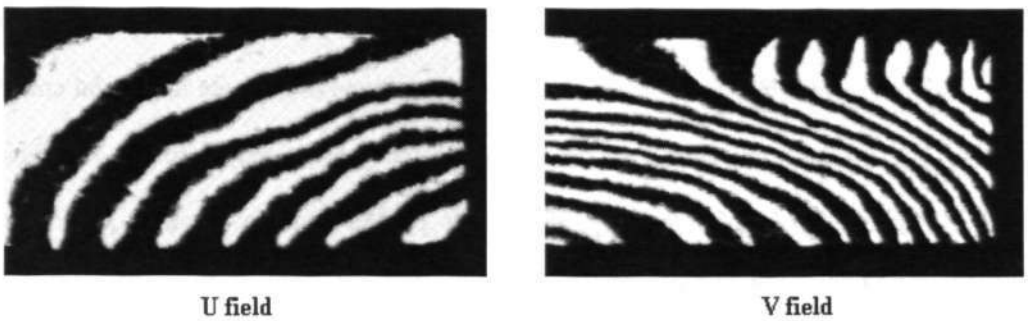

U field V field

(b) Cooled down to 75 °C

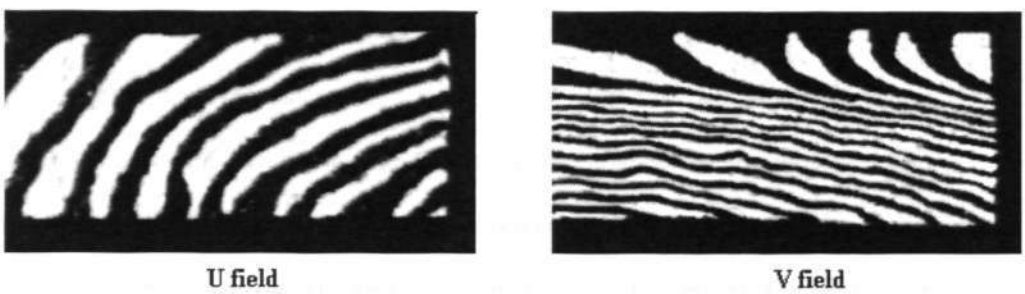

U field V field

(c) Cooled down to –25 °C

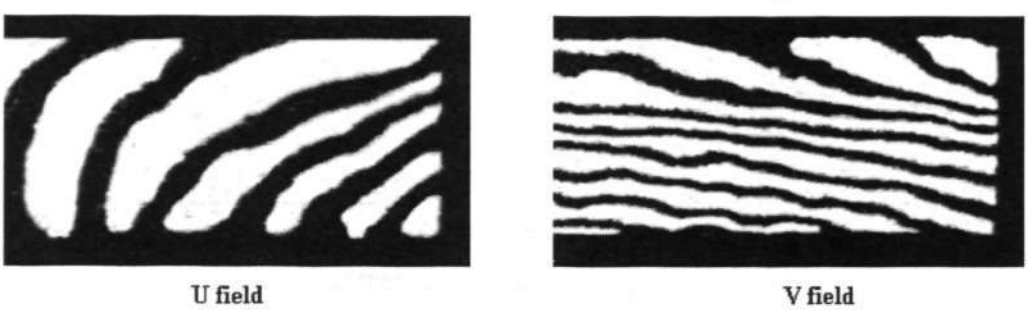

U field V field

(d) Heated up to 0 °C

Fig. 4.6 Representative U and V field fringe patterns during thermal cycling

ATTENTION: The Singapore Copyright Act applies to the use of this document. Nanyang Technological University Library

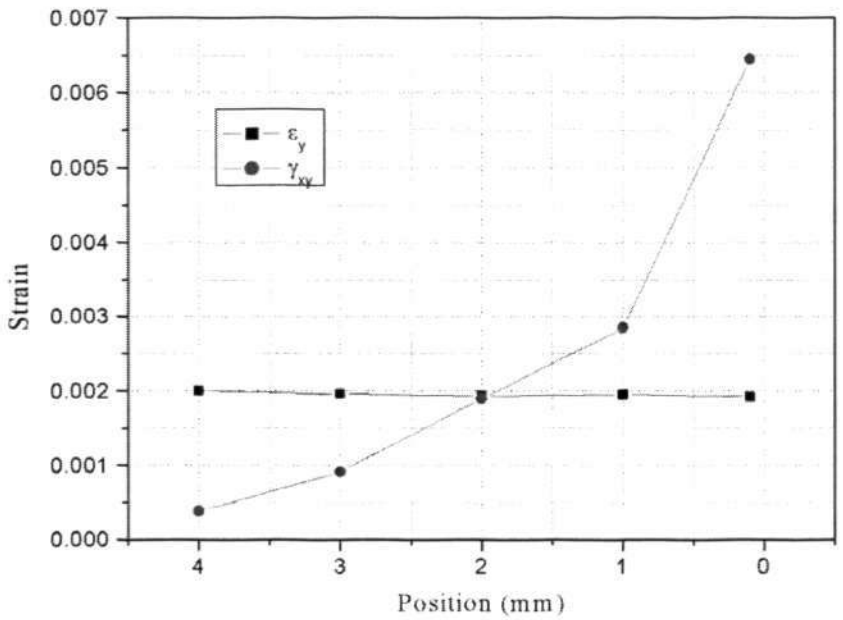

(a) Strains along Si/underfill interface at the temperature 100 °C

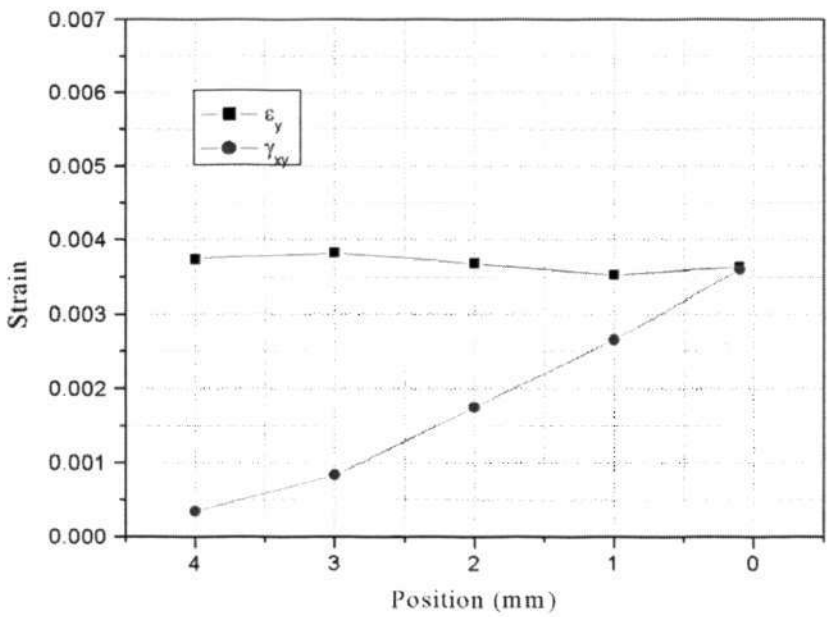

(b) Strains along FR-4/underfill interface at the temperature 100 °C

Fig. 4.7 Calculated strains along underfill adjacent interfaces

ATTENTION: The Singapore Copyright Act applies to the use of this document. Nanyang Technological University Library

4.6 Thermal Cycling Test on Specimen Type A

Fig. 4.8 and Fig. 4.9 show typical U field and V field moiré fringe patterns around the crack-tip obtained from the different temperatures. From the fringe patterns, the thermal deformations at the different temperatures were calculated according to Eq. (3.6), as shown in Fig. 4.10 a). The schematic deformation throughout the whole temperature cycling is shown in Fig. 4.10 b). Because of low CTE and high Young's modulus, silicon chip deformed the least compared to the other two materials. It can be observed that, during heating process, the adherent FR-4/underfill structure behind the crack tip bended down. The slight loss of warpage was observed during the dwelling at extremely high 125 °C. It is because of the rubbery or leathery nature of underfill when the temperature was above T_g of the underfill. The coupling between silicon and FR-4 through underfill material tended to diminish and the assembly is in the stress-release state. However, since the underfill experienced large inelastic deformation at this state due to large CTE (110 *ppm*/°C), the large strain would also consequently affect the interfacial reliability.

When the assembly was cooled down to room temperature, the structure lost warpage. However, the residual warpage remained in the assembly due to viscoelasticity nature of underfill at high temperature, especially at the temperature loading (e.g. 125 °C) higher than T_g of the underfill. When the assembly was cooled down to minus temperature, due to the CTE mismatch as well as the stiffness mismatch between underfill and FR-4, the warpage of the structure became significant again for the part of coupled underfill and FR-4 component and

ATTENTION: The Singapore Copyright Act applies to the use of this document. Nanyang Technological University Library

the magnitude of warpage increased continuously throughout the entire cooling process.

(a) Heated up to 50 °C

(b) Heated up to 75 °C

(c) Heated up to 100 °C

(d) Heated up to 125 °C

ATTENTION: The Singapore Copyright Act applies to the use of this document. Nanyang Technological University Library

(e) Held at 125 °C after 12 mins

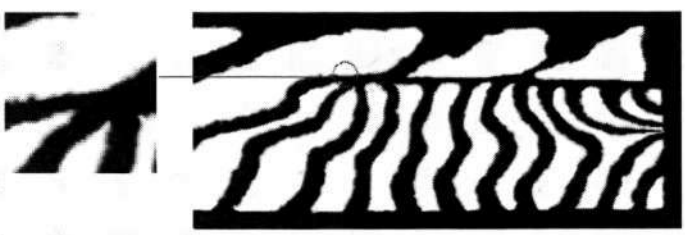

(f) Cooled down to 100 °C

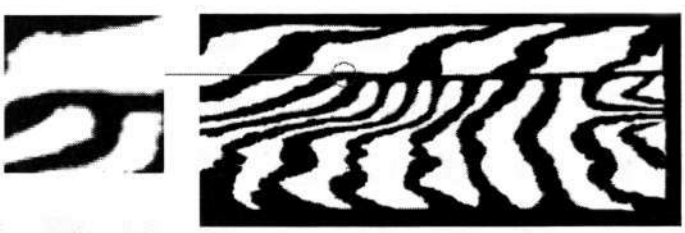

(g) Cooled down to 75 °C

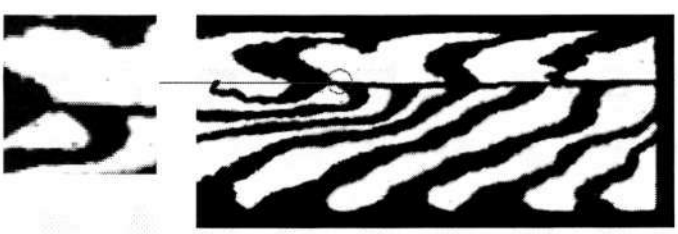

(h) Cooled down to 50 °C

ATTENTION: The Singapore Copyright Act applies to the use of this document. Nanyang Technological University Library

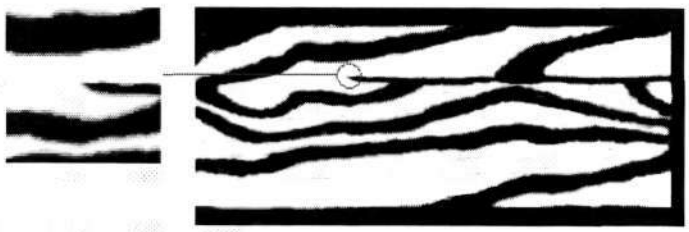

(i) Cooled down to 25 °C

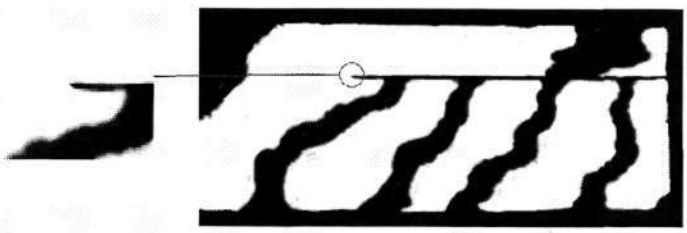

(j) Cooled down to 0 °C

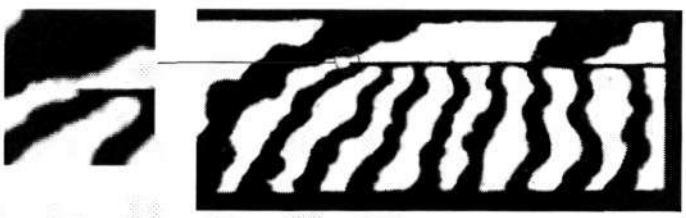

(k) Cooled down to –25 °C

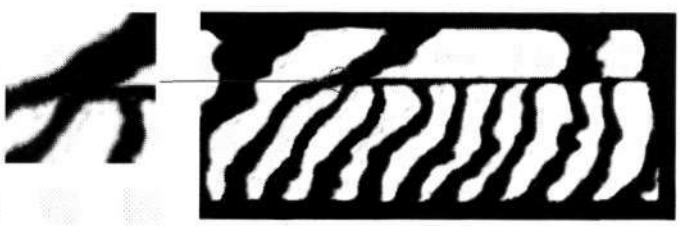

(l) Cooled down to –40 °C

ATTENTION: The Singapore Copyright Act applies to the use of this document. Nanyang Technological University Library

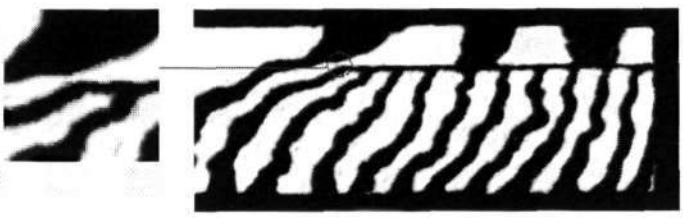

(m) Held at –40 °C after 12 mins

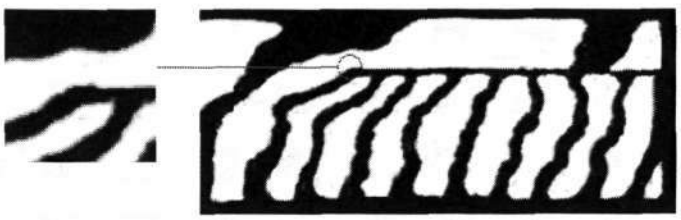

(n) Heated up to –25 °C

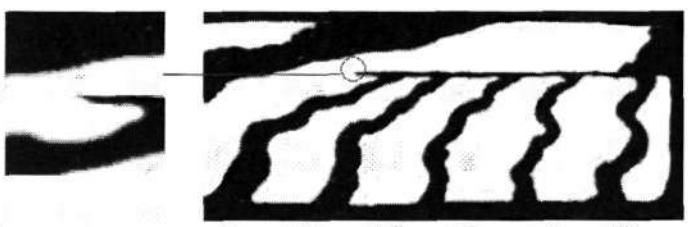

(o) Heated up to 0 °C

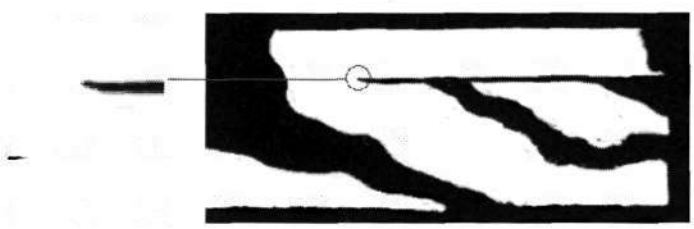

(p) Heated up to 25 °C

Fig. 4.8 U field fringe patterns throughout the whole temperature cycling range

ATTENTION: The Singapore Copyright Act applies to the use of this document. Nanyang Technological University Library

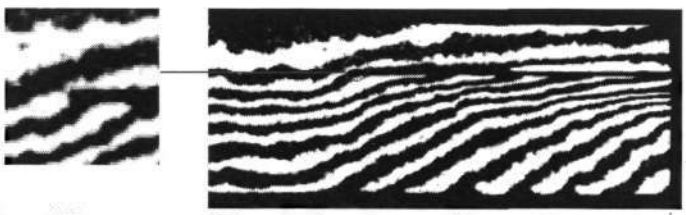

(a) Heated up to 50 °C

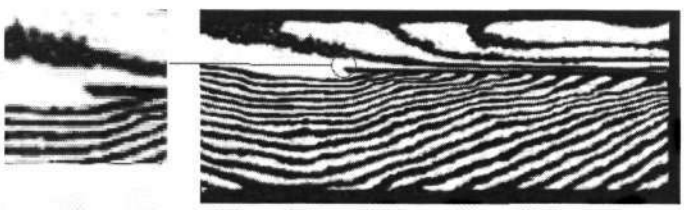

(b) Heated up to 75 °C

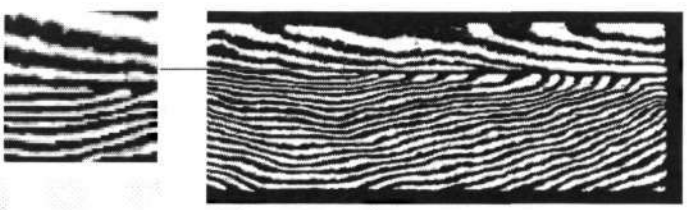

(c) Heated up to 100 °C

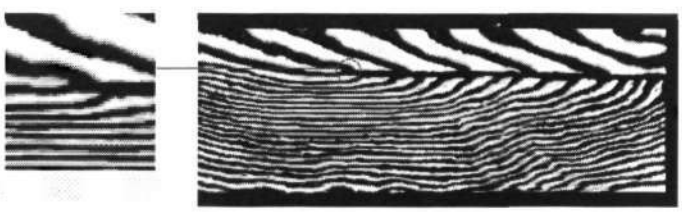

(d) Heated up to 125 °C

ATTENTION: The Singapore Copyright Act applies to the use of this document. Nanyang Technological University Library

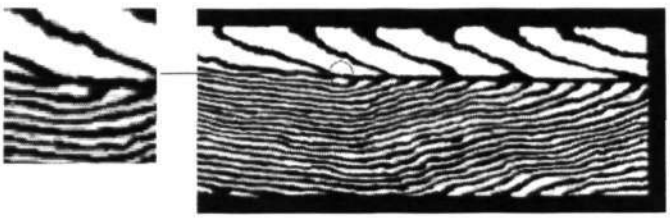

(e) Held at 125 °C after 12 mins

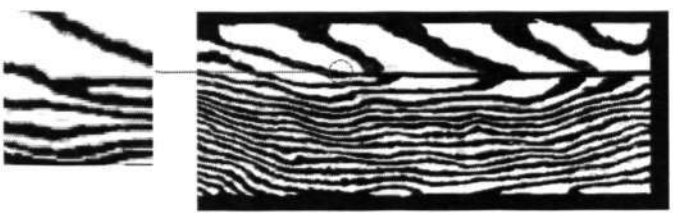

(f) Cooled down to 100 °C

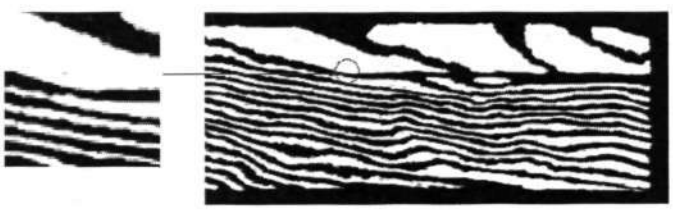

(g) Cooled down to 75 °C

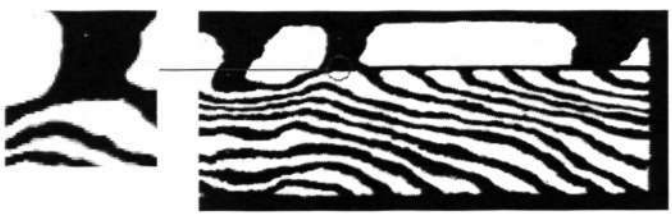

(h) Cooled down to 50 °C

ATTENTION: The Singapore Copyright Act applies to the use of this document. Nanyang Technological University Library

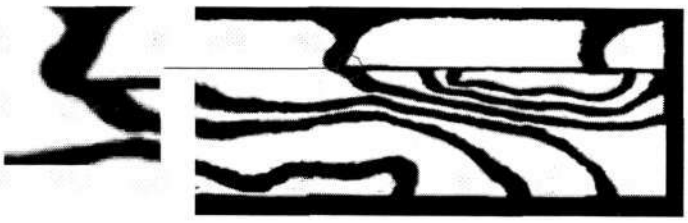

(i) Cooled down to 25 °C

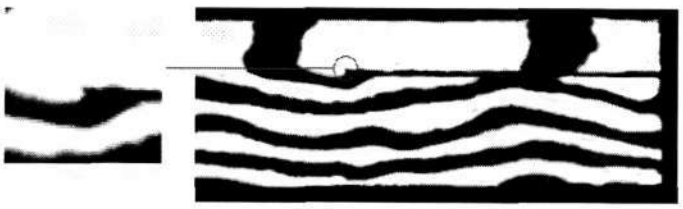

(j) Cooled down to 0 °C

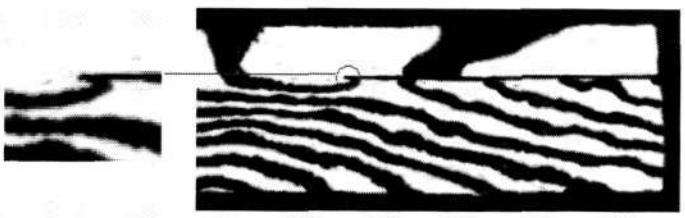

(k) Cooled down to –25 °C

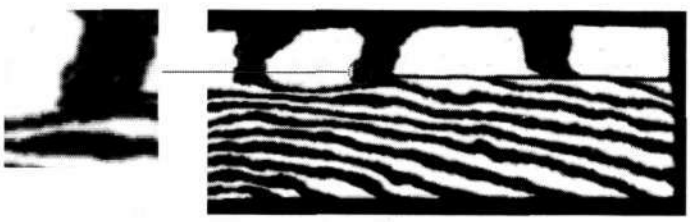

(l) Cooled down to –40 °C

ATTENTION: The Singapore Copyright Act applies to the use of this document. Nanyang Technological University Library

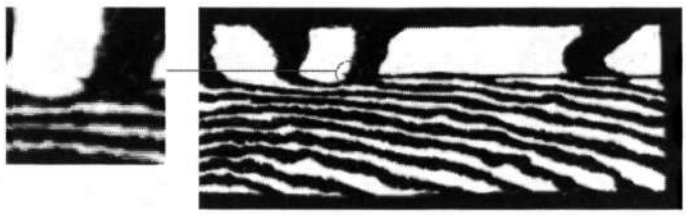

(m) Held at –40 °C after 12 mins

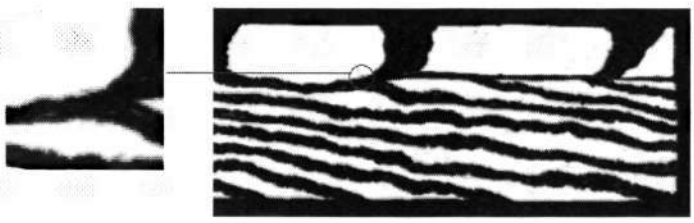

(n) Heated up to –25 °C

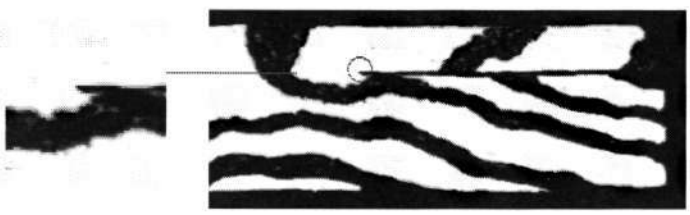

(o) Heated up to 0 °C

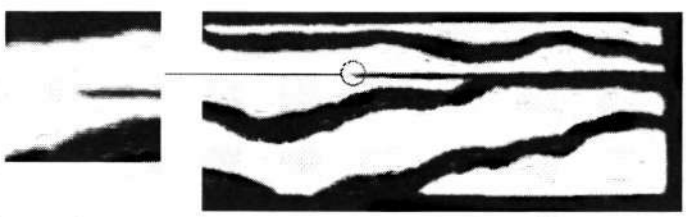

(p) Heated up to 25 °C

Fig. 4.9 V field fringe patterns throughout the whole temperature cycling range

ATTENTION: The Singapore Copyright Act applies to the use of this document. Nanyang Technological University Library

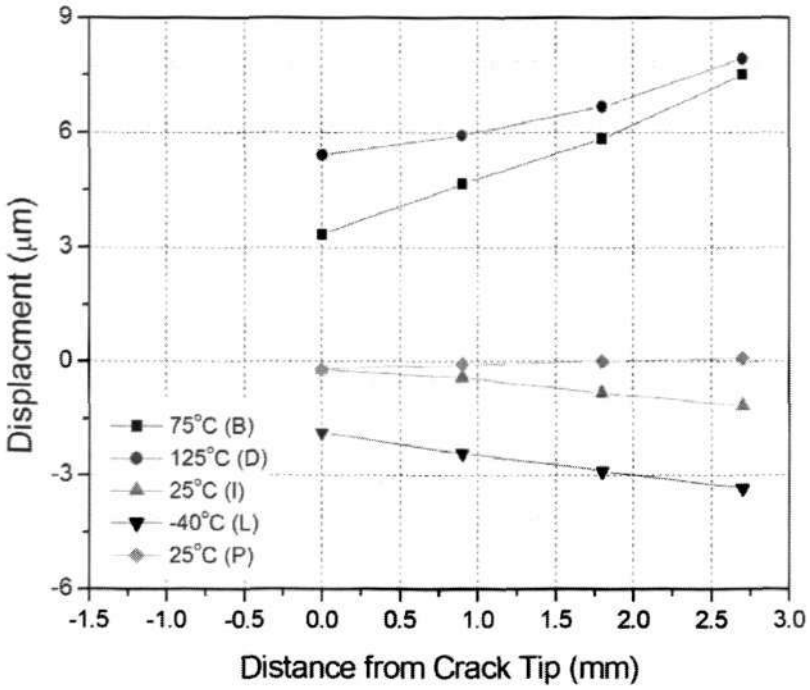

a) Relative vertical displacements along the interface of underfill/FR-4 obtained from the moiré patterns

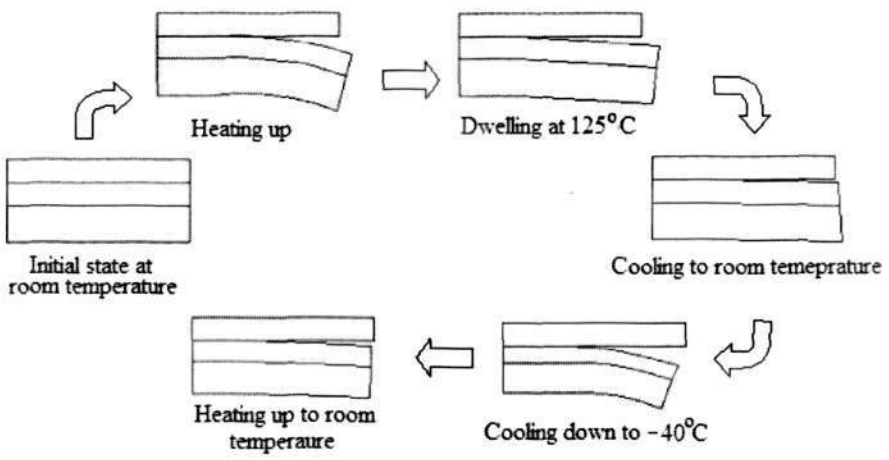

b) Schematic diagram of deformed shape within whole temperature cycling

Fig. 4.10 Deformation from fringe patterns

ATTENTION: The Singapore Copyright Act applies to the use of this document. Nanyang Technological University Library

4.7 FEA examination

Fig. 4.11 to Fig. 4.13 shows the deformation patterns around the crack tip of the assembly under the three temperatures of 75 ℃ under heating process, 50 ℃ under cooling process and –40 ℃ under cooling process. It was noted that the displacements attained from FEA were in agreement with those obtained from the moiré test. In addition, the results proved the tendency of deformation described before. It was also an evidence that the viscoelastic properties of underfill and the temperature-dependent properties of FR-4 and silicon wafer modelled in FEA could more veritably describe the thermal deformation of the sandwich flip-chip specimen. It is therefore proved that, in case the material model of underfill is accurately modelled, the more realistic results could be obtained through numerical simulation.

ATTENTION: The Singapore Copyright Act applies to the use of this document. Nanyang Technological University Library

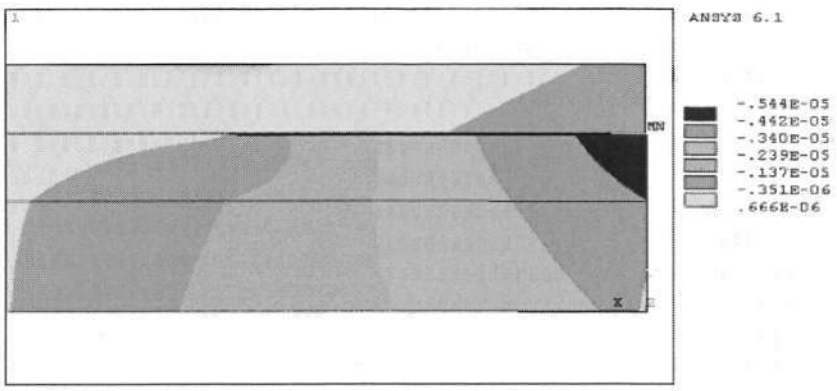

U field

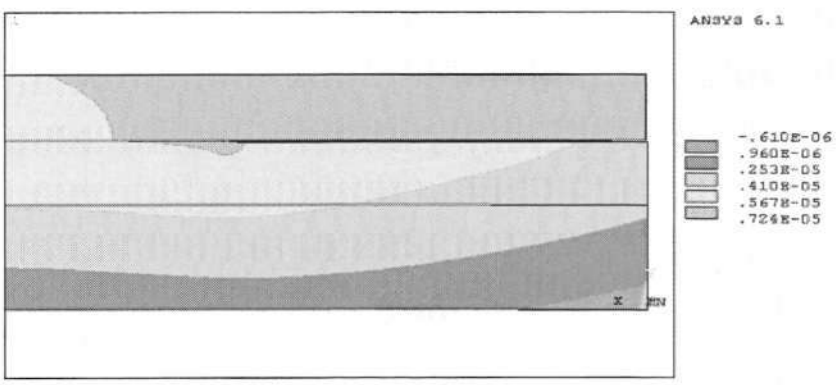

V field

U field

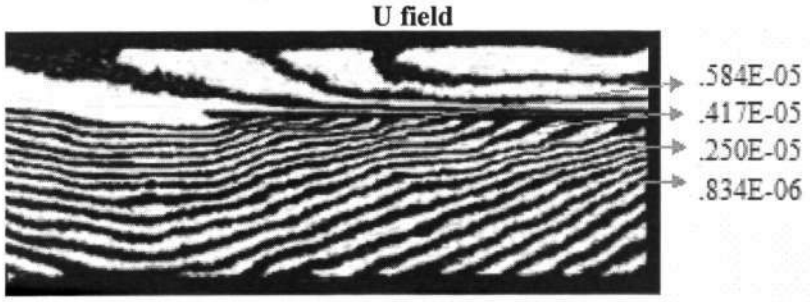

V field

Fig. 4.11 U and V comparison at 75 °C during heating up (Unit: m) (stage B in Fig. 3.13)

ATTENTION: The Singapore Copyright Act applies to the use of this document. Nanyang Technological University Library

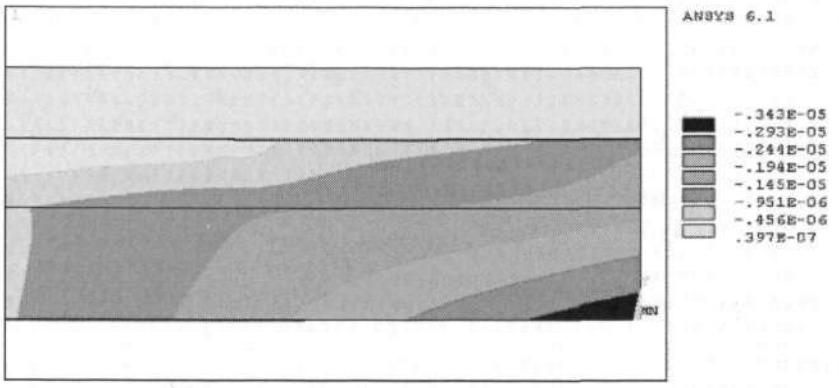

U field

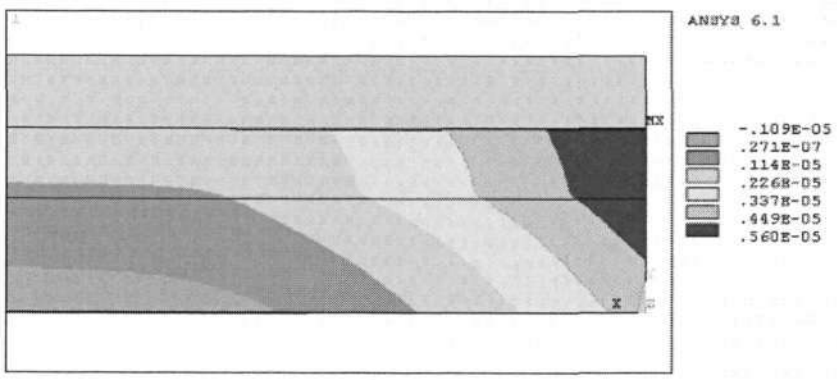

V field

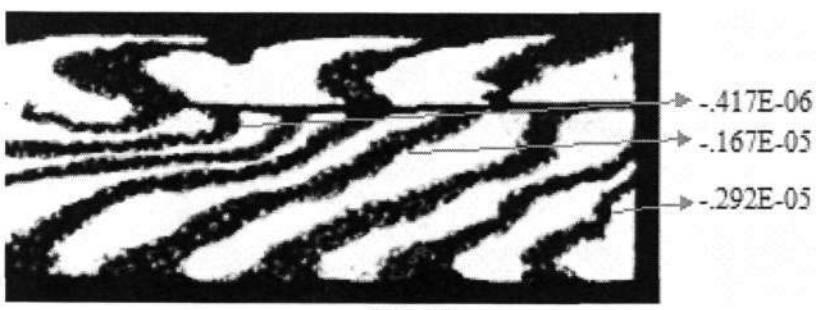

U field

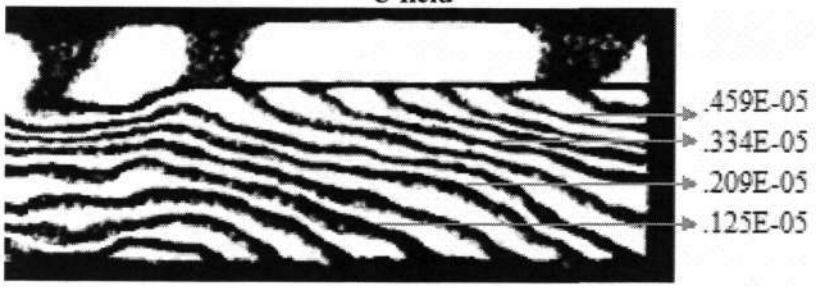

V field

Fig. 4.12 U and V comparison at 50 °C during cooling-down (Unit: m) (stage H in Fig. 3.13)

ATTENTION: The Singapore Copyright Act applies to the use of this document. Nanyang Technological University Library

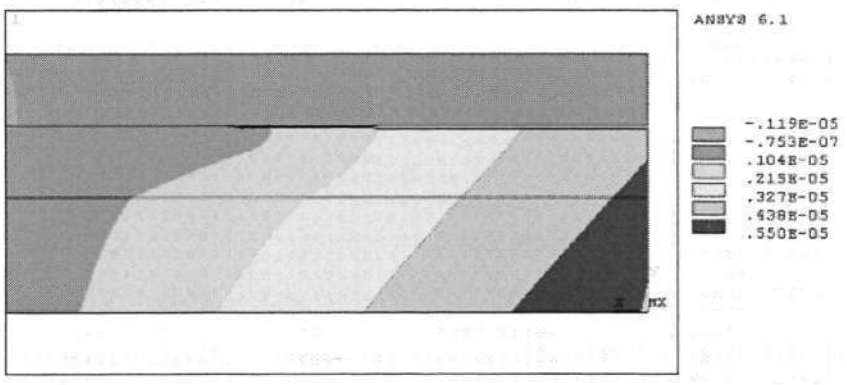

U field

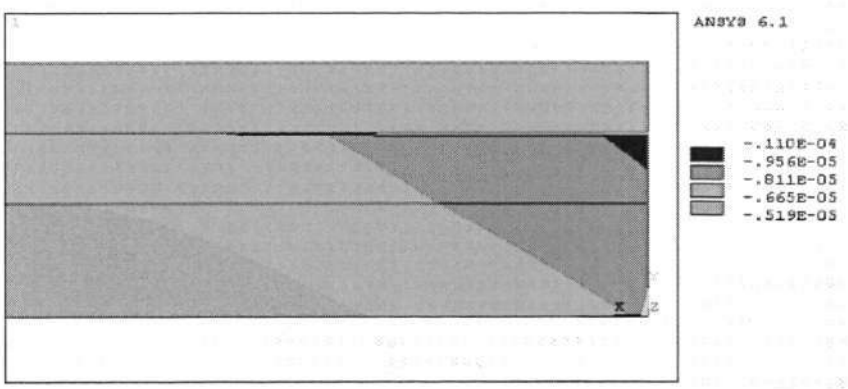

V field

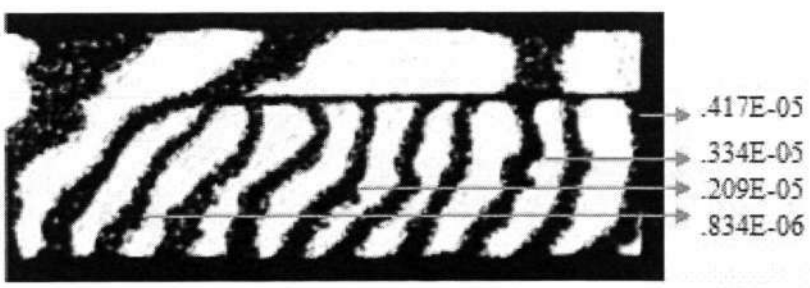

U field

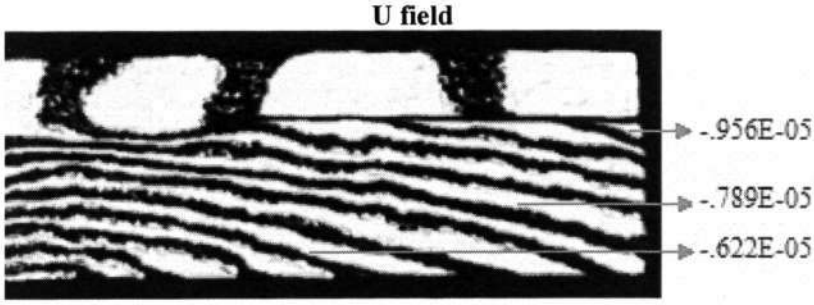

V field

Fig. 4.13 U and V comparison at –40 °C during cooling down (Unit: m) (stage L in Fig. 3.13)

ATTENTION: The Singapore Copyright Act applies to the use of this document. Nanyang Technological University Library

4.8 Fracture Behavior Investigation

Note that the Dundurs' parameters change as a function of elastic mismatch between chip/underfill. In case the elastic moduli of underfill varied significantly when temperature went up around and even above the T_g, the corresponding interfacial toughness was changed significantly. In the experiment, the CTODs were derived from the moiré fringe patterns representing displacement along the two crack flanks. Typical CTODs of the whole temperature cycling are displayed in Fig. 4.14. As seen, when the temperature cooled down to the room temperature, excessive CTODs were found along the crack. The residual deformation was caused by the viscoelastic behavior of the underfill at the high temperature. When the assembly loaded in the temperature below 0 degree, the viscoelasticity of the underfill was not significant since the underfill material exhibit elastic characteristic at low temperature.

The schematic diagram of crack tip movement is shown in Fig. 4.15. It was assumed that silicon wafer was relatively stationary during the loading history in the figure since the deformation of silicon was much smaller than the other two materials. The time effect became more significant when the temperature was around or even above T_g. The open-close-reopen history was also an evident of the loss of warpage during the dwelling at extreme high temperature. This can be proved through V field displacement obtained from both moiré experimental results and FEA numerical simulation results. It is shown that the time-dependent deformation can be well simulated through FEA technique if the viscoelastic properties of underfill were implemented.

ATTENTION: The Singapore Copyright Act applies to the use of this document. Nanyang Technological University Library

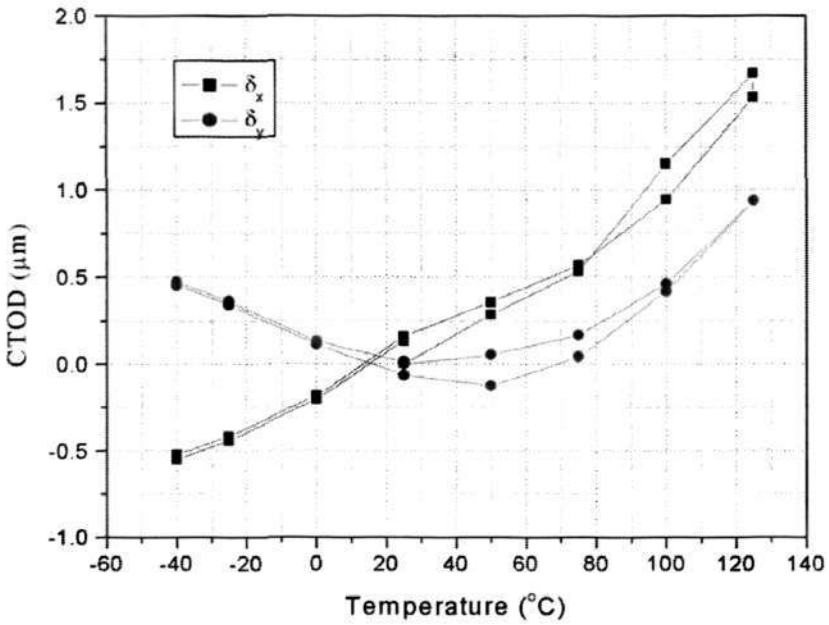

Fig. 4.14 CTODs at the distance of $r/l = 0.3$ obtained from moiré experiment for the whole temperature cycle ($l = 0.5$ *mm*)

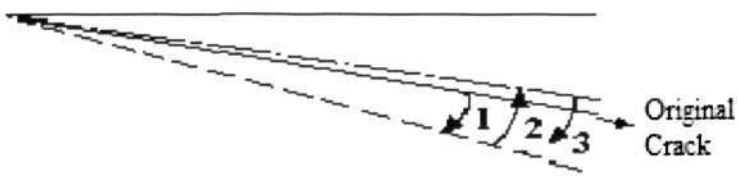

Fig. 4.15 Schematic diagram for the macro crack flank deformation. 1. Crack opening during heating; 2. Crack closure with temperature went down to room temperature; 3. Crack opens again in the temperatures of cold.

In this study, a characteristic length $l = h_{underfill}$ valued 0.5 *mm* was selected as the reference length. The selection of l was within the zone of dominance of the K-field, i.e. elastic zone of bimaterial, where the variation of l is negligible even

ATTENTION: The Singapore Copyright Act applies to the use of this document. Nanyang Technological University Library

for changes of l of several orders of magnitude since ε is small in the case of Si/underfill interface (Hutchinson and Suo 1992). With the length l, the nominal SIFs were calculated as function of $r^{1/2}$ (Pang et al. 2002). As shown in Fig. 4.16, the nominal $K_1^{'}$ increased when $r^{1/2}$ decreased, while the nominal $K_2^{'}$ almost remain as constant. The two nominal SIFs showed an approximate linear relationship with $r^{1/2}$. It is reasonable to assume that the deformation field around the crack-tip was dominated by the K-field, and the linear extrapolation method (Owen and Fawkes 1983) could be employed to determine the fracture toughness at the crack-tip. By curve fitting, the experimental and FEM results were extrapolated to the y-axis using straight line, which represented the interfacial toughness K_1 and K_2 at the crack tip. The values of K_{eff} and ψ were then calculated with Eq. (4.10) and Eq. (4.11) and the results are plotted in Fig. 4.17.

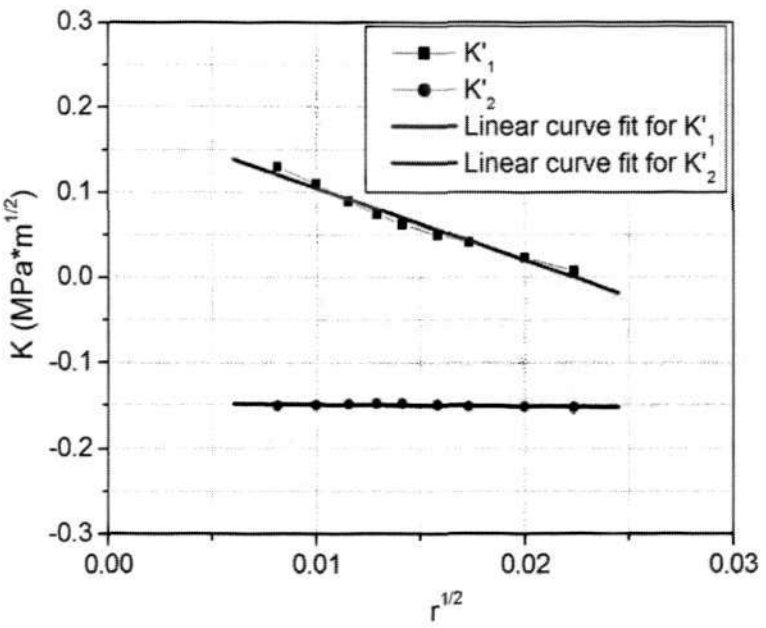

Fig. 4.16 SIFs obtained at –25 °C as functions of $r^{1/2}$

ATTENTION: The Singapore Copyright Act applies to the use of this document. Nanyang Technological University Library

As aforementioned, K_{eff} decreased as stress relaxation happened in the glass transition state of underfill. However, one cannot determine that the most dangerous stage in the thermal cycling was located at the point with the highest K_{eff}, since the interfacial toughness varies with the mode mixity at the same time (Hutchinson and Suo 1992). According to the definition of interfacial fracture extension, the expression can be

$$\left.\begin{aligned} K_{eff} &= K_{eff}(\psi) \\ \psi &= \tan^{-1}\left[\frac{\mathrm{Im}(KL^{i\varepsilon})}{\mathrm{Re}(KL^{i\varepsilon})}\right] \end{aligned}\right\} \tag{4.13}$$

where ψ is the mode mixity. From Eq. (4.13), it can be seen that the value of K_{eff} is a curve as a function of mode mixity ψ rather than an independent point. Thus, referring to the work done by Suo 1989, it is known that the smaller phase angle has corresponding smaller K_{eff} since mode I failure is more fatal than mode II. Apart from mode mixity, it was anticipated that a change of material stiffness (modulus) induced by temperature variation would also decrease the interfacial fracture toughness when the phase angle is fixed (Nguyen et al. 1997). Therefore, according to eq. (4.6), both interfacial toughness and interfacial fracture toughness are expressed as a function of temperature, which is $\overline{E_i}(T) = E_i(T)/(1-\nu_i)$.

During the heating process, it was observed in Fig. 4.17(a) that the highest value of K_{eff} happened at the temperature between 75 ℃ and 100 ℃ rather than 125 ℃. From Eq. (4.1) to Eq. (4.9), it can be seen that changes of E^* will affect the value of K_{eff} (Pang et al. 2002). The possible explanation might be that both CTE and stiffness mismatch inside layered structure could significantly influence the deformation and corresponding fracture behaviours. Particularly, when temperature went up to T_g of the underfill, the underfill is malleable because of the

ATTENTION: The Singapore Copyright Act applies to the use of this document. Nanyang Technological University Library

continuing rearrangement of molecular segments, which is influenced by the secondary bonds in the crystalline region. The rearrangement results in the dramatic decease in Young's modulus of underfill, and therefore alters the mechanical relationship in the sandwich structure. Mathematically, it is expressed as rapid decrease in E^* as defined in Eq. (4.6). Accordingly, SIFs are prone to decrease significantly as the temperature is close to or higher than the T_g of the underfill. It could be expressed as

$$\text{CTE mismatch factor: } F_1 = f_1(\left|CTE_{underfill}(T) - CTE_{FR-4}(T)\right|)$$

$$\text{Stiffness mismatch factor: } F_2 = f_2(\left|E_{underfill}(T) - E_{FR-4}(T)\right|)$$

$$\text{Warpage: } W = g(F_1 - F_2) \tag{4.14}$$

where f_1 and f_2 represented that the influence of CTE and stiffness on the warpage were the functions of absolute value of the difference between dissimilar materials respectively, g showed that the CTE mismatch and stiffness mismatch had opposite effect on the comprehensive warpage of the assembly.

Similarly, the increase of underfill modulus at the temperatures below 0 degree was helpful to increase the K_{eff}. When the temperature went down, there was residual K_{eff} generated with the comparison of the K_{eff} at the same temperature during the heating-up process. This residual value was aroused by viscoelastic deformation especially when the temperature exceeded the T_g. The phase angle shifted from positive to negative during cooling process, as presented in Fig. 4.17 (b), showed alteration of the direction of shear stress inside the specimen.

ATTENTION: The Singapore Copyright Act applies to the use of this document. Nanyang Technological University Library

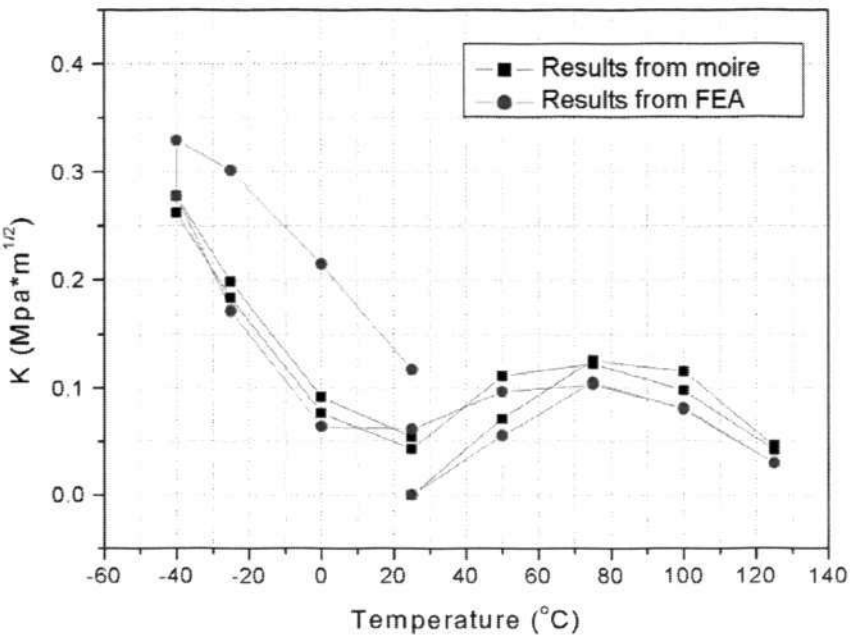

(a)

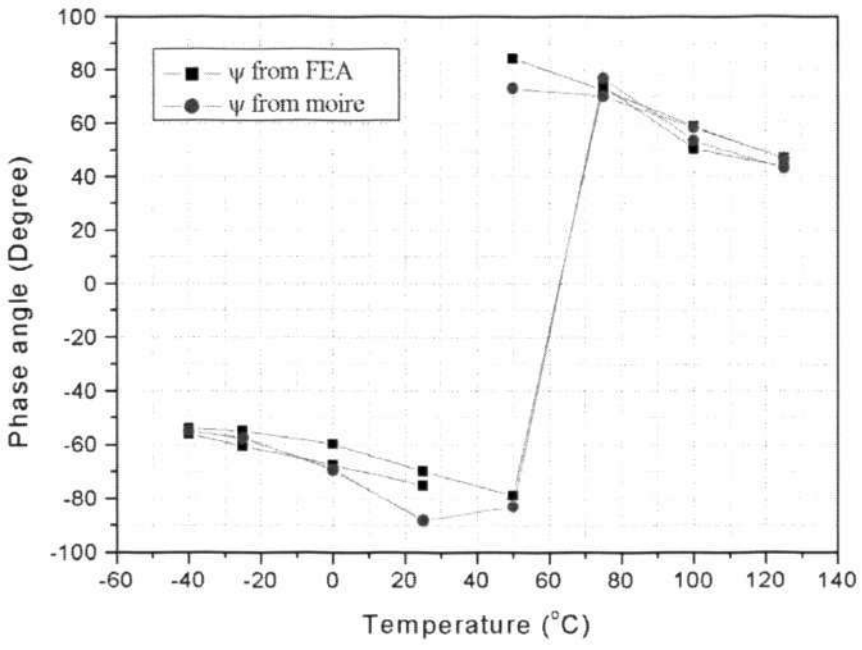

(b)

Fig. 4.17 Representative interfacial toughness and phase angle obtained from FEA and moiré. (a) comparison of FEA and moiré with respect to K_{eff}; (b) comparison of FEA and moiré with respect to $\hat{\psi}$

ATTENTION: The Singapore Copyright Act applies to the use of this document. Nanyang Technological University Library

4.9 Summary

The results show good agreement between moiré experiment and numerical simulation results based on the assumptions of viscoelasticity of underfill material, perfect bonding without defects or damage initially and solely crack propagation condition rather than both crack initiation and propagation. It indicated that in-situ measurement could well reflect the structure response of flip chip assembly under thermal cycling. Both results showed that not only CTE mismatch is a main cause for interfacial delamination, but also stiffness mismatch plays an important role on structure deformation and consequently fracture behaviour. It is important to consider the coupling effect between CTE mismatch and stiffness mismatch in the design and material choices of flip chip manufacturing.

ATTENTION: The Singapore Copyright Act applies to the use of this document. Nanyang Technological University Library

Chapter 5 Interface Behavior of Chip/Underfill under Hygrothermal Aging

5.1 Introduction

Moisture migrating into plastic packaging induces hazardous effects on package reliability. As reviewed in Chapter 2, moisture induced swelling, degradation of material properties (Wong et al. 2002b), popcorn (McKague et al. 1978, Apicella et al. 1979) and loss of interfacial strength (Ferguson & Qu 2002) aggravate the potential of interfacial delamination during manufacturing and operation processes.

Considerable effort has been made to understand the hygrothermal behavior of plastic packages based upon finite element analyses. The results are irradiative to the knowledge of moisture induced reliability problems. With an appropriate thermal-moisture analogy, moisture diffusion of polymeric material can be modeled after thermal diffusion function of the finite element software. The approach gives good prediction of acceleration factors compared with the experimental values (Okura et al. 2002).

To solve the discontinuity of moisture concentration between adjacent materials, the wetness technique is introduced to normalize moisture concentration with the saturated concentration of the respective materials. The results indicate that the magnitude of hygroscopic stress in flip chip PBGA is significantly higher than that of thermal stress (Wong et al. 1998, Wong et al. 2002b). Recently, the

ATTENTION: The Singapore Copyright Act applies to the use of this document. Nanyang Technological University Library

wetness technique has been extended to model the vapor pressure in electronic packaging (Wong et al. 2002c).

These efforts do have remarkably improved the knowledge of moisture induced interfacial problem. However, in order to improve the interfacial reliability, apart from numerical analysis, it is necessary to understand the failure mechanism of FCOB assembly under hygrothermal aging using accurate experimental measurement technique. Moreover, to the author's best knowledge, few studies have taken into consideration the time effect even though the underfill exhibits viscoelasticity in hygrothermal aging, which is normally carried out under high temperature for long duration. The difficulties of experimental work may exist inherently since the hygrothermal deformation is a 3 dimensional problem with the consideration of the nature of moisture diffusion.

However, it is estimated that, if the structure response under saturated condition with C_{sat} can be understood, it is possible to evaluate the reliability of the package under varying unsaturated moisture concentration. Therefore, the first step in the study was to carry out 2-dimensional in-situ measurement with the assumption of saturated moisture concentration on the in-plane surface, consistent with boundary condition applied in the finite element analysis.

In this study, a moiré interferometry system was developed (see detailed description in Chapter 3) and used to investigate the interfacial fracture behavior of FCOB assembly under hygrothermal aging. In order to study the time effect on FCOB assembly, the thermal aging study was simultaneously carried out.

ATTENTION: The Singapore Copyright Act applies to the use of this document. Nanyang Technological University Library

5.2 Hygrothermal Displacement

In this study, specimen type A was tested in M^3I system with a miniaturized moisture chamber. Following the introduction of specimen type A preparation in section 3.2.1 and the testing program in section 3.5.2.1, the displacements of specimen type A under the hygrothermal aging were measured using the M^3I system. The fringe patterns in both the x and y-directions at the initial state (t=0, 85 °C/dry) and different time intervals are presented in Fig. 5.1. It can be observed from the figure that the number of fringe patterns increased at the initial several hours. The increase is the result of the swelling of the underfill material upon moisture absorption.

When water migrated into epoxy-based underfill, it broke the interchain bonds by forming hydrogen bonds with chain interruption (Kwei 1966). The formation of hydrogen bonds permits the resin network to expand through relaxation of the stresses produced by osmotic pressure (Xiao & Shanahan 1998). Afterwards, the increase of fringe orders was not significant.

Determined with Eqs. (3.6) and (3.7), the normal strain ε_x and shear strain γ_{xy} along the interfaces of Si/underfill and FR-4/underfill are plotted in Fig. 5.2 and 5.3 respectively. The geometric positions of the data points are defined according to the coordinate system in Fig. 3.2 (b). The strains were observed to increase drastically when they approached the free edges. This is caused by the singularity nature of the free edges. The normal stress σ_x and the shear stress τ_{xy} in particular concentrated in regions close to the free edges and thus facilitated the interfacial delamination at these sites. It is also noted that the strains along the interfaces increased more significantly in the initial 3-hour than in the subsequent period (from 3-hour to 168-hour aging).

ATTENTION: The Singapore Copyright Act applies to the use of this document. Nanyang Technological University Library

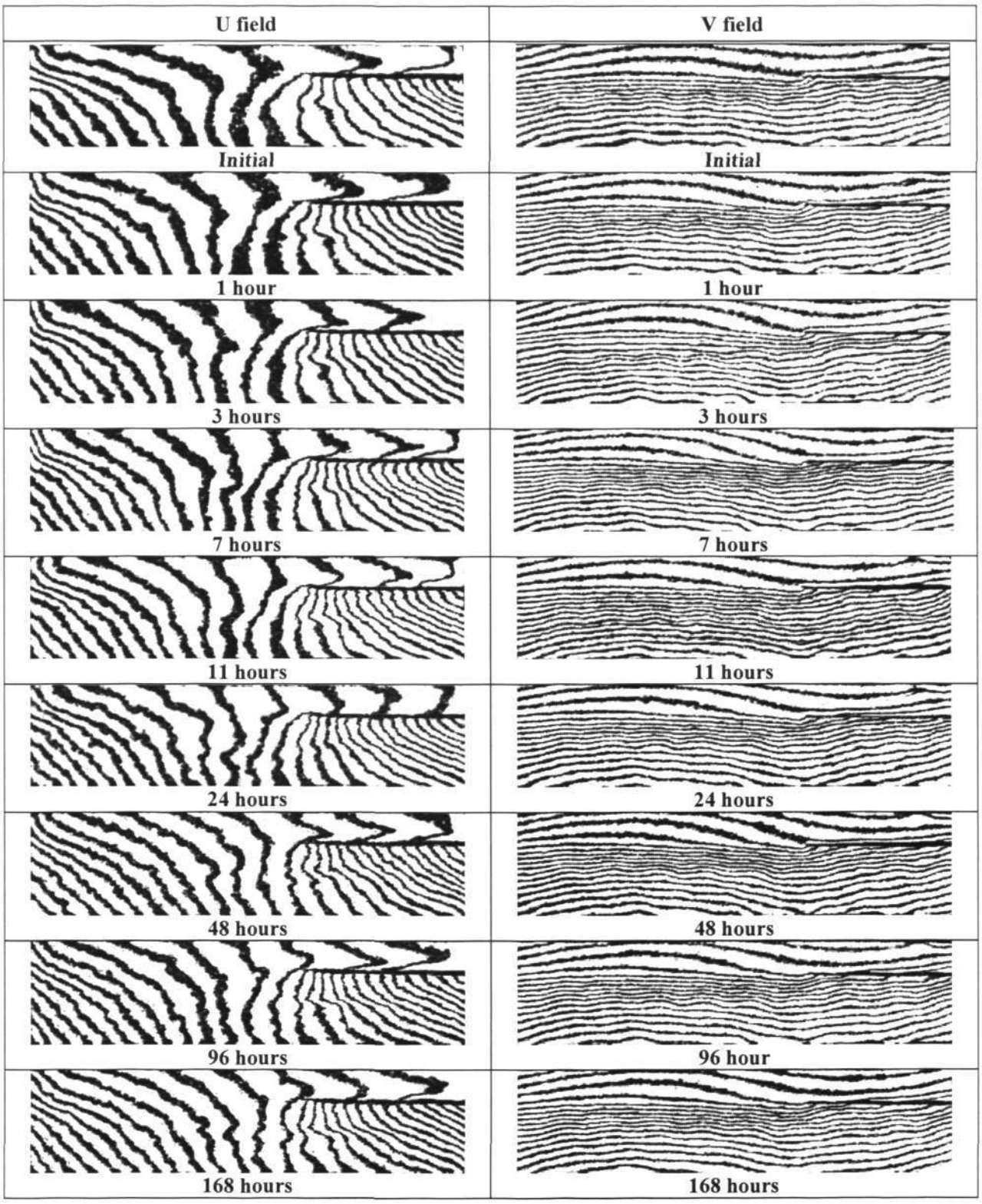

Fig. 5.1 Fringe patterns during hygrothermal aging under 85 °C/85%RH

ATTENTION: The Singapore Copyright Act applies to the use of this document. Nanyang Technological University Library

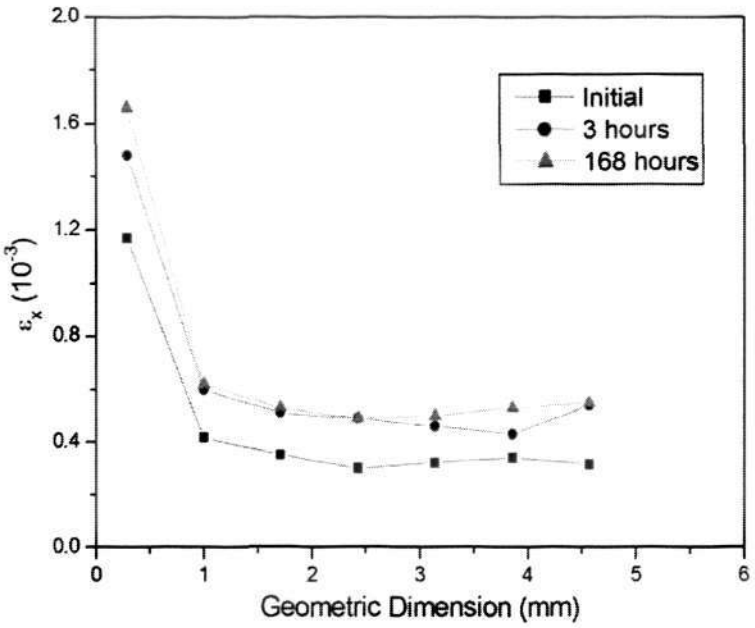

(a) ε_x

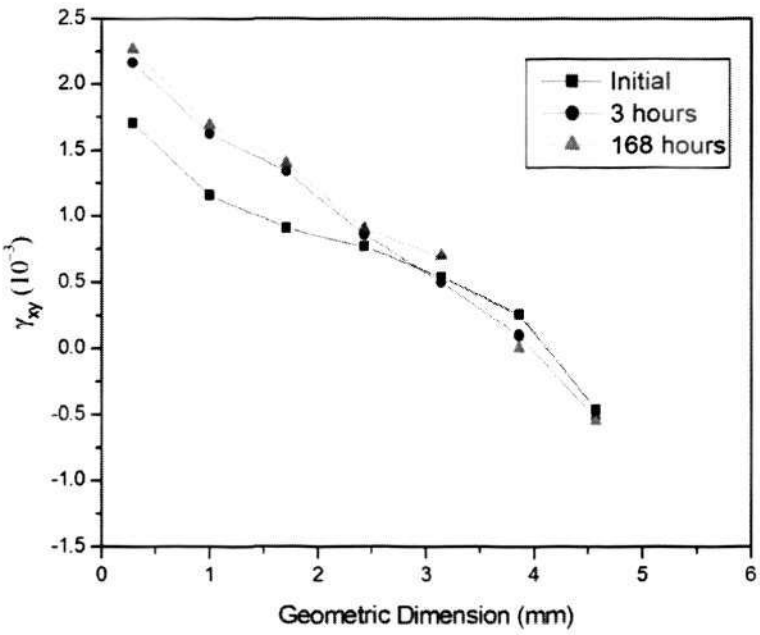

(b) γ_{xy}

Fig. 5.2 ε_x and γ_{xy} along the Si/underfill interface

ATTENTION: The Singapore Copyright Act applies to the use of this document. Nanyang Technological University Library

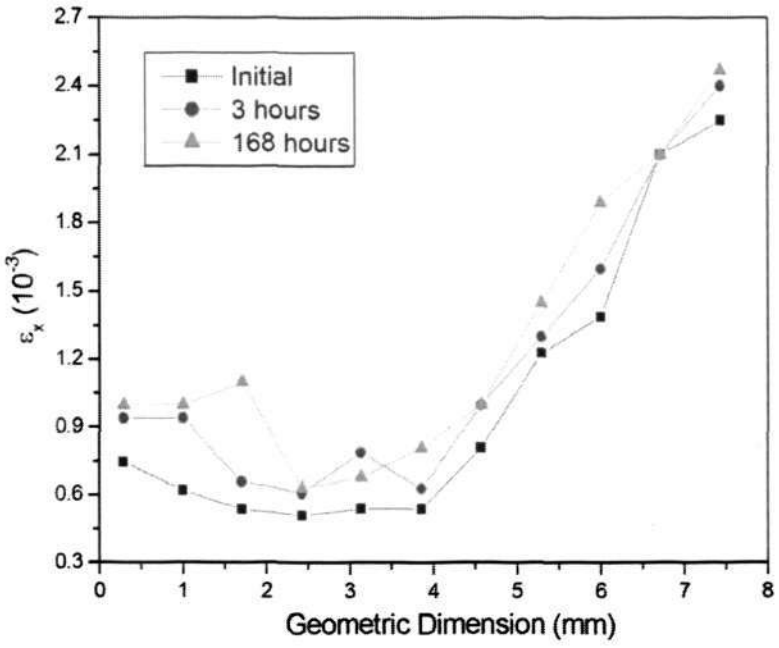

(a) ε_x

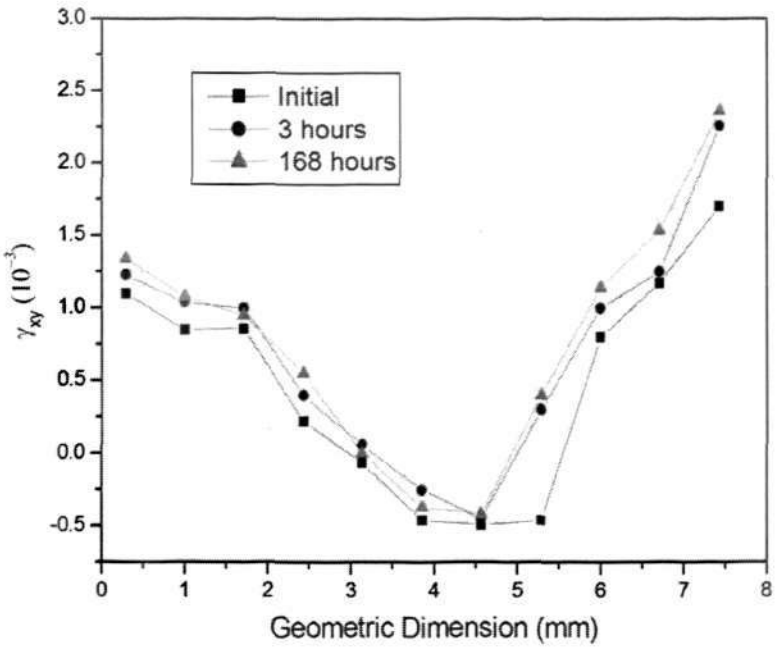

(b) γ_{xy}

Fig. 5.3 ε_x and γ_{xy} along the FR-4/underfill interface

ATTENTION: The Singapore Copyright Act applies to the use of this document. Nanyang Technological University Library

In order to understand the relationship between the moisture absorption and the hygrothermal deformation, the moisture absorption test of the underfill material was carried out under the hygrothermal condition 85 °C/85%RH. It is found from the experimental results that the absorption property of the underfill is Fickian, as shown in Fig. 5.4.

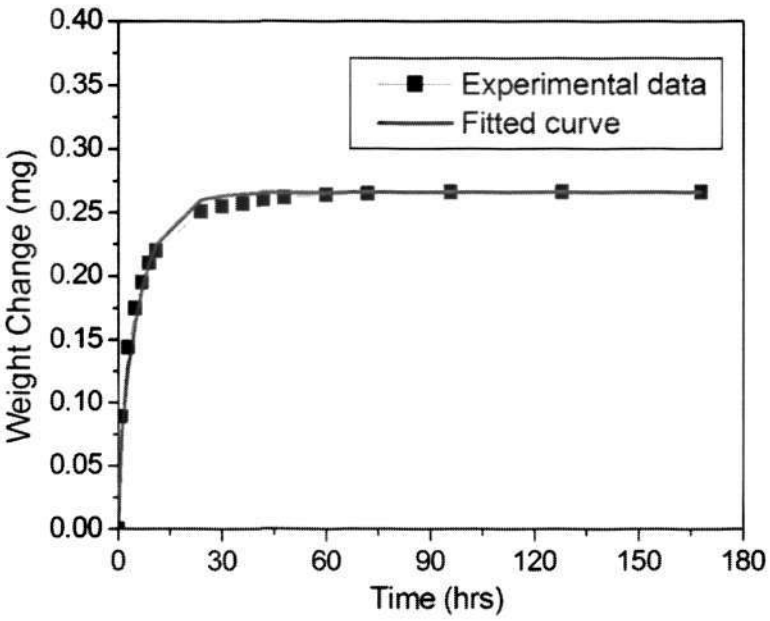

Fig. 5.4 Weight gain for underfill 3563 tested at 85 °C/85%RH and Fickian curve fitting

Note that since the moisture diffusion of underfill material in the sandwiched specimen was predominantly one-dimensional, the moisture uptake was described with Eq. (5.1), which was an asymptotic curve as a function of time (Crank & Park 1956)

$$\frac{M_t}{M_{sat}} = 1 - \frac{8}{\pi^2}\sum_{n=1}^{\infty}\frac{1}{(2n+1)^2}\exp\left[-\frac{D_z t}{z_0^2}[(2n+1)\pi]^2\right] \tag{5.1}$$

ATTENTION: The Singapore Copyright Act applies to the use of this document. Nanyang Technological University Library

where D is the diffusion coefficient, z_0 is the total film thickness, M_t is total mass of the diffusing substance absorbed by the sample at time t, and M_∞ is the equilibrium mass of the absorbed substance. The similarity between the moisture absorption of underfill and hygrothermal deformation indicates that there is inherent relationship between them.

The observation indicates that the initial moisture uptake caused most of swelling in the underfill. With the slowing of moisture absorption for a long period of time, the corresponding swelling induced deformation became inconspicuous. The normal and shear strains at the leftward edge of Si/underfill interface are plotted in Fig. 5.5. The figure shows that the strains increased as time increased. Since both normal strain and shear strain showed similar trends, which was in asymptotic manner, it is believed that hygrothermal deformation was analogous to the moisture diffusion in underfill since moisture absorbed in the underfill has chemical reaction with interchain bonds and therefore causes swelling (Kwei 1966). This observation also physically, apart from chemical point of view, proved that the swelling of underfill was related to the concentration of moisture diffusion at a certain extent.

ATTENTION: The Singapore Copyright Act applies to the use of this document. Nanyang Technological University Library

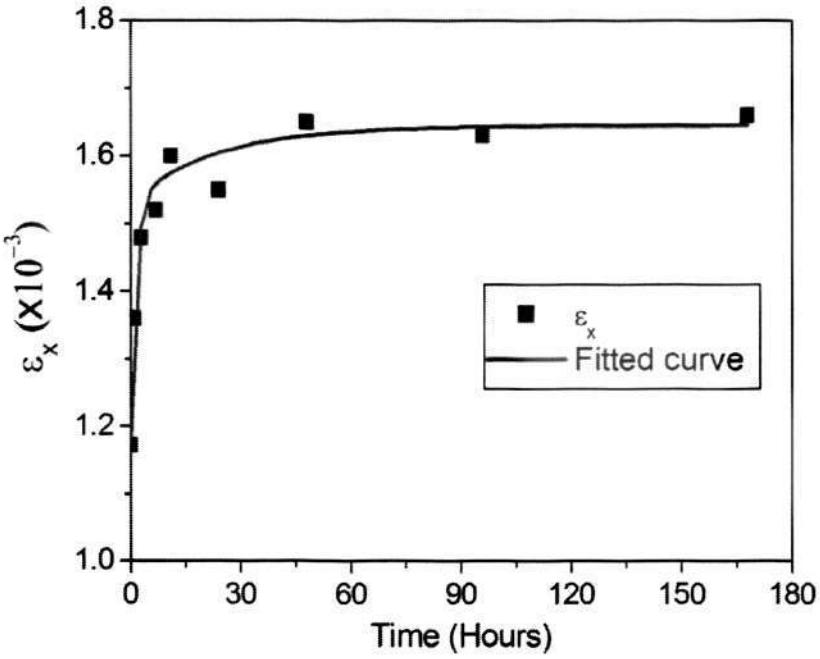

(a) ε_x

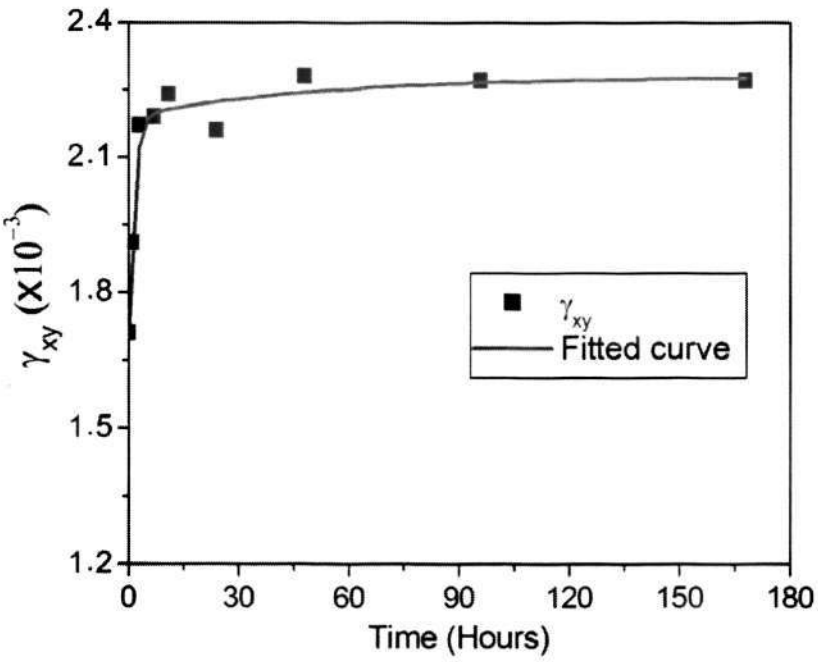

(b) γ_{xy}

Fig. 5.5 Strains at the left free edge of Si/underfill interface in hygrothermal aging (85 °C/85%RH)

ATTENTION: The Singapore Copyright Act applies to the use of this document. Nanyang Technological University Library

5.3 Thermal Aging Deformation

The study of thermal deformation was performed to understand the time effect on the reliability of FCOB assembly under the hygrothermal aging. The representative fringe patterns under different intervals are shown in Fig. 5.6. The normal and shear strains at the leftward edge of Si/underfill interface are plotted in Fig. 5.7. It can be seen from Fig. 5.6 that, analogous to hygrothermal aging effect, the time effect was significant at the beginning.

The strains reduced fast since the stresses caused by thermal mismatch of dissimilar materials were initially large. As time going on, time effect became less obvious. Up to 60% to 70% decrease of strains occurred at the beginning, while the remainder occurred within a relatively long period due to the stress relaxation. Therefore, it is believed that thermal aging, which was related to stress relaxation during aging under high temperature, helped to gradually reduce the magnitude of deformation of sandwiched structure.

Wang et al. (1998) presented similar results that an FCOB assembly without pre-crack exhibited significant time effect under high aging temperature, and stress relaxation happened rapidly at the very beginning of several hours.

Following the temperature-moisture analogous technique presented by Wong et al. (1998), the deformation caused by hygroscopic swelling and CTE/thermal creep can be separated individually. According to this method, superposition principle is used to separate the deformation caused by thermal aging from that caused by hygroscopic swelling. With the consideration of stress relaxation, the actual swelling induced strains are expected to be greater than those measured in hygrothermal aging, as shown in Fig. 5.8.

ATTENTION: The Singapore Copyright Act applies to the use of this document. Nanyang Technological University Library

In Fig. 5.8, the losses of strains induced by thermal aging are added to the strains measured in hygrothermal aging. As a result, the values of swelling induced strains are enlarged by 20%-30%. It is therefore thought that time effect should be considered in hygrothermal aging, which is beneficial to assembly reliability since it reduces the strains induced by material swelling during moisture immigration. It is also a hint that it is of necessity to include the time effect when finite element simulation is performed; otherwise the hygrothermal effect might be overestimated in reliability evaluation.

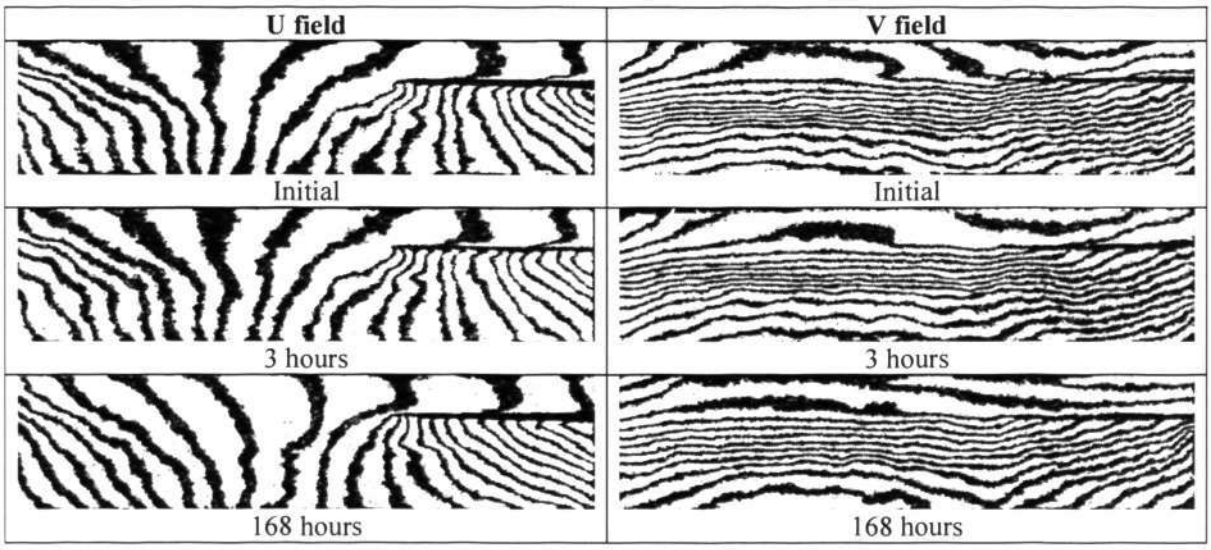

Fig. 5.6 Representative fringe patterns under the thermal aging test (168 hours under 85 °C)

ATTENTION: The Singapore Copyright Act applies to the use of this document. Nanyang Technological University Library

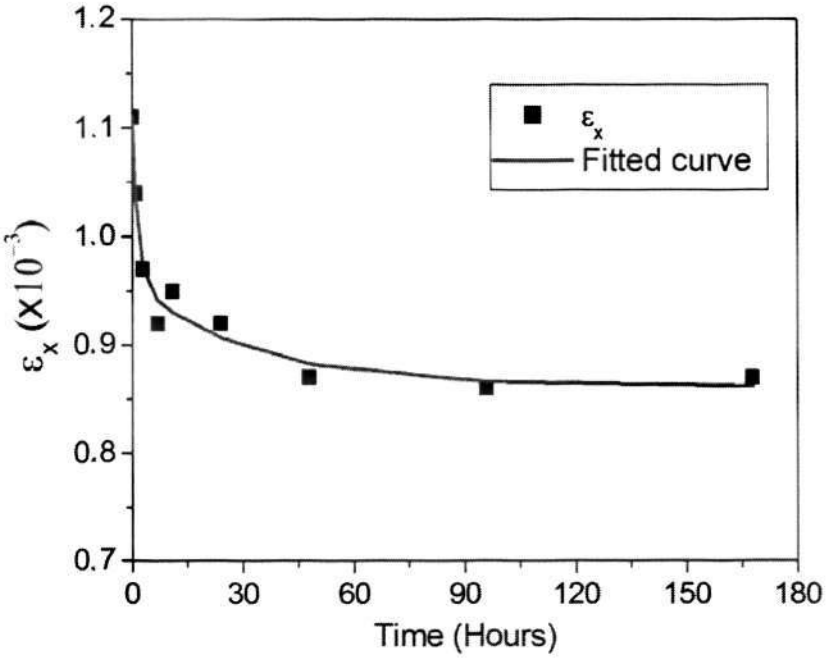

(a) ε_x

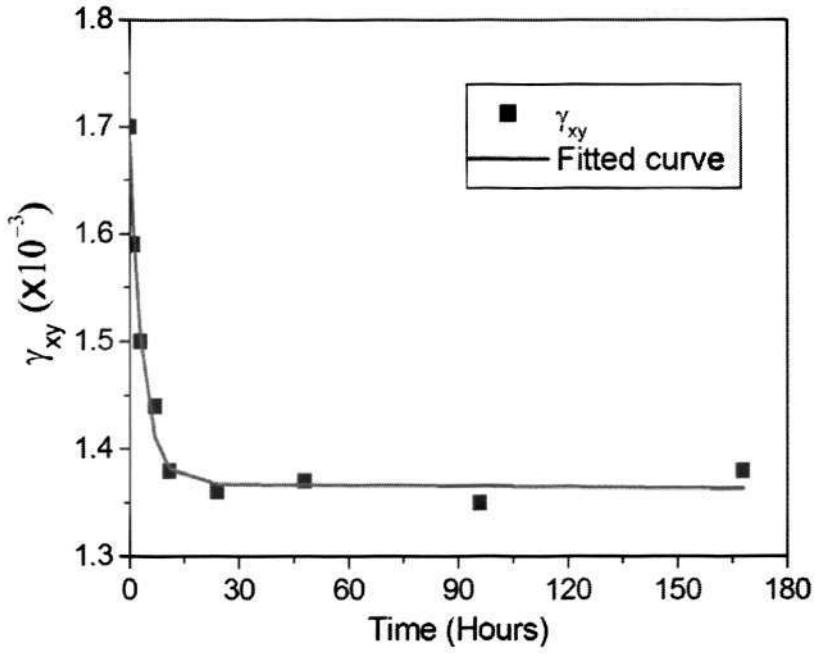

(b) γ_{xy}

Fig. 5.7 Strain gradients at the leftward of Si/underfill interface in thermal aging at 85 °C

ATTENTION: The Singapore Copyright Act applies to the use of this document. Nanyang Technological University Library

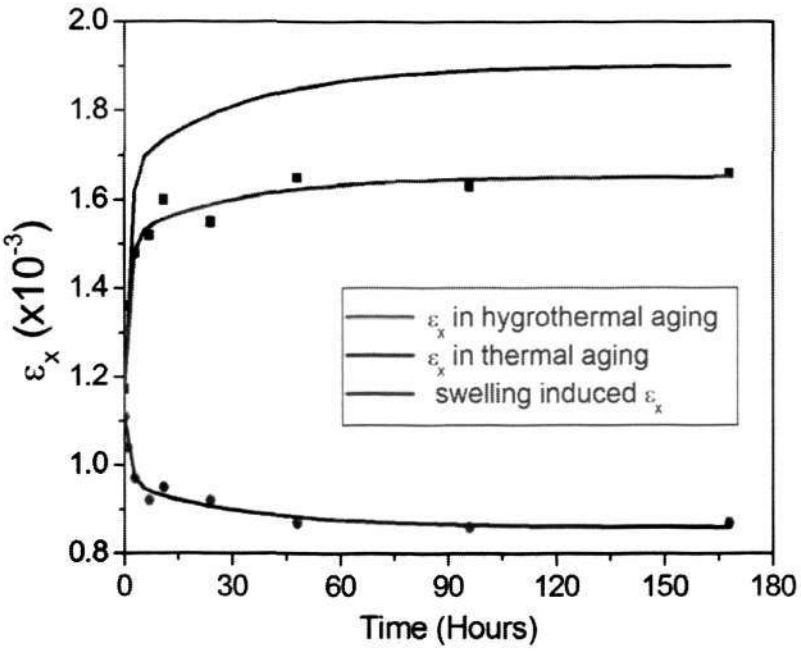

(a) ε_x

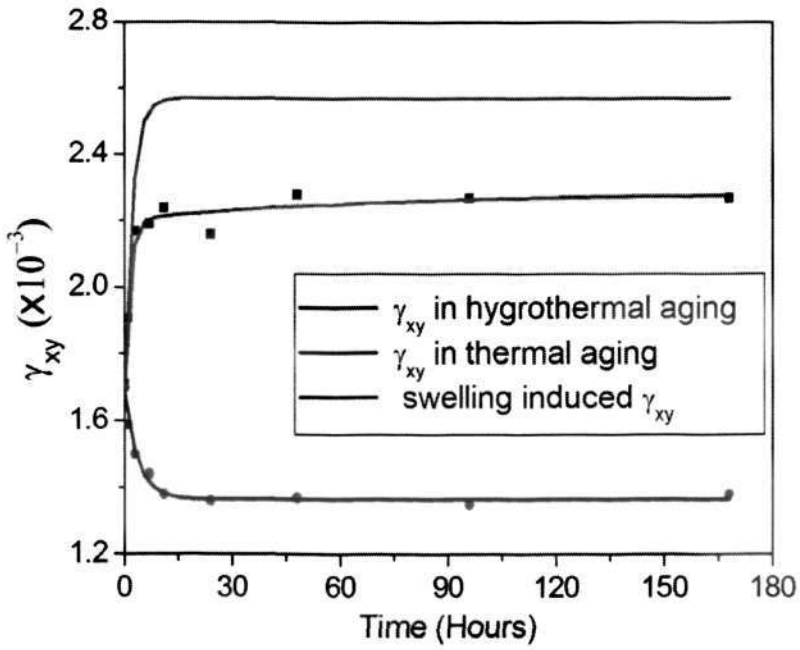

(b) γ_{xy}

Fig. 5.8 Swelling induced strains by using superposition method

ATTENTION: The Singapore Copyright Act applies to the use of this document. Nanyang Technological University Library

5.4 Fracture Behavior under Hygrothermal Aging

It is reported that the adhesion of interface can markedly reduce after moisture conditioning (Yi et al. 1997, Gurumurthy et al. 2001). In case the interfacial toughness is measured as a result of hygrothermal aging, it is convenient to quantitatively evaluate the potential of fracture propagation by comparing with the interfacial fracture toughness and thus understand the reliability of Si/underfill interface under the moisture attack. This section illustrated the results of the interfacial toughness under the hygrothermal aging. The method for characterization of interfacial fracture toughness is presented in Chapter 6.

Based on the displacement fields in moiré test, the nominal K'_1 and K'_2 can be determined using Eq. (4.1) to (4.9) for any given distance r away from the crack-tip. According to Eq. (4.8) and Eq. (4.9), $K_1^{'}$ and $K_2^{'}$ are proportional to $\sqrt{r}$, as shown in Fig. 5.9. It is noticed that the value of the nominal $K_2^{'}$ increases as the square root of distance $\sqrt{r}$ decreases, while $K_1^{'}$ remains the same.

The K_1 and K_2 at the crack tip can be obtained using extrapolation method based on nominal K'_1 and K'_2 with respect to various distance r away from crack tip (Owen and Fawkes 1983). As seen in Fig. 5.9, the nominal SIFs showed an approximate linear relationship with $\sqrt{r}$. The extrapolation method can then be employed to determine the interfacial toughness at the crack tip (Shi, et al. 2003). By curve fitting, the experimental results were extrapolated to $r=0$, representing the interfacial toughness K_1 and K_2 at the crack tip.

ATTENTION: The Singapore Copyright Act applies to the use of this document. Nanyang Technological University Library

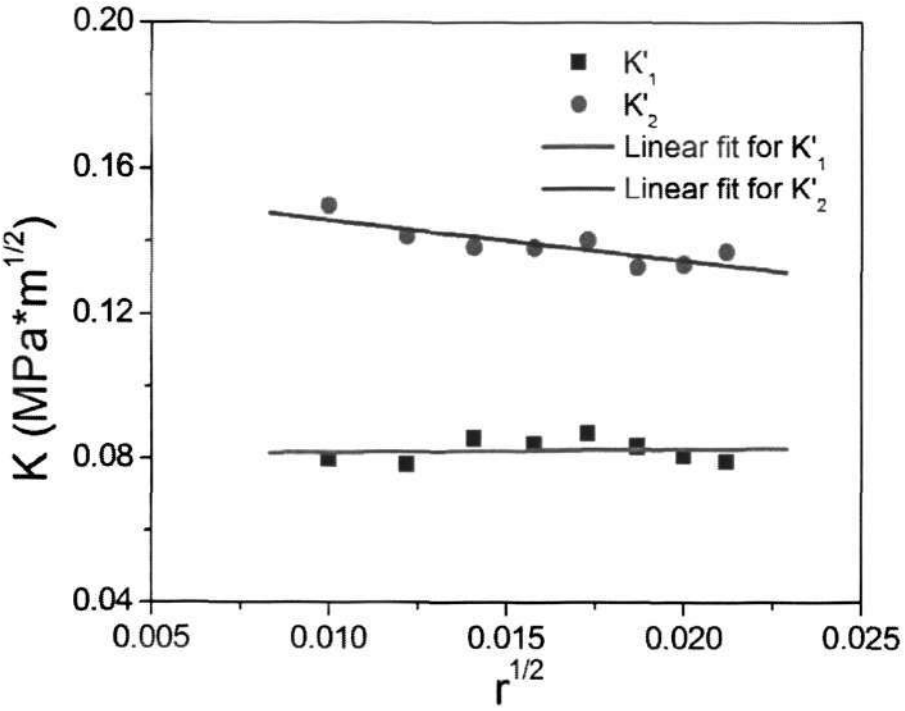

Fig. 5.9 Determination of extrapolation according to linear relationship

With this method, the values of SIFs at different hygrothermal aging times were determined and the results are presented in Fig. 5.10. It was observed that a large percentage of increase in toughness occurred at the early stage of aging, which was the same as the strain gradients calculated at the interface. K_1 increased 33% and K_2 increased 23% respectively. Both K_1 and K_2 increased in the asymptotic manner, which were similar to the moisture diffusion nature in the underfill material. On the other hand, the asymptotic curve suggested that the change of the fracture behavior induced by moisture absorption was gradual rather than instant, although the in-plane surface measured was under saturated moisture concentration at the boundary.

ATTENTION: The Singapore Copyright Act applies to the use of this document. Nanyang Technological University Library

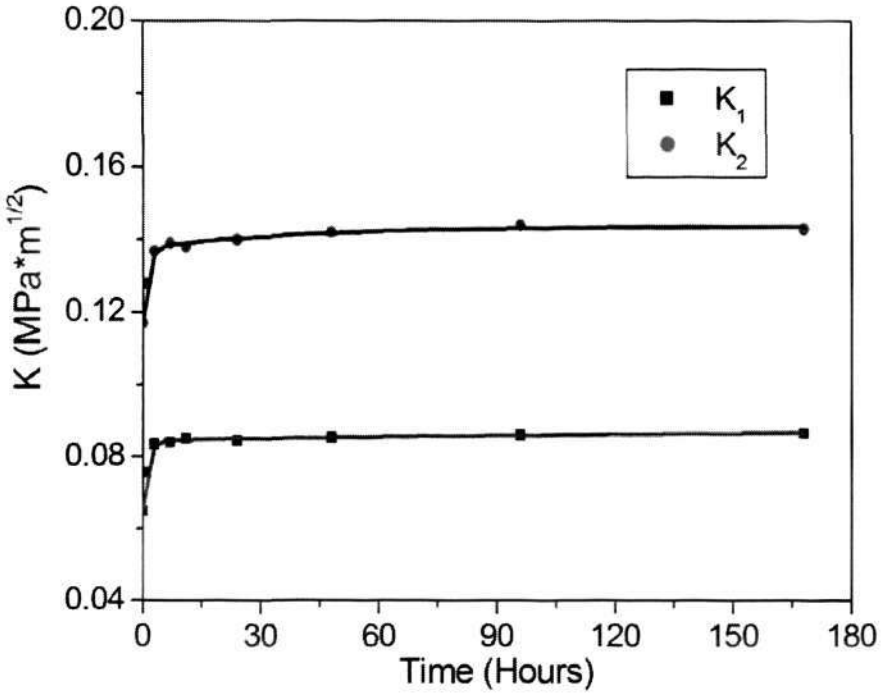

Fig. 5.10 K_1 and K_2 with respect to different hygrothermal aging time (85 °C/85%RH)

The values of SIF under thermal aging were determined and the results are plotted in Fig. 5.11. It is noted that both K_1 and K_2 reduced faster at the beginning. It was thought that the creep behavior of underfill and solder joints greatly relieved the part of stresses and thereby prevented interfaces from cracking (Wang et al. 1998). Likely, it was observed in this study, for an assembly with crack, the time effect could play a considerable role on fracture toughness although the change of the CTODs were in the small scale.

Therefore, both strains and SIFs showed that the time effect was significant in hygrothermal aging, especially at the high temperature. In addition, it can be seen that the magnitude of stresses or fracture parameters on time effect was

ATTENTION: The Singapore Copyright Act applies to the use of this document. Nanyang Technological University Library

comparable to that on hygrothermal induced swelling. Therefore, the results indicate that the interfacial toughness induced by the moisture swelling may be overestimated if the time effect is not considered. Since the interfacial toughness is an important parameter to evaluate the life of assembly during thermal cycling (Paris & Erdogan 1963, Lau, Chang & Lee 2001), the greater change of the interfacial toughness will result in shorter reliability life eventually. Therefore, if the overestimated fracture toughness is used to calculate the fatigue life under moisture conditioning, the reliability issues tend to be more severe and give improper estimation. As a result, it is obvious that viscosity (time-temperature behavior) of underfill is of necessity to be included in the reliability study.

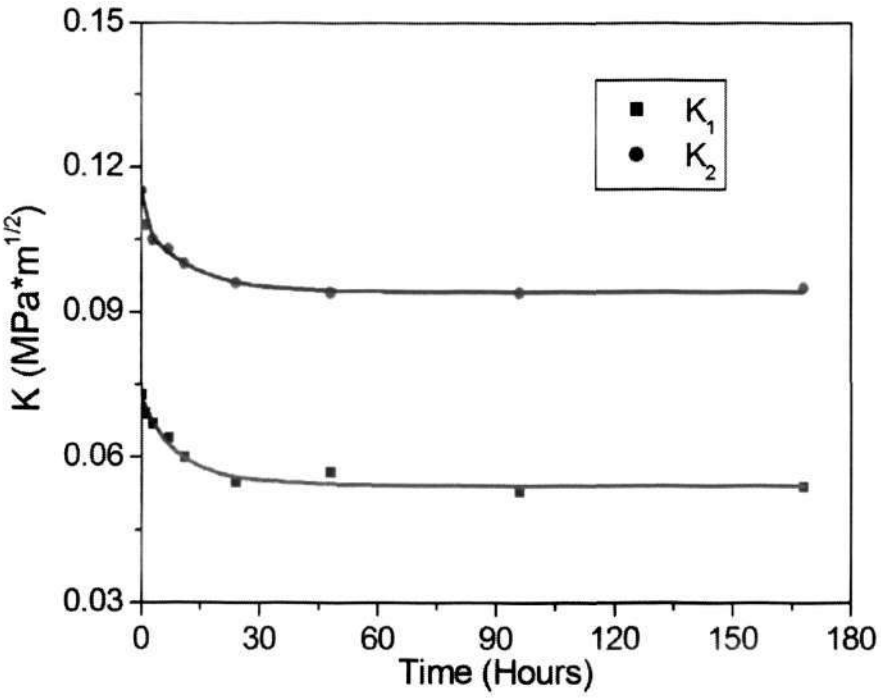

Fig. 5.11 K_1 and K_2 with respect to different thermal aging time (85 °C)

ATTENTION: The Singapore Copyright Act applies to the use of this document. Nanyang Technological University Library

5.5 Summary

In this study, moiré interferometry with miniaturized moisture chamber was used to investigate the deformation as well as interfacial toughness of a cracked FCOB assembly during 168 hours of exposure at 85 °C/85%RH. The thermal aging test at 85 °C was carried out to separate two time-effects, i.e. moisture diffusion induced swelling and stress relaxation caused by the viscoelasticity of underfill.

In strain calculation at the interface of Si/underfill, both hygrothermal loading and thermal aging are found to have significant effect. It is also found that thermal aging relieved the stresses induced by hygrothermal mismatch between dissimilar materials involved. As a result, thermal aging effectively prevented interfaces from fracture propagation. Further study on fracture parameters presented the same trend as the conclusions made in strain gradients study. Since the magnitude of strains and SIFs of thermal aging and hygrothermal loading were quantitatively comparable, time effect was supposed to be considered in hygrothermal aging. The viscoelasticity nature of underfill was found to be beneficial to assembly reliability since it reduced the strains and SIFs induced by material swelling during moisture immigration. In case of simulation of hygrothermal conditioning, the creep behavior of underfill material, i.e. viscoelastic properties of underfill material should be included to alleviate the potential fracture threat since time effect can do positive impact on reliability of assembly. Otherwise, since both temperature and moisture have analogous effect on assembly deformation, it is likely to overestimate the moisture swelling induced failure if temperature-moisture superposition principle is to be applied.

ATTENTION: The Singapore Copyright Act applies to the use of this document. Nanyang Technological University Library

Chapter 6 Characterization of Interfacial Fracture Toughness of Si/Underfill

6.1 Introduction

Interfacial cracking between underfill and its adherends initiates during thermal cycling, which introduces interfacial shear stress concentration as a result of solder joint failure and its extension into the die (Bartoszyk et al. 2000). The defects at the underfill/silicon interface can be microcracks that lead to serious reliability issue of interface delamination in flip chip assembly. Interfacial fracture toughness, which is a measure of resistance of interface to fracture, is usually used as a fracture criterion of underfill/silicon interface. However, limited work has been carried out in the field of characterizing critical interfacial fracture toughness for flip chip assembly till recently.

Commonly, two categories of methods are used in the measurement of critical fracture toughness. One is based on analytical method. Different three-point-bending (TPB) and four-point-bending (FPB) test based experimental methodologies have been developed to characterize the interfacial fracture toughness at different temperatures (Yan & Agarwal 1998, Jiao et al. 1998). However, these testing techniques are not suitable for the measurement of wide range of mode mixity since they vary the mode mixity only by changing the thickness ratio of adjacent layers. Therefore, the data obtained from those methodologies may not represent real fracture toughness of the interface, as during service conditions the interface is subjected to mixed mode loading (Pang et al.

ATTENTION: The Singapore Copyright Act applies to the use of this document. Nanyang Technological University Library

2002). In order to achieve wide mode mixity, the cracked Brazilian disk was introduced to analytically measure the combined mode fracture (Atkinson et al. 1982, Wang & Suo 1990). The second category is FEA-assisted method, which resorts to FEA commercial software to acquire the fracture parameters with the sources of original experimental data (Wang et al. 1998, Pang et al. 2002). Kuhl and Qu (2000) also used Brazil-nut specimens to quantitatively characterize interfacial fracture toughness over a wide range of phase angles, whose solutions to non-dimensional calibrations factors were based on finite element simulations.

In the establishment of interfacial reliability, the configuration of the package and the loading condition (e.g. temperature, external force and creep/relaxation) lead to complexity in reliability evolution. Some errors may be introduced in the determination of interfacial fracture toughness by inaccurate materials description and package structure configuration. Therefore, it is of importance to develop advanced experimental measurement techniques for the characterization of the interfacial fracture toughness and the validation of the findings of theoretical solution and numerical results.

In this study, with a specially designed brazil-nut (BN) specimen type B as illustrated in section 3.2.2, digital image correlation (DIC) technique was employed to characterize the interfacial fracture toughness of underfill/silicon interface under various loading angles from 20° to 90° over a wide temperature range from 25 °C to 125 °C and 85 °C/85%RH hygrothermal aging, to study the effects of loading angle, temperature and moisture effects on the interfacial fracture toughness. The material properties of underfill and silicon can be determined with the method introduced in Shi et al. (2004) and the results are summarized in Table 6.1.

ATTENTION: The Singapore Copyright Act applies to the use of this document. Nanyang Technological University Library

In order to examine the findings of μ-DiSC technique, an interfacial fracture mechanics based finite element (FE) model was implemented into ANSYS™ to calculate the values of crack-tip opening displacement (CTOD) of underfill/chip with different temperatures and loading angles. Furthermore, the effects of temperature, moisture and mode mixity on fracture toughness and fractography of underfill/chip interface were investigated.

Table 6.1 Material Constants used for underfill and silicon

Constants	Temperature (°C)		
	25	75	125
Effective modulus E* (*GPa*)	11.18	8.29	0.81
Material constant ε	0.0695	0.0709	0.0744

6.2 Interfacial Fracture Toughness under Temperature Loading

Following the test programs described in section 3.5.1.3, the interfacial fracture toughness of Si/underfill over a wide range of temperatures and loading angles was characterized using specimen type B.

6.2.1 Critical Load Level

There are two sets of experimental data that can be obtained during fracture toughness test. Apart from images recorded by the μ-DiSC system, the load-time/load-displacement curves were saved by Instron® system. The data were a reference for the choice of image before fracture occurred as well as the source of

ATTENTION: The Singapore Copyright Act applies to the use of this document. Nanyang Technological University Library

data for determination of critical load level for FEA simulation. In this work, both the time and fracture load were recorded throughout the whole loading history. Fig. 6.1 shows typical load-displacement curve in fracture toughness measurement for underfill/chip interface. With the acquisition of tensile data, images and critical load can be determined subsequently.

The experimental results of critical force are represented in Fig. 6.2 and Table 6.2. From the results, it can be seen that critical force increased rapidly when the loading angle decreased, especially when the loading angles were lower than 45°. This indicated that loading in shear dominant mode could sustain more force or fracture toughness than loading in opening dominant mode.

At large loading angle (90°, 75° and 60°), it was thought that mode I open loading dominated, indicating that the interface delamination was governed by the mode I opening loading under mode I/mode II loading mixity. When the loading angle was smaller than 45° (45°, 30°, 20°), mode II shear loading inversely dominated, meaning that interface delamination was governed by the mode II opening loading under mode I and mode II loading mixity.

From the figure, it can be seen that the relation between loading and loading angle also indicated that the interface is stronger in mode II dominated fracture (during 45°, 30°, 20°) than in mode I dominated fracture (during 90°, 75°, 60°). Therefore, the interface of Si/underfill is more liable to delaminate when the structure is subjected to the loading with opening mode (mode I).

ATTENTION: The Singapore Copyright Act applies to the use of this document. Nanyang Technological University Library

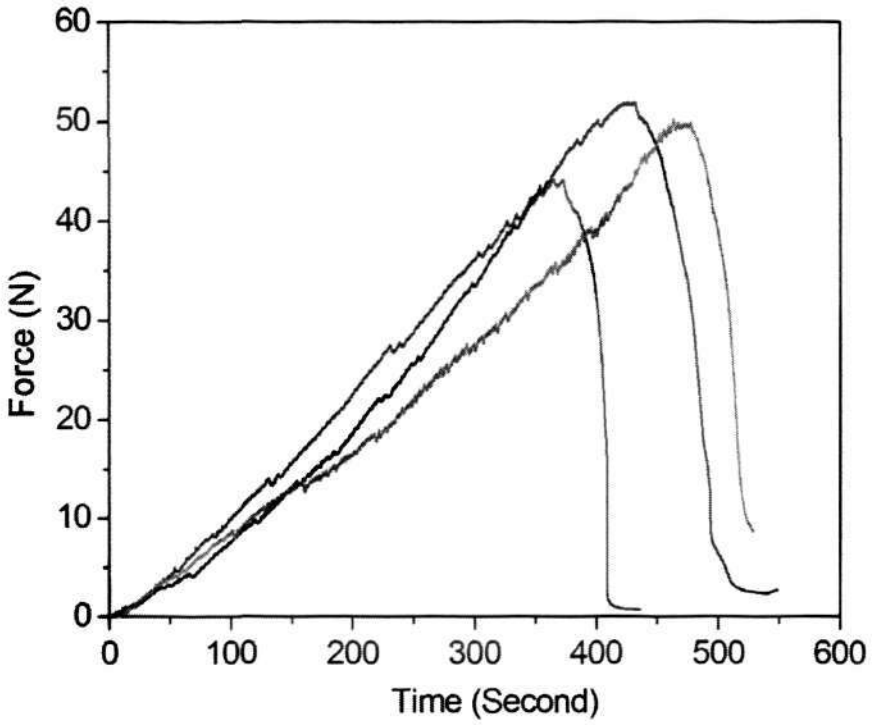

Fig. 6.1 Three load-displacement curves obtained from the fracture toughness test at the temperature of 125 °C and under the loading angle of 60°

Table 6.2 Critical load with different temperatures and loading angles

Temperature / L. A.	25 °C		75 °C		125 °C	
	Ave. (N)	Err. (N)	Ave. (N)	Err. (N)	Ave. (N)	Err. (N)
90°	71.433	±7.638	67.900	±2.513	34.303	±1.965
75°	75.833	±4.692	71.793	±4.387	41.753	±3.054
60°	86.606	±2.568	82.680	±3.602	51.790	±3.402
45°	104.436	±6.487	98.796	±6.355	62.103	±3.550
30°	145.233	±5.320	127.233	±5.050	80.986	±4.416
20°	196.053	±3.355	166.513	±9.501	103.033	±4.945

L.A.=Loading Angle; Ave.=Average; Err.=Error.

ATTENTION: The Singapore Copyright Act applies to the use of this document. Nanyang Technological University Library

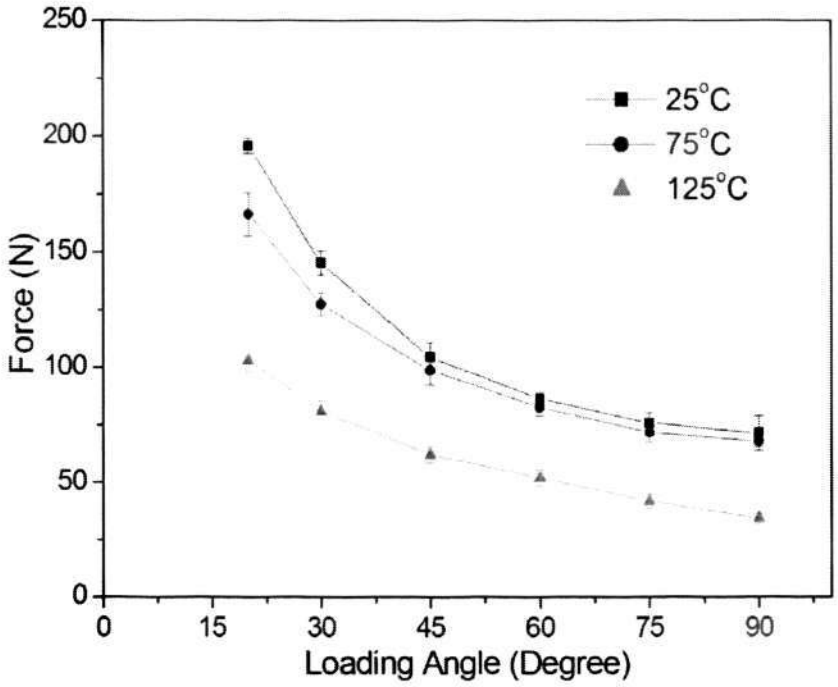

Fig. 6.2 Critical forces with respect to different loading angles

6.2.2 Fracture Toughness Characterization

With the digitised images obtained before and after deformation, the displacement distribution around the crack-tip can be determined using the correlation software. The representative displacement fields along crack flanks are shown in Fig. 6.3. With the correlation software, the CTODs can be obtained along two crack flanks. The typical CTOD distributions along crack franks obtained from different loading angles and temperatures are shown in Fig. 6.4. δ_y was found to increase with the distance away from the crack-tip, while δ_x was observed to remain at almost the same level when the distance increased. With the measured

ATTENTION: The Singapore Copyright Act applies to the use of this document. Nanyang Technological University Library

data of CTODs, the nominal SIFs at certain distance away from the crack-tip were calculated with Eq. (4.8) and Eq. (4.9). The corresponding nominal $K_1^{'}$ and $K_2^{'}$ with respect to the distance away from the crack-tip are shown in Fig. 6.5. It can be seen that when the r/L ratio ranges from 0.2 to 0.9, an approximate linear relationship existed with the distance away from the crack-tip. Accordingly, a linear extrapolation method was developed and implemented to determine the critical fracture toughness at the crack-tip. It was noted that both nominal $K_1^{'}$ and $K_2^{'}$ showed approximately linear relationships with the normalized distance away from the crack-tip. With the linear extrapolation method explained in section 4.8 and section 5.4, the values of K_1 and K_2 at the crack-tip were then determined respectively. For instance, the K_1 and K_2 for the condition of 25°C and 90 degree was determined to be 0.45 $MPa \cdot m^{1/2}$ and 0.05 $MPa \cdot m^{1/2}$. Since the data were determined for the critical load, they were defined as the interfacial fracture toughness for the condition of 25 °C and 90 degree. Using the same method, the values of interfacial fracture toughness were determined for the temperature of 25°C but different loading angles of 75, 60, 45, 30 and 20 degree.

ATTENTION: The Singapore Copyright Act applies to the use of this document. Nanyang Technological University Library

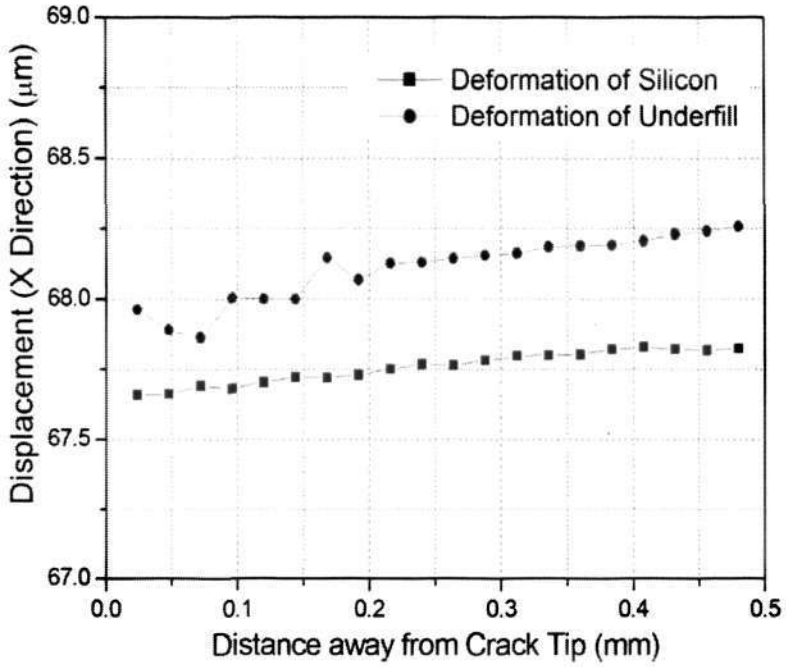

(a)

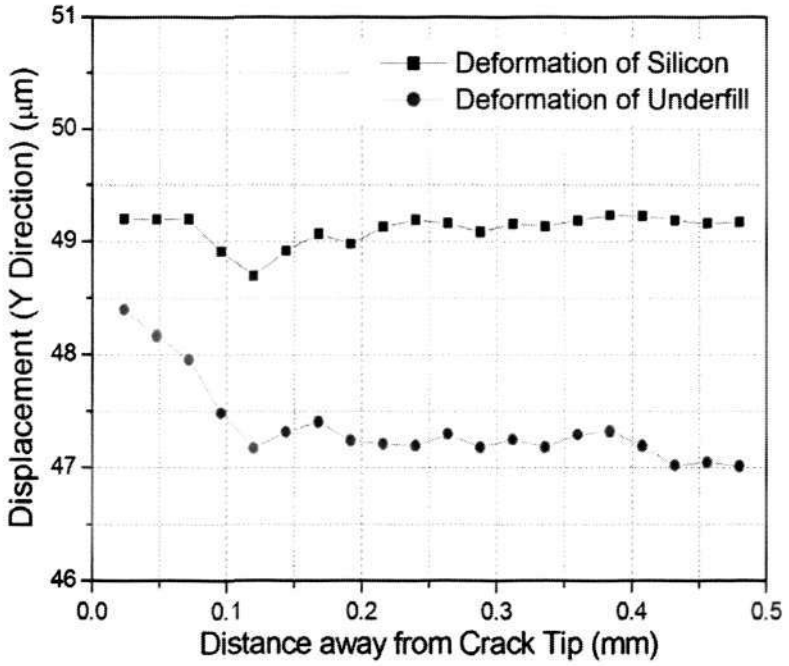

(b)

Fig. 6.3 Representative displacement field along crack flanks at 75 °C and loading angle 75°: (a) x displacement; (b) y displacement

ATTENTION: The Singapore Copyright Act applies to the use of this document. Nanyang Technological University Library

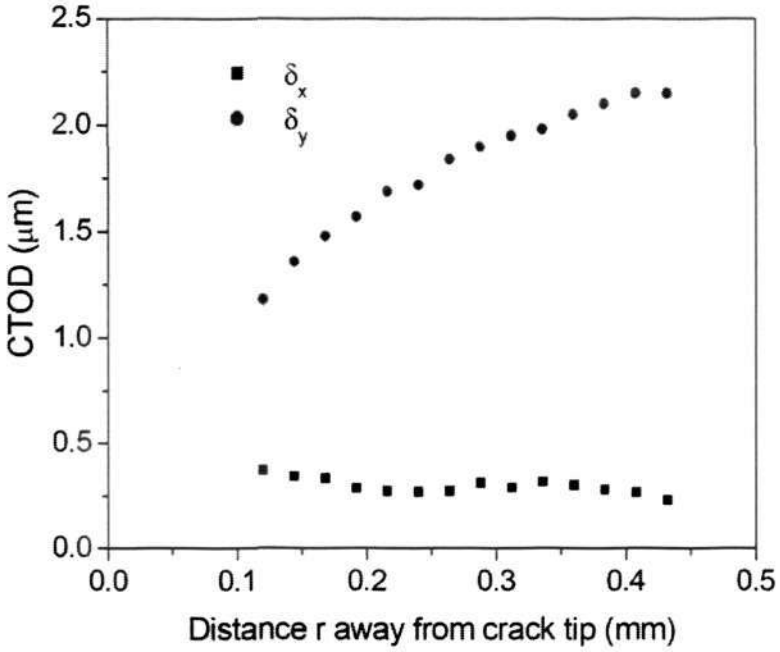

(a)

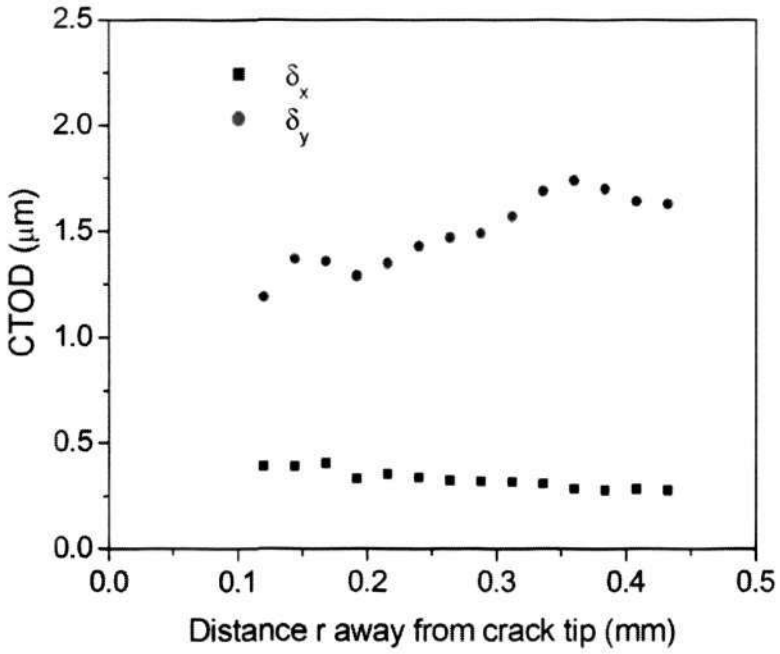

(b)

ATTENTION: The Singapore Copyright Act applies to the use of this document. Nanyang Technological University Library

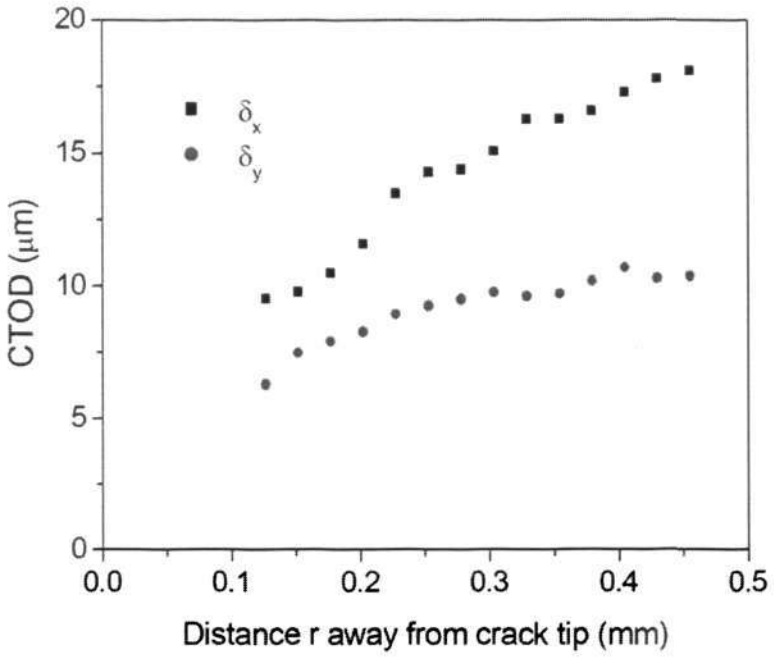

(c)

Fig. 6.4 Typical CTOD distribution. (a) temperature 25 °C and loading angle 90°; (b) temperature 25 °C and loading angle of 60°; (c) temperature 125 °C and loading angle of 20°

ATTENTION: The Singapore Copyright Act applies to the use of this document. Nanyang Technological University Library

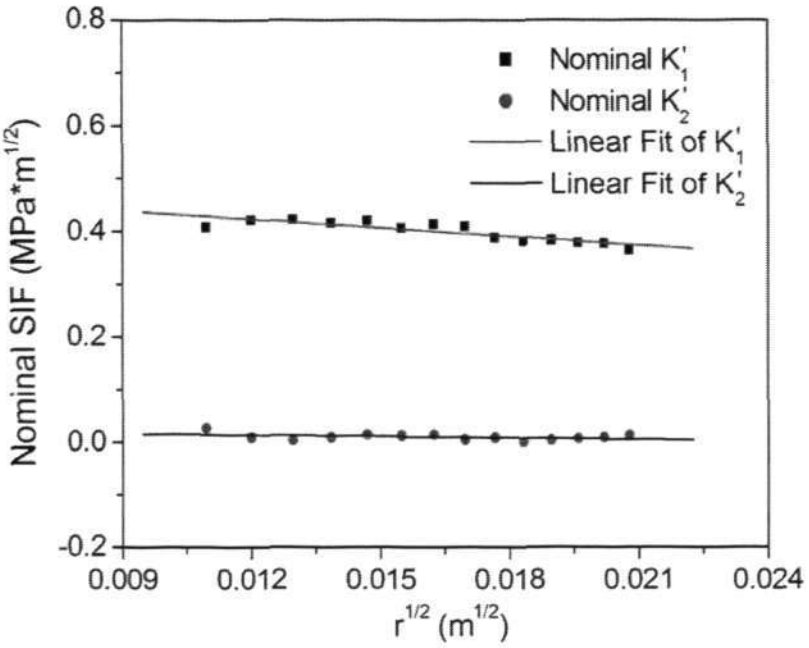

(a)

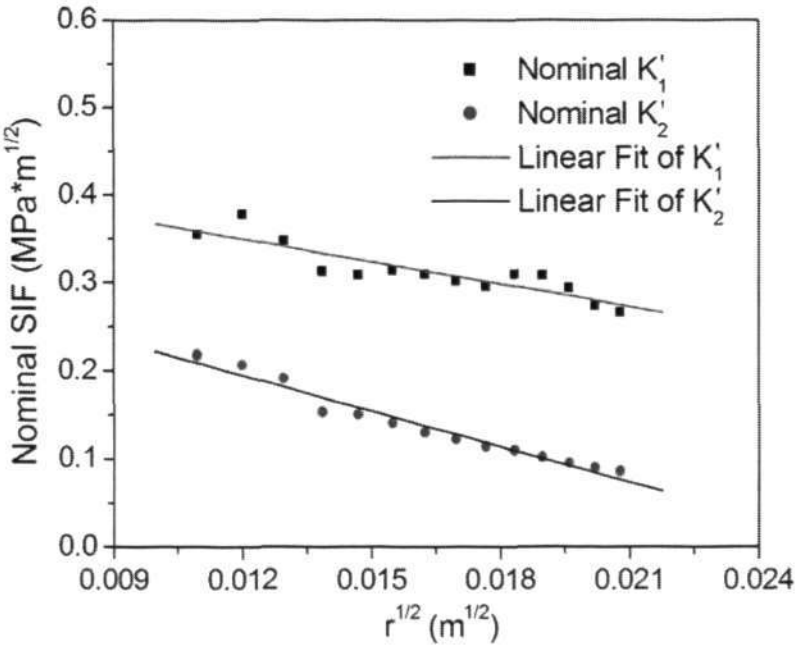

(b)

ATTENTION: The Singapore Copyright Act applies to the use of this document. Nanyang Technological University Library

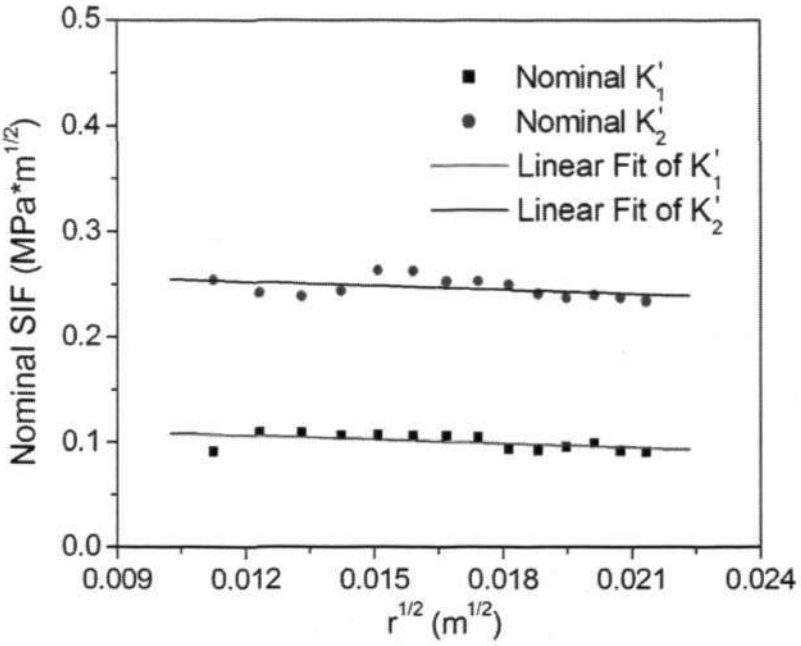

(c)

Fig. 6.5 Typical nominal SIFs. (a) temperature 25 °C and loading angle 90°; (b) temperature 25 °C and loading angle of 60°; (c) temperature 125 °C and loading angle of 20°

6.2.3 Effect of Loading Angle on Interfacial Fracture Toughness

As a result, the fracture toughness for underfill/chip interface can be calculated with respect to different loading angles and temperatures. Fig. 6.6 shows the effect of loading angles on the critical toughness for BN specimen at room temperature. It was noted that the mode I interfacial toughness increased with increasing loading angles, while the mode II interfacial toughness decreased with increasing loading angle. Moreover, with the loading angle getting smaller, K_2 increased rapidly, while K_1 dropped slowly even when the shear mode seemed to play a dominant role on fracture behavior. This observation implied that even if the fracture behavior and the critical fracture load were shear-dominant, K_1 still could

ATTENTION: The Singapore Copyright Act applies to the use of this document. Nanyang Technological University Library

significantly affect the fracture tolerance at the end. The phase angles with respect to the loading angles are given in Fig. 6.7. As seen, the phase angle increased with a decrease on loading angle, indicating the fracture mixity changed from mode I dominant to mode II dominant fracture. The observation showed that the Brazil-Nut specimen type B could effectively achieve a wide range of mode mixity by varying the loading directions from 90° to 20°. It was found that the relation between phase angle and loading angle was generally linear, which indicated that one could control the expected phase angle by manipulating the loading angle considering linearity relationship.

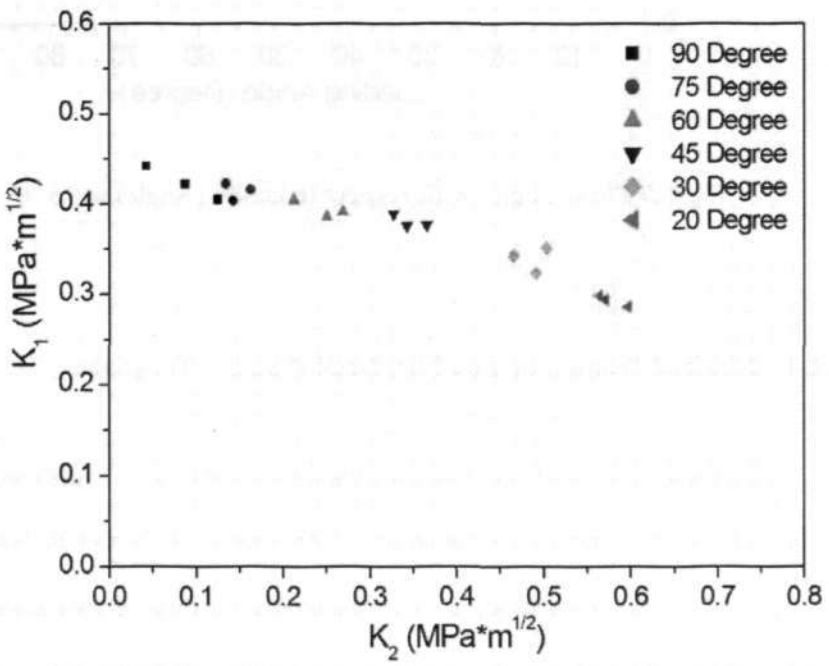

Fig. 6.6 Mode I and mode II interfacial fracture toughness obtained at the temperature of 25 °C but different loading angles

ATTENTION: The Singapore Copyright Act applies to the use of this document. Nanyang Technological University Library

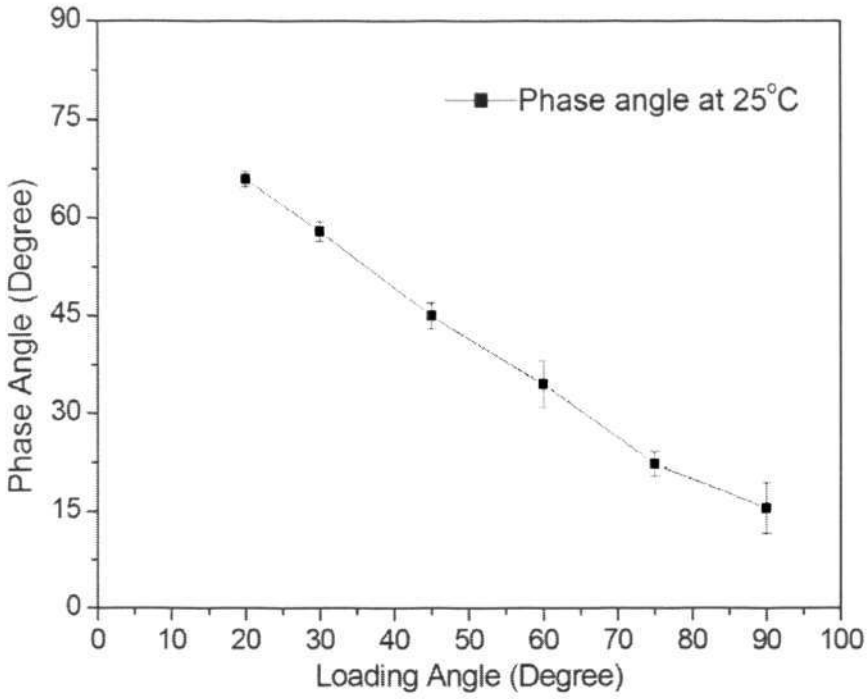

Fig. 6.7 Phase angles with respect to loading angles at 25 °C

6.2.4 Effect of Temperature on Interfacial Fracture Toughness

Similarly, the interfacial fracture toughness at other two temperatures of 75 °C and 125 °C for different loading angles of 90, 75, 60, 45, 30 and 20 degree were measured. Fig. 6.8 represents all the data obtained at the three temperatures and six loading angles. It was found that for the two temperatures, both mode I and mode II interfacial fracture toughness exhibited similar trends as observed at the temperature of 25 °C. When the temperature increased, the values of mode I and mode II interfacial fracture toughness became smaller. However, the temperature effect showed nonlinear trend. Compared with the temperature of 25 °C, both

ATTENTION: The Singapore Copyright Act applies to the use of this document. Nanyang Technological University Library

mode I and mode II interfacial fracture toughness were observed to reduce slightly at the temperature of 75 °C, but they were found to drop tremendously at the temperature 125 °C. The possible reason for the phenomenon was that the transition temperature of the underfill was 105 °C (Shi, Wang & Pickering 2003), when the temperature was above 100 °C, the epoxy matrix was in the transition from the glassy state to rubbery state, the strength of the cross-links in the matrix decreased largely and the material strength was reduced sharply, causing the large reduction in the interfacial fracture toughness.

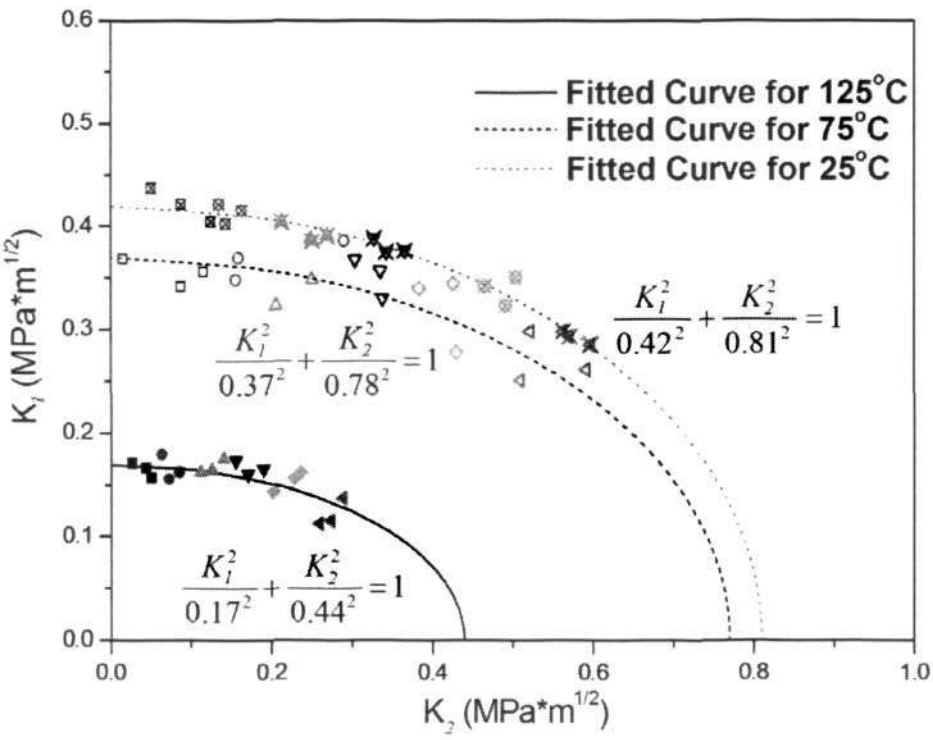

Fig. 6.8 Failure assessment diagram (FAD) determined with the interfacial toughness results obtained at different temperatures and loading angles

ATTENTION: The Singapore Copyright Act applies to the use of this document. Nanyang Technological University Library

With the experimental data, the curve fitting was performed for the three temperatures, and empirical equations were obtained. Based on the equations, a failure assessment diagram (FAD) was established, as displayed in Fig. 6.8. The diagram can be used for reliability design of the silicon/underfill/silicon sandwiched system. In other words, for any given temperature, when the fracture toughness of an interface fell inside the area defined by the boundary and x and y axes, the interface was safe, otherwise, it would open and caused interface delamination problem. For instance, the interfacial toughness at 125 °C obtained from moiré experiment, as illustrated in chapter 4, was 0.030 for K_1 and 0.034 for K_2. The corresponding point fell inside the FAD tested at 125 °C, which means the interface was safe for the first temperature cycling.

6.2.5 FEA Simulation

FEA simulation was performed to make comparison with experimental results, using commercial FE software ANSYS™ 6.1. In this verification, 2D plane strain was taken as the assumption of SBN specimen. Some assumptions are made: a) perfect bond of materials except the pre-crack region; b) the properties of underfill is temperature dependent; c) only crack propagation is considered, there is no crack initiation. The typical numerical model and zoned-in area around the crack-tip are plotted in Fig. 6.9. The model was meshed with 2D solid 95 eight-node elements, including a total of 2554 elements and 7871 nodes. The element size at the crack tip is 0.01 *mm* compared with overall crack size 4 *mm*. According to the critical load obtained from the mechanical test, the CTOD distribution along the crack franks can be simulated. Typical results are presented in Fig. 6.10. For

ATTENTION: The Singapore Copyright Act applies to the use of this document. Nanyang Technological University Library

comparison, both experimental and simulation results are combined in the figure with respect to different loading angles. Both trend and value of CTODs determined by the correlation technique were close to those obtained from the simulation. The match indicates that the μ-DiSC correlation methodology could be used as an accurate method for the determination of the interfacial fracture toughness.

Comparison of nominal SIFs is subsequently given between experimental and simulation, as is plotted in Fig. 6.11. The extrapolation method was then used to determine the fracture toughness at the crack-tip. By curve-fitting the numerical results and linearly extrapolating nominal SIFs to *y*-axis, the fracture toughness was determined from the intersection, as shown in Fig. 6.11. By repeating the above procedures, the SIFs with respect to different loading angles were obtained, which is shown in Fig. 6.12. The comparison of critical toughness obtained from the experiment and simulation can consequently made referring to Fig. 6.8 and Fig. 6.12, which showed same trend between each other. Through the comparison for all data acquisition procedures, it can be seen that the experimental methodology can well determine the interfacial fracture toughness for different loading conditions.

ATTENTION: The Singapore Copyright Act applies to the use of this document. Nanyang Technological University Library

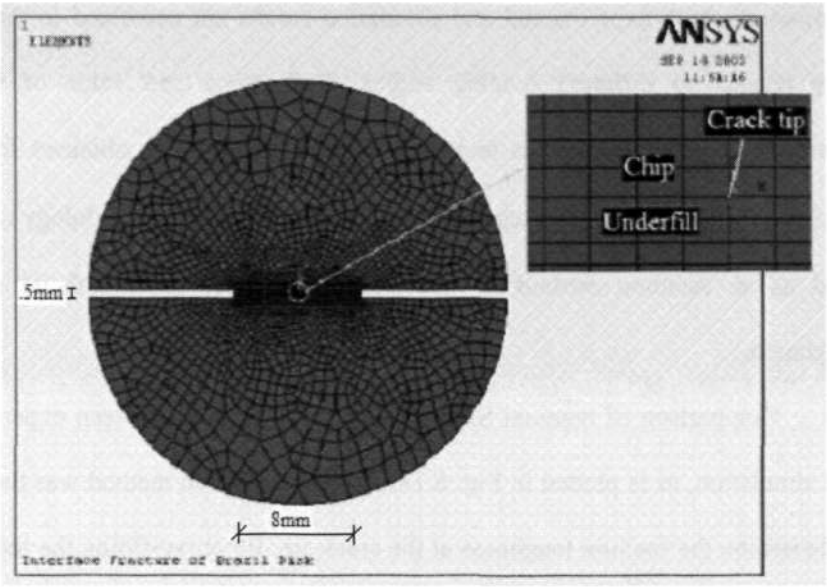

Fig. 6.9 FEA model used in the simulation

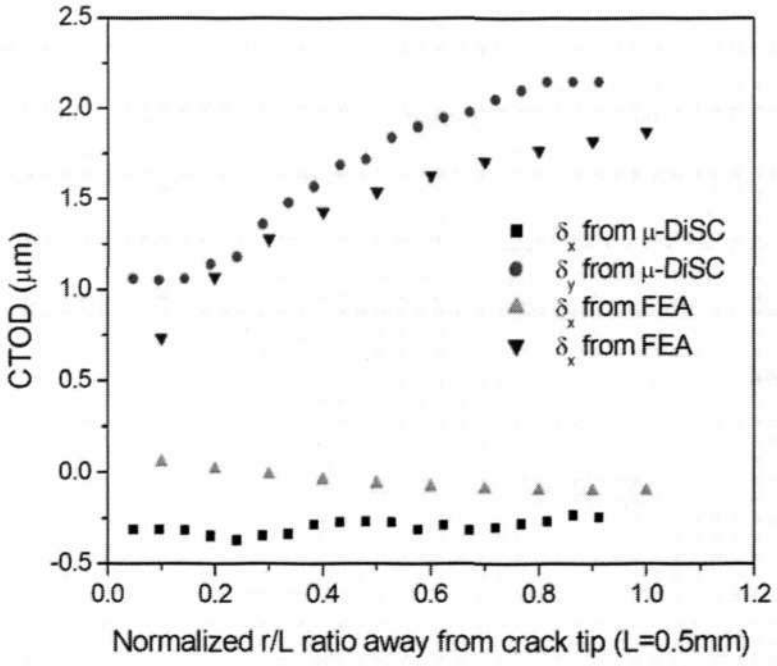

(a)

ATTENTION: The Singapore Copyright Act applies to the use of this document. Nanyang Technological University Library

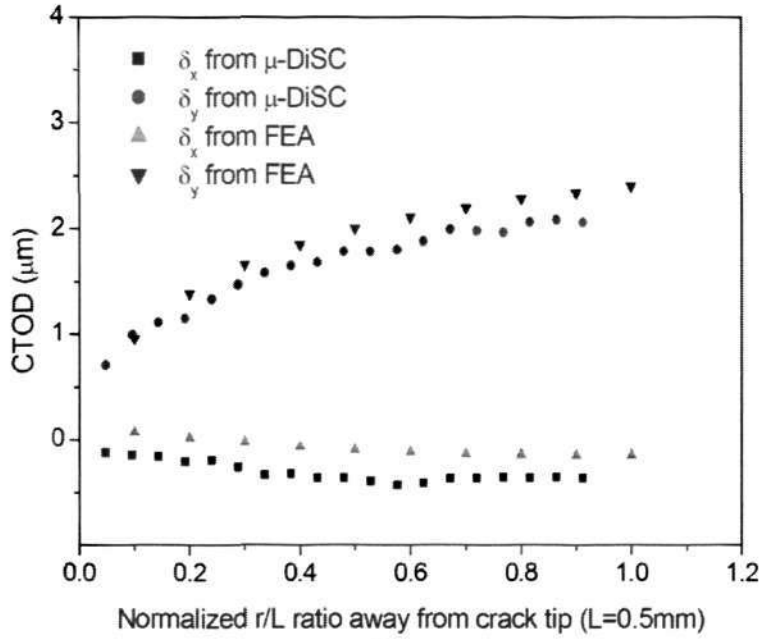

(b)

Fig. 6.10 Comparison of CTOD distribution. (a) temperature 25 °C and loading angle 90°; (b) temperature 75 °C and loading angle 90°

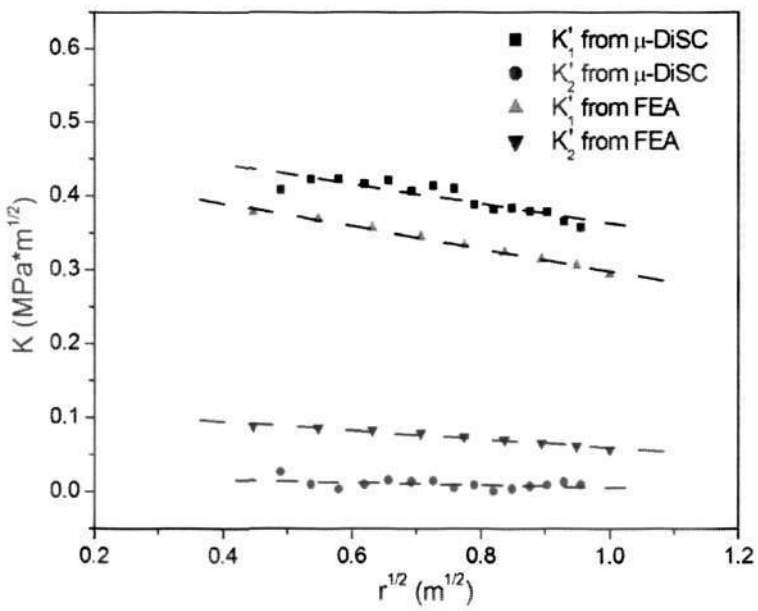

(a)

ATTENTION: The Singapore Copyright Act applies to the use of this document. Nanyang Technological University Library

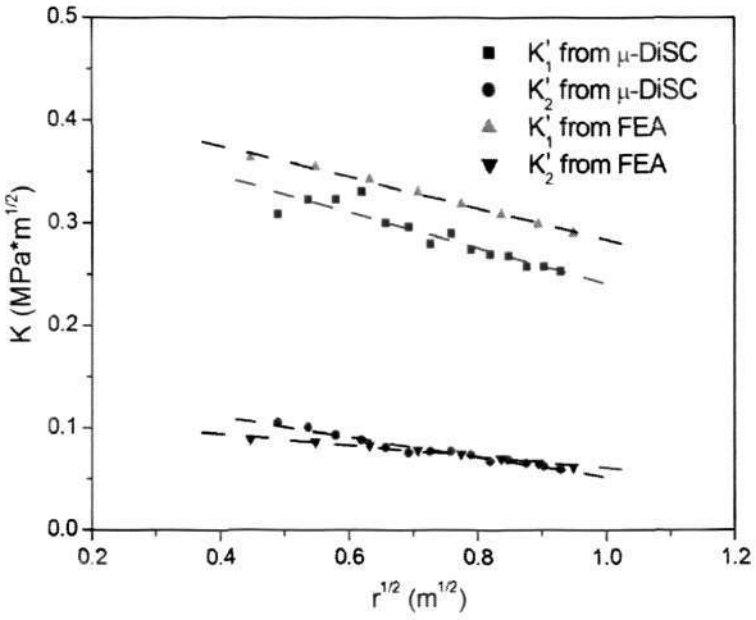

(b)

Fig. 6.11 Comparison of K distribution. (a) temperature 25 °C and loading angle 90°; (b) temperature 75 °C and loading angle 90°

ATTENTION: The Singapore Copyright Act applies to the use of this document. Nanyang Technological University Library

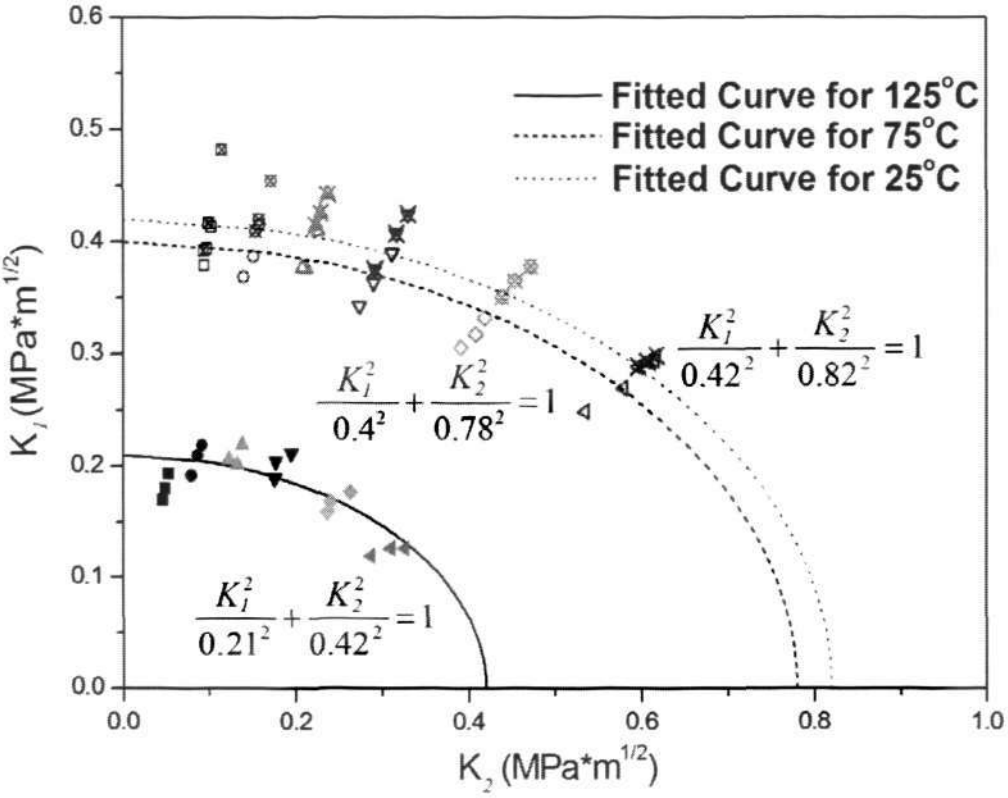

Fig. 6.12 Finite element results for FAD determined with the interfacial toughness results obtained at different temperatures and loading angles

As mentioned in section 4.8, K_{eff} decreased as stress relaxation happened in the glass transition state of underfill. However, one cannot determine that the most dangerous stage in thermal cycling was located at the point with highest K_{eff}, since the interfacial toughness varies with the mode mixity at the same time (Hutchinson and Suo 1992). Referring to Eq. (4.13), the value of K_{eff} becomes a curve as a function of mode mixity ψ rather than an independent point. Therefore, the smaller phase angle has corresponding smaller K_{eff}, since mode I failure is more fatal than mode II. In order to examine the possibility of assembly failure, the ratio of effective interfacial toughness K_{eff} and critical interfacial toughness K_{Ceff} was

ATTENTION: The Singapore Copyright Act applies to the use of this document. Nanyang Technological University Library

introduced to describe the fracture behavior of underfill/chip interface under ATC loading. As a result, the ratio of K_{eff} and K_{Ceff} at 75 °C was found to be smaller than that at 125 °C, i.e. $\left(\frac{K_{eff}}{K_{Ceff}}\right)_{75^\circ C} = 0.185 < \left(\frac{K_{eff}}{K_{Ceff}}\right)_{125^\circ C} = 0.2$. This showed that 125 °C was supposed to be the most catastrophic point during high temperature loading. Similarly, the ratio of K_{eff} and K_{Ceff} at –40 °C was determined to be 0.4, which is even greater than the ratio at 125 °C. It implied that it is also possible to induce crack propagation at –40 °C. Therefore, it is expected that interface delamination is prone to propagate at both extreme temperatures, i.e. 125 °C and –40 °C, during thermal cycling.

6.2.6 Failure Mode Analysis

6.2.6.1 Temperature Effect

Following the mechanical test for each BN specimen type B, the fracture morphology was studied using scanning electron microscope (SEM). It was observed that the fracture morphology changed significantly with respect to the loading angle and temperature under fracture toughness test. At 25 °C and 75 °C, crack kinking into the interior of silicon was observed. The typical SEM photo at room temperature is shown in Fig. 6.13 a). The fracture resistance of silicon is determined to be 1.2 $GPa \times m^{1/2}$, which is around 3 times higher than the interfacial critical fracture toughness (0.4 $GPa \times m^{1/2}$). Although fracture should follow the path requiring the lower delamination energy, the specimen exhibit kinking into silicon. This preference for a high-energy path over a low energy path in close proximity highlights the importance of understanding the mechanics of crack path

ATTENTION: The Singapore Copyright Act applies to the use of this document. Nanyang Technological University Library

selection. Wang and Suo (1990) started their cracks on the interface and observed a small amount of interfacial crack growth prior to the crack kinking into the interior of the layer. This observation was similar with the SEM photo in Fig. 6.13(a). The possible explanation is that the kink might result from the initial defect in silicon material. After crack kinking into the silicon material, predominantly opening mode and increasing K_{II} might result from the large elastic mismatch between bimaterials.

When the testing temperature went up to 125 °C, the fracture went along interface between underfill and silicon all the way, indicating ductile delamination might happen during fracture propagation (Fig. 6.13(b)). The possible explanation might be that the T_g of underfill was 105 °C, the increase of plasticity of underfill had a significant effect on delamination behavior, which greatly lowered the interface of delamination energy.

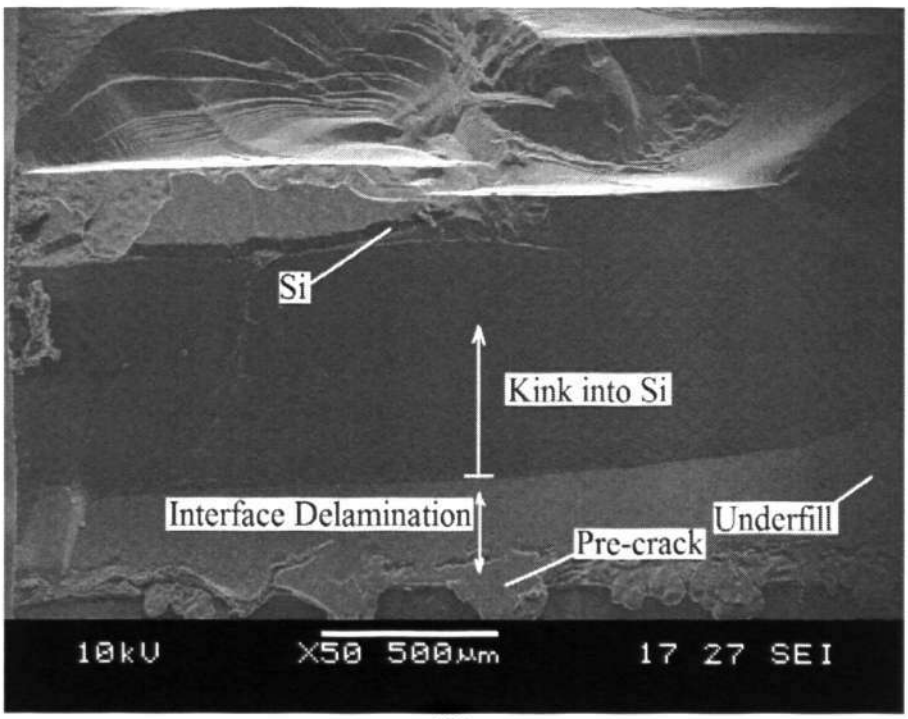

(a)

ATTENTION: The Singapore Copyright Act applies to the use of this document. Nanyang Technological University Library

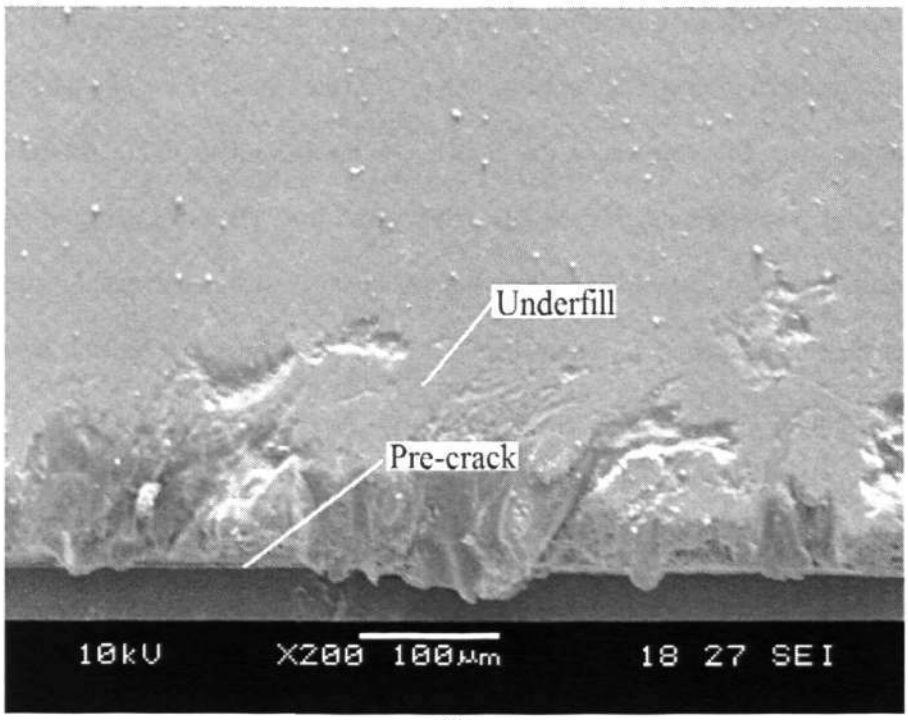

(b)

Fig. 6.13 Effect of temperature on fracture morphology. (a) kinking observed at the temperature of 25 °C and the loading angle is 20°; (b) Pure delamination observed at the temperature of 125 °C and the loading angle of 45°

6.2.6.2 Loading Angle Effect

Since the failure modes at 125 °C with respect to loading angles are pure interfacial fracture propagation, only the effects of loading angles under 25 °C and 75 °C are discussed.

Under mode-I dominated fracture, the main failure happened at the interface between underfill and silicon, as shown in Fig. 6.14(a). In addition, small pieces of silicon leftover were observed at the edge of the specimen type B, as shown in Fig. 6.14(b). The leftover was thought to be the results of initial defects generated during the polishing process in specimen preparation. The interfacial crack may interact with flaws in the layer adjacent to the interface and nuclear

ATTENTION: The Singapore Copyright Act applies to the use of this document. Nanyang Technological University Library

microcrack. The effect of the mixed mode loading is to grow these microcracks back towards the interface (Hutchinson & Suo 1992). The resulting fracture surface will be covered with tiny chunks of the silicon material.

However, under loading angle 60 degree and 45 degree, which were related to mixed mode interfacial fracture, the crack was observed to kink into silicon material, followed by short distance of interfacial delamination. The pyramid-shape kinking crack was generated when crack direction headed to silicon bulk material, as shown in Fig. 6.15. The mechanism of this phenomenon remains an open question. The wavy and rough natures on the silicon were also reported elsewhere (Deegan et al. 2003). However, the mechanism at the interface was not obvious. The possible explanation for this observation was that the fracture energy provided by Instron machine was concentrated on some points of interfacial delamination route due to defects or particles imbedded in the interface. It introduced a high stress concentration at these points. As a result, the fracture kinked into silicon, if fracture energy density was greater than the silicon fracture energy. Subsequently, the dissipation of energy due to the high-speed brittle fracture in the silicon produced the corresponding pyramid shape fracture morphology. The centre of the pyramid silicon, which is the fracture in the bulk silicon, showed higher fracture energy. While the edge of the pyramid silicon, which is the fracture at the underfill/silicon interface, indicated lower fracture energy due to the dissipation of energy.

The crack kinking into silicon was found to be more obvious if loading angle changed to 30 degrees and 20 degrees, as shown in Fig. 6.13(a). The kinking angle was significantly larger than that for the loading angles of 60 and 45 degrees, indicating there contained greater fracture energy prior to kinking for shear

ATTENTION: The Singapore Copyright Act applies to the use of this document. Nanyang Technological University Library

dominated fracture (mode II dominated). A typical kinking was observed with constant kinking angle as large as 52.58 degree, as shown in Fig. 6.16, which was consistent with the simulation results given by Chai and Chiang (1998) and the experimental observation for the single crystal silicon (Cramer, Wanner & Gumbsch 2000). The angles were also indicated the fracture inside silicon was diverted onto the {111} plane, which was 54.7 degree. The difference of kinking angle with respect to various loading angles are thought to be the result of the difference in fracture energy (He & Hutchinson 1989).

ATTENTION: The Singapore Copyright Act applies to the use of this document. Nanyang Technological University Library

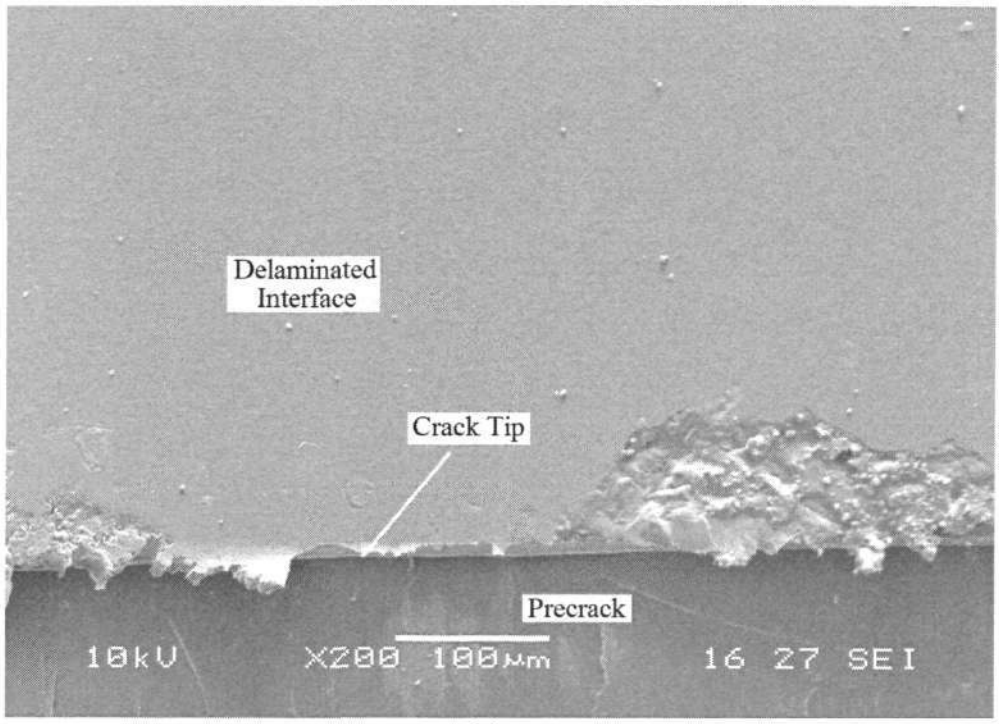

(a)

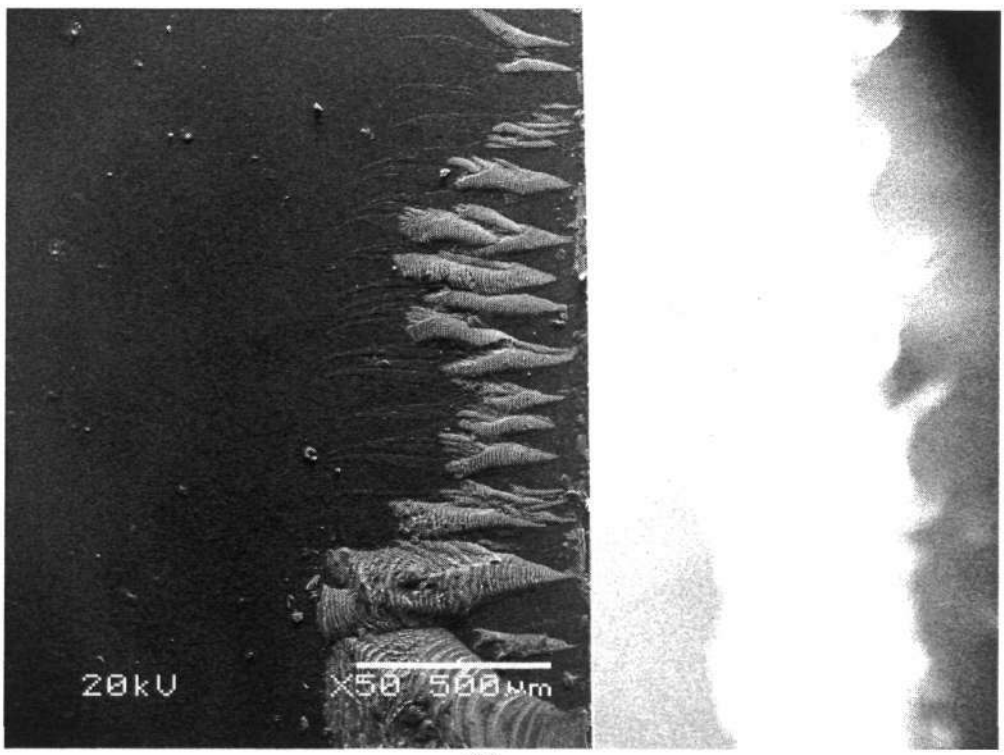

(b)

Fig. 6.14 SEM photo for the fracture morphology with the temperature of 75 °C and the loading angle 90°. (a) interface delamination; (b) silicon leftover at the edge of the specimen

ATTENTION: The Singapore Copyright Act applies to the use of this document. Nanyang Technological University Library

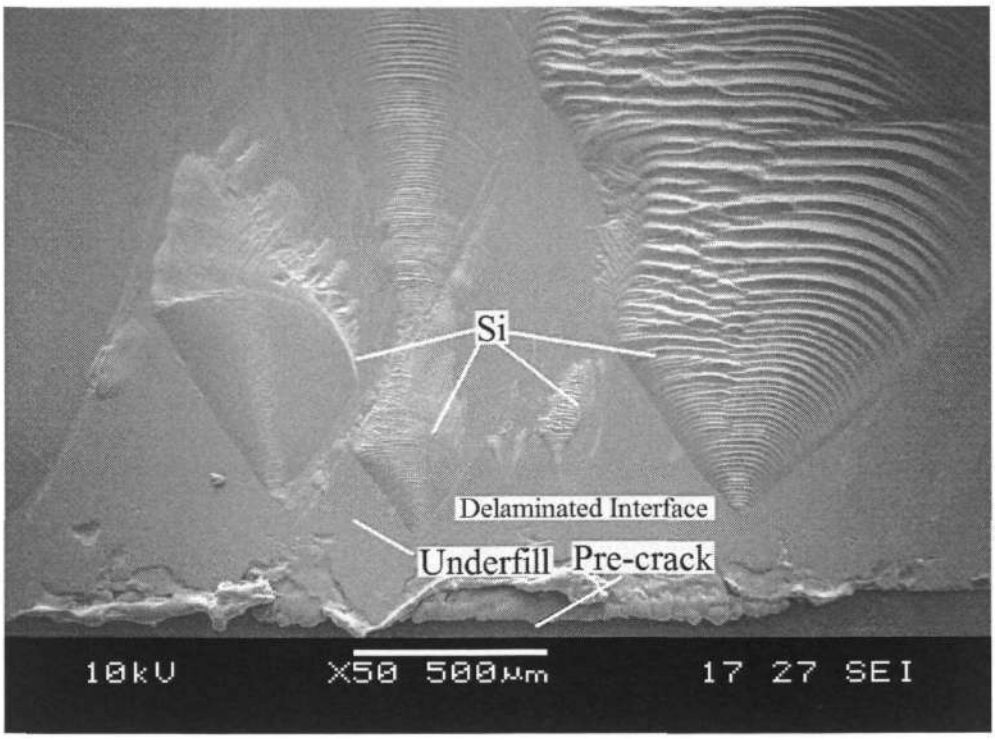

Fig. 6.15 Typical pyramid-shape kinking into silicon observed at the temperature of 25°C and the loading angle of 60 degree

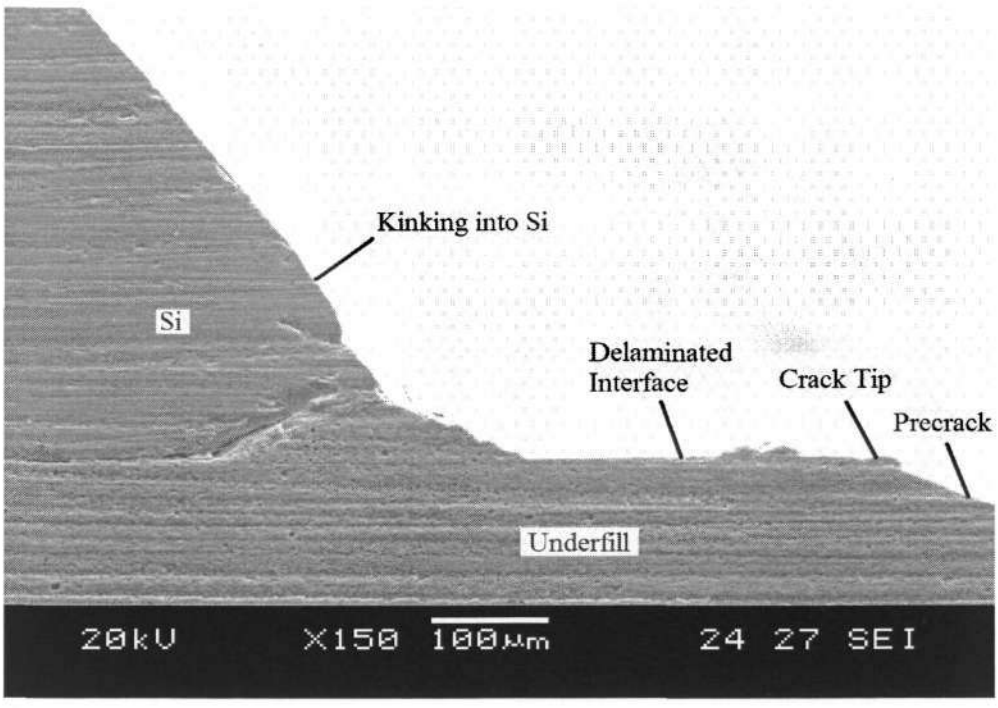

Fig. 6.16 Side view of specimen tested at the temperature of 25 °C and loading angle of 20 degree

ATTENTION: The Singapore Copyright Act applies to the use of this document. Nanyang Technological University Library

6.3 Interfacial Fracture Toughness after Hygrothermal Aging

Micro-digital image speckle correlation (μ-DiSC) technique was applied to measure critical interfacial fracture toughness of Si/UF interface. The measurand showed that moisture would significantly reduce the interfacial strength due to the break of hydrogen bonding. By combining the moiré and μ-DiSC results, it was concluded that the hygrothermal loading would increase the possibility of interface delamination in FCOB. The morphologies of fracture were studied with the aid of SEM. Remarkable changes of failure mode were observed and were related to moisture-induced reaction.

6.3.1 Critical Interfacial Fracture Toughness

Since the values of interfacial toughness under hygrothermal aging, as shown in Chapter 5, were understood, it was easy to quantitatively estimate the possibility of fracture propagation by comparing with the interfacial fracture toughness. Based on the μ-DiSC system and interfacial fracture mechanics, the CTODs obtained in the fracture test were calculated to interfacial fracture toughness with respect to different phase angles. Brazil-Nut-specimen type B was used to achieve this variety. The linear extrapolation method was also used to obtain SIFs at the crack tip. The measured results are presented in Fig. 6.17. It can be seen the interfacial fracture toughness K_1 and K_2 followed the ellipse law with respect to different phase angles. After the hygrothermal aging, the critical interfacial fracture toughness decreased significantly compared with the interfacial fracture toughness of dry specimen tested at room temperature, as shown in Fig.

ATTENTION: The Singapore Copyright Act applies to the use of this document. Nanyang Technological University Library

6.6. Other authors also observed the significant decrease (Ferguson & Qu 2002), which indicated that moisture could invade into the defects and remarkably decrease the interfacial strength by intercepting the inter- and intra-molecular hydrogen bonding provided by the hydroxyl groups (Kwei 1966). Therefore, it demonstrated that the hygrothermal loading would increase the possibility of interface delamination in FCOB assembly. In addition, compared to the dry specimen tested at room temperature, it was observed that more decrease happened in case of mode I (36% for pure mode I fracture and 32% for pure mode II fracture), which means that more severe reliability issues lie in the opening mode. The possible explanation of this phenomenon is due to a displacement type reaction where water modules displace the polymer chain in the Van-der Waals bonding of the polymer adhesive to the glass surface (Kinloch 1987). In order to demonstrate it, the fracture morphology was to be studied in the next section.

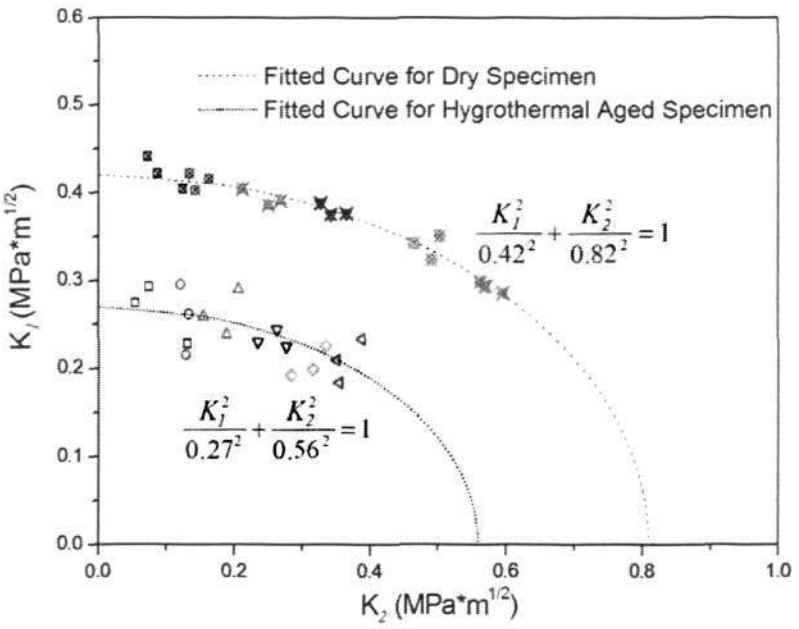

Fig. 6.17 Critical interfacial toughness of dry and wet (85°C/85%) SBN specimen

ATTENTION: The Singapore Copyright Act applies to the use of this document. Nanyang Technological University Library

6.3.2 Fracture Morphology Study

It was found that the fracture modes were generally interface delamination with respect to all loading angles, which were similar to those of dry specimen tested at 125 °C (Zhang et al. 2004). However, in the microscopic view, the morphologies of interface delamination were surprisingly different. For the delamination happened at 125 °C, it was observed that granular bulges distributed over the whole fractured interface of the underfill part of the dry sample, as shown in Fig. 6.18(a). It indicated that chemical bonding was destroyed by high stresses-at-break, which exceeded the local yield stress of underfill material. However, for hygrothermal-aged sample, its fracture morphology showed smooth surface without granulae, as shown in Fig. 6.18(b). It indicated that the stresses causing debonding were not large enough to make the underfill material yield locally. It is evidence from a mechanical point of view that the moisture leads to bonding interception. This observation also demonstrated that moisture could hydrolyze the chemical bonding between UF and Si apart from making epoxy-based UF swell as reported in moiré experiment.

ATTENTION: The Singapore Copyright Act applies to the use of this document. Nanyang Technological University Library

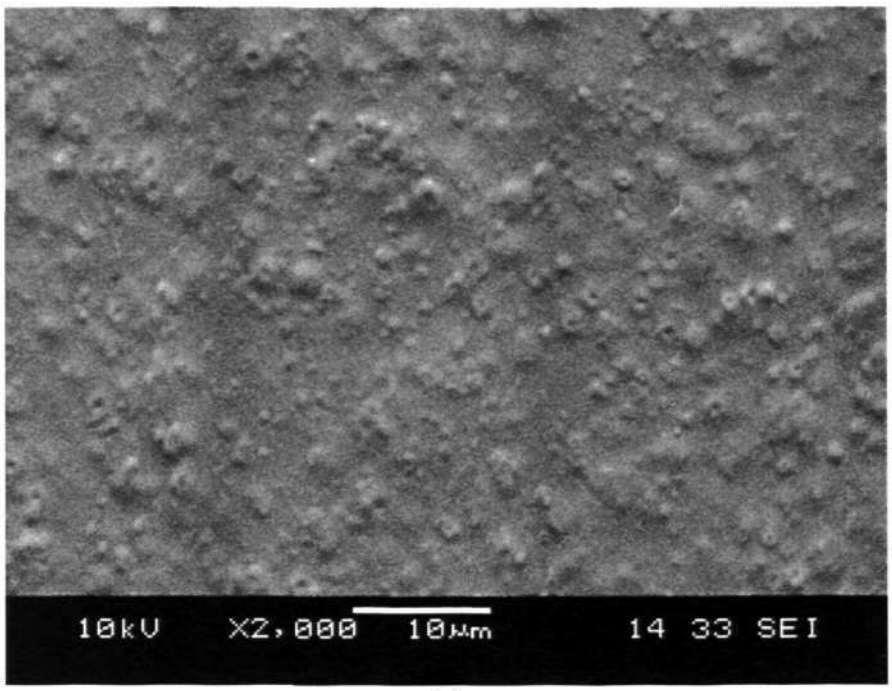

(a)

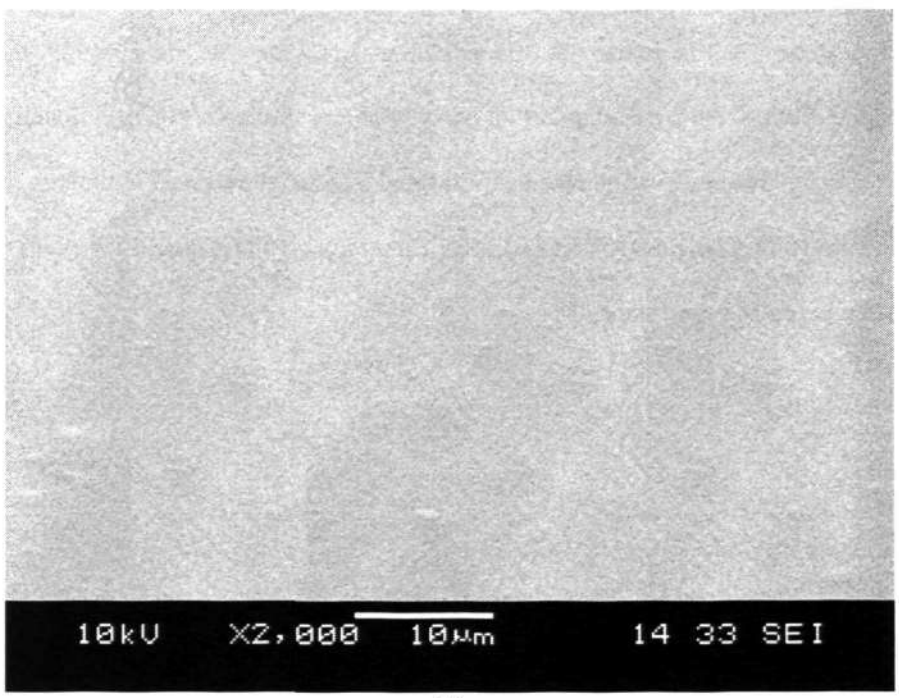

(b)

Fig. 6.18 Fracture morphology of interface delamination. (a) interface delamination of dry specimen under 125°C; (b) interface delamination of hygrothermal aged specimen under the room temperature

ATTENTION: The Singapore Copyright Act applies to the use of this document. Nanyang Technological University Library

6.4 Summary

Fracture toughness of underfill/chip interface was determined as function of temperature and mode mixity. It is shown that the μ-DiSC technique can measure the CTODs along the crack-tip and therefore determine the critical interfacial fracture toughness according to interfacial fracture mechanics. BN type specimens show good feasibility of characterizing toughness with a wide range of mode mixity.

The measurement results under thermal loading indicate that critical toughness could drop dramatically if temperature went close or above glass transition temperature of underfill material. The ellipse manner of interfacial fracture toughness can be a useful reference for the reliability design of flip chip packages to reduce experimental and numerical simulation size for other electronic packages. The fracture morphology was observed and related to loading angles and temperatures. Kinking into silicon could happen for small loading angle, i.e., in the case of shear dominant fracture.

The measurement results after hygrothermal aging show that moisture significantly reduced the interfacial strength compared with dry specimens tested at the room temperature. The interception of the inter- and intra-molecular hydrogen bonding provided by the hydroxyl groups is thought to take place with respect to wide range of mode mixity. The fracture morphology study revealed granular bulges distributed over the whole interface of underfill part at 125 °C in our previous study. However, the surface without granular was seen for hygrothermal-aged specimen tested under ambient condition. The observation indicates that moisture severed the chemical bonding between Si/underfill and decreased the debonding stresses.

ATTENTION: The Singapore Copyright Act applies to the use of this document. Nanyang Technological University Library

Chapter 7 Conclusions and Recommendations for Further Research

7.1 Summary and Conclusions

Although many other researchers have studied reliability issues in flip chip assembly, the present research has made significant contributions in establishing in-situ measurement techniques, i.e. moiré interferometer and speckle correlation systems, to monitor real-time interface behavior under thermal and moisture loading conditions. The techniques were used to obtain failure assessment diagram (FAD), and they may be used to investigate other types of electronic packages under the temperature variation or moisture surrounding. The major conclusions are drawn as follows:

(1) In the flip chip assembly, the interface between the silicon chip and the underfill is the most susceptible interface to delaminate. Both CTE mismatch and stiffness mismatch have significant effect on the interfacial behavior under thermal cycling

(2) Based on the assumptions in section 4.4, good agreement between FEA simulation results and the moiré experimental results is concluded. It indicates that the viscoelastic properties of the underfill material are the key to precisely determine the thermal response of the flip chip assembly in the numerical simulation.

ATTENTION: The Singapore Copyright Act applies to the use of this document. Nanyang Technological University Library

(3) The temperature dependent material properties of underfill also have a strong effect on the interfacial fracture toughness of Si/underfill, especially when the temperature is above T_g of the underfill.

(4) Moisture induced underfill swelling has a significant effect on the assembly's deformation. However, the time effect at high temperature or during long aging period is not negligible since the magnitude of strain is comparable to that caused by material swelling. Therefore, the hazard of moisture attack in the flip chip assembly may be overestimated if the time effect is excluded in the numerical simulation.

(5) After moisture aging, there is significant decrease of interfacial fracture toughness with respect to different mode mixities – up to 36% decrease for pure mode I fracture and 32% decrease for pure mode II fracture.

(6) The fracture morphology is related to loading angles, temperatures and moisture immigration. Kinking into silicon could happen in the case of shear dominant fracture at relatively low temperature. Moisture immigrating into the underfill material severs the chemical bonding between Si/underfill and induces the interfacial delamination without kinking observed.

(7) This research is the first to use the speckle correlation technique to carry out in-situ deformation measurement and the characterization of interfacial fracture toughness in the electronic packaging area. This technique has been shown to be

ATTENTION: The Singapore Copyright Act applies to the use of this document. Nanyang Technological University Library

feasible to evaluate the interfacial reliability issues by establishing the failure assessment diagram for various electronic packaging. The curve-fitted ellipse formula indicated that the interfacial fracture toughness follows $x^2/a^2 + y^2/b^2 = 1$ manner, so that the experimental sample size for interfacial fracture toughness could be reduced.

7.2 Recommendations for Further Research

From the results obtained so far, it can be seen that it is of importance to formulate the underfill material with proper mechanical properties, good adhesion and high moisture resistance. The glass transition temperature of the epoxy, the adhesion behavior of the epoxy and the content of filler in the underfill material are the major concerns in the improvement of interfacial reliability issues of underfill and its adjacent materials. The "hard" underfill with moderated CTE (Rzepka et al. 1998) may be ideal. In addition, the precise way to measure material hygrothermal behavior becomes outstanding. The moisture expansion and material properties degradation have significant effect on interfacial behavior, which is not adequately characterized in this study. Therefore, further research can be carried out to optimise the thermal & mechanical properties of the underfill material.

Since the no-flow underfill material, with the advantages of being fast and flexible in large-die application, is expected to have a great future in the industrial application, it is suggested that further research be carried out in this area. Since the in-situ testing methods established in this study are shown to be broadly applicable to understand reliability issues of the interfaces, it is possible to use

ATTENTION: The Singapore Copyright Act applies to the use of this document. Nanyang Technological University Library

these methods to evaluate any other interfaces in all kinds of electronic packages. It is certain that if there be an analytical model developed to describe the interfacial toughness as a function of thermal and moisture, it would be a great contribution to electronic packaging field. This work needs enormous experiment and simulation verification as a database to have insight in interfacial behavior.

Another recommendation for further research is to use the embedded viscoelastic model to take into consideration effect of time in simulation of the flip chip package response under moisture loading condition.

ATTENTION: The Singapore Copyright Act applies to the use of this document. Nanyang Technological University Library

References

Adamson, M.J., (1980), "*Thermal Expansion and Swelling of Cured Epoxy Resin Used in Graphite/Epoxy Composite Materials*", Journal of Materials Science, Vol. 15, No. 7, pp. 1736-1745.

Akay, M., Kong Ah Mun, S., and Stanley, A., (1997), "*Influence of Moisture on the Thermal and Mechanical Properties of Autoclaved and Oven–Cured Kevlar–49/Epoxy Laminates*," Composites Science and Technology, 57, pp.565–571.

Alpern, P., Lee, K.C., Dudek, R., and Tilgner, R., (2000), "*A Simple Model for the Mode I Popcorn Effect for IC Packages*," Microelectronics Reliability, Vol. 40, pp. 1503–1508.

Apicella, A., Nicolais, L., Astarita, G., and Drioli, E., (1979), "*Effect of Thermal History on Water Sorption, Elastic Properties and The Glass Transition of Epoxy Resins*", Polymer, Vol. 20, pp. 1143-1148.

Atkinson, C., Smelser, R.E., and Sanchez, J., (1982), "*Combined mode fracture via the cracked Brazilian disk test*," International Journal of Fracture, Vol. 18, pp. 279.

Bao, L.R., Yee, A.F., and Lee, Charles Y.–C., (2001), "*Moisture Absorption and Hygrothermal Aging in a Bismaleimide Resin*," Polymer, 42, pp. 7327–7333.

Bartoszyk, A., Cho, S., Han, C.W., Jin, H.Q., and Lee, Y., (2000), "*Flip Chip Technology Development*," ENME808z Final Report.

Baschek, G., Hartwig, G., and Zahradnik, F., (1999), "*Effect of Water Absorption in Polymers at Low and High Temperature*," Polymer, Vol. 40, pp. 3433–3441.

ATTENTION: The Singapore Copyright Act applies to the use of this document. Nanyang Technological University Library

Borgesen, P., Blass, D., and Sribari, K., (2000), "*Flip Chip Reliability*," Universal Instrument.

Bruck, H.A., McNeill, S.R., Sutton, M.A., and Peters, W.H., (1989), "*Digital image correlation using Newton-Raphson method of partial differential correlation.*" Experimental Mechanics, Vol. 29, pp. 261–267.

Chai, H., and Chiang, M.Y.M., (1998) "*Finite Element Analysis of interfacial fracture propagation Based on Local Shear, Part II Fracture*," International Journal of Solids and Structures, Vol. 35, No. 9, pp. 815-829.

Chen, L., Zhang, Q., Wang, G.Z., Xie, X.M., and Cheng, Z.N., (2001), "*The Effects of underfill and its Material Models on Thermomechanical Behaviours of a Flip Chip Package*," IEEE Transactions on Advanced Packaging, Vol. 24, No. 1, pp. 17–24.

Cho, S.-M., Cho, S.-Y. and Han, B. (2002), "*Observing Real-Time Thermal Deformation in Electronic Packaging*", Experimental Techniques, Vol. 26, No. 3, pp. 25-29.

Cho, S.-M., Han, B. and Joo, J., (2004), "*Temperature Dependent Deformation Analysis of Ball Grid Array Package Assembly under Accelerated Thermal Cycling Condition*", Journal of Electronic Packaging, Vol. 126, pp. 41-47.

Cramer, T., Wanner, A., and Gumbsch, P., (2000), "*Energy Dissipation and Path Instabilities in Dynamic Fracture of Silicon Single Crystal*", Physical Review Letters, Vol. 85, No. 4, pp. 788-791.

Crank, J., and Park, G.S., (1956), "*The Mathematics of Diffusion*," Oxford University Press.

Dai, X., Brillhart, M.V., Roesch, M., and Ho, P.S., (2000),"*Adhesion and Toughening Mechanisms at Underfill Interfaces for Flip-Chip-On-Organic-*

ATTENTION: The Singapore Copyright Act applies to the use of this document. Nanyang Technological University Library

Substrate Packaging," IEEE Transactions on Components and Packaging Technology., Vol. 23, No. 1, pp. 117–127.

Deegan, R.D., Chheda, S., Patel, L., Marder, M., Swinney, H.L.K.J., and Alex de Lozanne, (2003), "*Wavy and rough cracks in silicon*", Physical Review E, Vol. 67, 066209, pp. 1-7.

Derveaux, D., and Mawer, A., (1995), "*Thermal and Power Cycling Limits of Plastic Ball Grid Array (PBGA),*" Conf. Proc. Surface Mount Int., pp. 315-325.

Desai, C.S., and Whitenack, R., (2001), "*Review of Models and the Disturbed State Concept for Thermomechanical Analysis in Electronic Packaging*," Journal of Electronic Packaging, Vol. 123, pp. 19–33.

Doi, K., Hirano, N., Okada, T., Hiruta, Y., and Sudo, T., (1996), "*Prediction of Thermal Fatigue Life for Encapsulated Flip–Chip Interconnection*," International Journal of Microcircuit Electronic Packaging, Vol 19, pp. 231–237.

Dundurs, J., (1969), "*Edge-Bonded Dissimilar Orthogonal Elastic Wedges*," ASME J. Appl. Mech., Vol. 36, pp. 650–652.

Dutta, I., Gopinath, A., and Marshall, C., (2002), "*Underfill Constraint Effects during Thermomechanical Cycling of Flip-Chip Solder Joints*", Journal of Electronic Materials, Vol. 31, Issue 4, pp. 253–264.

Fan, X.J., Wang, H.B., and Lim, T.B., (2001), "*Investigation of the Underfill Delamination and Cracking in Flip–Chip Modules under Temperature Cyclic Loading*," IEEE Transactions on Components and Packaging Technologies, Vol. 24, No. 1, pp. 84–90.

Ferguson, T., and Qu, J.M., (2002), "*Effect of Moisture on the Interfacial Adhesion of the Underfill/Solder Mask Interface*," Journal of Electronic Packaging, Vol. 124, pp. 106–110.

ATTENTION: The Singapore Copyright Act applies to the use of this document. Nanyang Technological University Library

Fukuzawa, I., (1985), "*Moisture Resistance Degradation of Plastic LSI's by Reflow Soldering*," IEEE/IRPS, pp. 192–197.

Galloway, J.E., and Miles, B.M., (1996), "*Moisture Absorption and Desorption Prediction for Plastic Ball Grid Array Packages*," IEEE InterSociety Conference on Thermal Phenomena, pp.180–186.

Gektin, V., Bar-Cohen, A., and Ames, J., (1997), "*Coffin-Manson Fatigue Model of Underfilled Flip-chip,"* IEEE Trans. Comp., Packag., and Manufact. Technol., Vol. 20, pp. 317–325.

Ghaffarian, R., (2000), "*Accelerated Thermal Cycling and Failure mechanisms for BGA and CSP Assemblies*," Journal of Electronic Packaging, Vol. 122, pp. 335–340.

Gonon, P., Sylvestre, A., Teysseyre, J., and Prior, C., (2001), "*Combined Effects of Humidity and Thermal Stress on the Dielectric Properties of Epoxy–Silica Composites*," Materials Science and Engineering, B83, pp. 158–164.

Guedes, R.M., Morais, José J.L., Marques, A.T., and Cardon, A.H., (2000), "*Prediction of Long–Term Behaviour of Composite Materials*," Computers & Structures, Vol. 76, pp. 183–194.

Guo, Y., and Liu, S., (1998), "*Development in Optical Methods for Reliability Analysis in Electronic Packaging Applications*," Journal of Electronic Packaging, Vol. 120, pp. 186–193.

Gurumurthy, C.K., Jiao, J., Norris, L.G., Hui, C.-Y., and Kramer, E.J., (1998), "*A Thermo–Mechanical Approach for Fatigue Testing of Polymer Bimaterial Interfaces*," Journal of Electronic Packaging, Vol. 120, pp. 372–378.

Gurumurthy, C.K., Kramer, E.J., and Hui, C.-Y., (2001), "*Water–Assisted Sub–critical Crack Growth along an Interface Between Polyimide Passivation and Epoxy Underfill*," International Journal of Fracture, Vol. 109, pp. 1–28.

ATTENTION: The Singapore Copyright Act applies to the use of this document. Nanyang Technological University Library

Haener, J., Ashbaugh, N., Chia, C.Y., and Fang, M.Y., (1967), "*Investigation of Micromechanical Behaviour of Fiber–Reinforced Plastics*," US Army Aviation Material laboratories Technical Report 66–67, Fort Eustis, VA.

Han, B., and Guo, Y., (1995), "*Thermal Deformation Analysis of Various ElectronicPackaging Products by Moiré and Microscopic Moiré Interferometry*," Journal of Electronic Packaging, Vol. 117, pp. 185–191.

Han, B., and Guo, Y., (1996a), "*Determination of an Effective Coefficient of Thermal Expansion of Electronic Packaging Components: A Whole–Field Approach,*" IEEE Transaction on Components, Packaging, and Manufacturing Technology–Part A, Vol. 19, No. 2, pp. 240–247.

Han, B., Guo, Y., Lim, C.K., and Caletka, (1996b), "*Verification of Numerical Models Used in Microelectronics Packaging Design by Interferometric Displacement Measurement Methods*," ASME Journal of Electronic Packaging, pp. 157–163.

Han, B., (2003), "*Thermal Stresses in Microelectronics Subassemblies: Quantitative Characterization using Photomechanics Methods*", Journal of Thermal Stresses, Vol. 26, pp.583-613.

He, M.-Y., and Hutchinson, J.W., (1989), "*Kinking of Crack Out of an Interface*," Journal of Applied Mechanics, Vol. 56, pp. 270-8.

Ho, P.S., Wang, G.T., Ding, M., Zhao, J.H., and Dai, X. (2004), "*Reliability Issues for Flip-Chip Packages*," Microelectronics Reliability, Vol. 44, pp. 719-737.

Hohlfelder, R.J., Maidenberg, D.A., Dauskardt, R.H., Wei, Y.G., and Hutchinson, J.W., (2001), "*Adhesion of Benzocyclobutene–Passivated Silicon in Epoxy Layered Structures*," Journal of Materials Research, Vol. 16, No. 1, pp. 243–255.

ATTENTION: The Singapore Copyright Act applies to the use of this document. Nanyang Technological University Library

Hu, K.X., Yeh, C.P., Wu, X.S., and Wyatt, K., (1995), "*An Interfacial Delamination Analysis for Multi-Chip Module Thin Film Interconnects*," EEP–Vol. 11/MD–Vol. 64, Application of Fracture Mechanics in Electronic Packaging and Materials, pp. 71–78.

Hutchinson, J.W., and Suo, Z.G., (1992), "*Mixed Mode Cracking in Layered Materials*," Advances in applied Mechanics, Vol. 29, pp. 63–191.

Jackson, R., and Carnevali, P., (1991), "*Finite Element Modeling of Encapsulated Flip-Chip Packaging Assemblies*," Proceedings 1991 International Symposium on Microelectronics, ISHM, pp. 82–85.

Jiang, Z.Q., Huang, Y., and Chandra, A., (1997), "*Thermal Stresses in layered Electronic Assemblies*," Journal of Electronic Packaging, Vol. 119, pp. 127–132.

Jiao, J., Gurumurthy, C.K., Kramer, E.J., Sha, Y., Hui, C.-Y., and Borgesen, P., (1998), "*Measurement of Interfacial Fracture Toughness Under Combined Mechanical and Thermal Stresses,,*" Journal of Electronic Packaging, Vol. 120, pp. 349-353.

Kawagoe, M., Doi, Y., Fuwa, N., Yasuda, T., and Takata, K., (1997), *"Effects of Absorbed Water on the Interfacial Fracture Between Two Layers of Unsaturated Polyester and Glass,"* Journal of Material Science, Vol. 36, pp.5161–6167.

Kenner, V.H., Harper, B.D., and Itkin, V.Y., (1997), "*Stress Relaxation in Molding Compounds*," Journal of Electronic Materials, Vol. 26, pp. 821–826.

Kinloch, A.J., (1987), "*Adhesion and Adhesives: Science and Technology*", Chapman and Hall, New York.

Kitano, M., Nishimura, A., and Kawai, S., (1988), "*Analysis of Package Cracking During Solder Reflow*," IEEE/IRPS, pp. 90–95.

ATTENTION: The Singapore Copyright Act applies to the use of this document. Nanyang Technological University Library

Kook, S.–Y., Snodgrass, J.M., Kirtikar, A., and Dauskardt, R.H., (1998), "*Adhesion and Reliability of Polymer/Inorganic Interfaces*," Journal of Electronic Packaging, Vol. 120, pp. 328–334.

Kuhl, A., and Qu, J.M., (2000), "*A Technique to Measure Interfacial Toughness Over a Range of Phase Angles*," Journal of Electronic Packaging, Vol. 122, pp. 147-151.

Kuo, C.-T., Yip, M.-C., and Chiang, K.-N., (2004), "*Time and Temperature-Dependent Mechanical Behavior of Underfill Materials in Electronic Packaging Application*," Microelectronics Reliability, Vol. 44, pp. 627–638.

Kwei, T.K., (1966), Journal of Applied Polymer Science, Vol. 10, pp. 1647.

Lau, J., (1993), "*Thermal Fatigue Life Prediction of Flip Chip Solder Joints by Fracture Mechanics Method*," Eng. Fract. Mech., Vol. 45, No. 5, pp. 643–654.

Lau, J.H., Lee, S.W.R., and Chang, C., (2000), "*Solder Joint Reliability of Wafer level Chip Scale Packages (WLCSP): A Time-Temperature-Dependent Creep Analysis*," Journal of Electronic Packaging, Vol. 122, pp. 311–316.

Lau, J.H., and Lee, S.W.R., (2000a), "*Temperature–Dependent Popcorning Analysis of Plastic Ball Grid Array Package during Solder Reflow with Fracture Mechanics Method*," Journal of Electronic Packaging, Vol. 122, pp. 34–41.

Lau, J.H., and Lee, S.W.R., (2000b) "*Fracture Mechanics Analysis of Low Cost Solder Bumped Flip Chip Assemblies with Imperfect Underfills*," Journal of Electronic Packaging, Vol. 122, pp. 306–310.

Lau, J.H., Chang, C., and Lee, S.W.R., (2001), "*Solder Joint Crack Propagation Analysis of Wafer-Level Chip Scale Package on Printed Circuit Board Assemblies*," IEEE Transactions on Components and Packaging Technologies, Vol. 24, No. 2, pp. 285–292.

ATTENTION: The Singapore Copyright Act applies to the use of this document. Nanyang Technological University Library

Lawrence, S.St., Willett, J.L., and Carriere, C.J., (2001), "*Effect of Moisture on the Tensile Properties of Poly (hydroxy ester ether),*" Polymer, Vol. 42, pp. 5643–5650.

Lee, B.L., Lewis, R.W., and Sacher, R.E., (1978), "*Effects of Static Immersion in Water on the Tensile Strength of Crossply Laminates*," Process of 2nd Interna7tional Conference on Composite Materials, pp. 1560–1583.

Li, Y.M., Miranda, J., and Sue, Hung–Jue, (2001), "*Hygrothermal Diffusion Behaviour in Bismaleimide Resin*," Polymer, Vol. 42, pp. 7791–7799.

Li, Y.M., and Sue, Hung-Jue, (2002), "*Moisture Diffusion Behaviour in Bismaleimide Resin Subjected to Hydrothermal Cycling*," Polymer Engineering and Science, Vol. 42, pp. 375-381.

Lim, J.H., Lee, K.W., Park, S.S., and Earmme, Y.Y., (1998), "*Vapor Pressure Analysis of Popcorn Cracking in Plastic IC Packages by Fracture Mechanics*," IEEE/CPMT Electronics Packaging Technology Conference, pp. 36–41.

Lin, R., (1988), "*Moisture Induced Package Cracking in Plastic Encapsulated Surface Mount Components during Reflow Soldering*," IEEE/IRPS, pp. 83–89.

Lin, T.Y., and Tay, A.A.O., (1997), "*A J–Integral Criterion for Delamination of Bi–material Interfaces Incorporating Hygrothermal Stress*," EEP-Vol. 19–2, Advances in Electronic Packaging, Volume 2, ASME, pp. 1421–1428.

Loh, W.K., Crocombe, A.D., Wahab, M.M.A., and Ashcroft, I.A., (2002), "*Environmental Degradation of the Interfacial Fracture Energy in an Adhesively Bonded Joint*," Engineering Fracture Mechanics, Vol. 69, pp. 2113–2128.

Madenci, E., Shkarayev, S., and Mahajan, R., (1998), "*Potential failure Sites in a Flip-Chip Package With and Without Underfill*," Journal of Electronic Packaging, Vol. 120, pp. 336–341.

ATTENTION: The Singapore Copyright Act applies to the use of this document. Nanyang Technological University Library

McKague, E.L.J.D., Reynolds, Jr., and Halkias, J.E., (1978), "*Swelling and glass transition relations for epoxy matrix material in humid environments*", Journal of Applied Polymer Science, Vol. 22, pp.1643-1654.

Nguyen, L.T., Chen, A.S., and Lo, R.Y., (1995), "*Interfacial Integrity in Electronic Packaging*, " EEP–Vol. 11/MD–Vol. 64, Application of Fracture Mechanics in Electronic Packaging and Materials, pp. 35–44.

Nguyen, L.T., Lee, G., Jones, C., Hsu, T.R., Fang, R., Kuo, A.Y., and Chen, W.T., (1997), "*Interfacial Fracture Toughness in Plastic Packages*," AMD–Vol.222/EEP–Vol.20, Application of Fracture mechanics in Electronic Packaging, pp. 15–24.

Nishimura, A., Hirose, I., and Tanaka, N., (1992), "*A New Method for Measuring Adhesion Strength of IC Molding Compounds*", Journal of Electronic Packaging, Vol.114, pp.407.

Oesterholt, (1997), "*Effect of Moisture on Flip Chip Assemblies*," Internal Report, Philips Center for Manufacturing Technology, The Netherlands.

Okura, J.H., Shetty, S., Ramakrishnan, B., Dasgupta, A., Caers, J.F.J.M., and Reinikainen, T., (2000), "*Guidelines to select underfills for flip chip on board assemblies and compliant interposers for chip scale package assemblies*," Microelectronics Reliability, Vol. 40, Issue 7, pp. 1173–1180.

Okura, J.H., Dasgupta, A., and Caers, J.F.J.M., (2002), "*Hygro-Mechanical Durability of Underfilled Flip-Chip-on-board (FCOB) Interconnects*," Journal of Electronic Packaging, Vol. 124, Sep, pp.184–187.

Owen, D.R.J., and Fawkes, A.J., (1983), *"Engineering Fracture Mechanics: Numerical Methods and Applications,"* Pineridge Press Ltd., Swansea, U. K..

Pang, H.L.J., Zhang, X.R., Shi, X.Q., and Wang, Z.P., (2002), "*Interfacial Fracture Toughness Test Methodology for Adhesive Bonded Joints*," IEEE

ATTENTION: The Singapore Copyright Act applies to the use of this document. Nanyang Technological University Library

Transactions on Components, Packaging and Manufacturing Technology, Part-A, Vol. 25, No. 2 , pp. 187-191.

Paris, P., and Erdogan, F., (1963), "*A critical analysis of crack propagation laws*," Journal of Basic Engineering, Vol. 85, pp. 528–534.

Park, C.E., Han, B.J., and Bair, H.E., (1997), "*Humidity Effects on Adhesion Strength Between Solder Ball and Epoxy Underfills*," Polymer, Vol. 38, No. 15, pp. 3811–3818.

Pearson, R.A., Lloyd, T.B., Azimi, H.R., Hsiung, J.C., and Brandenburger, P.D., (1995), "*Fundamentals of Adhesion, Manufacturability, and Reliability of Epoxy–Based Chip Attach Adhesives*," EEP–Vol. 11/MD–Vol. 64, Application of Fracture Mechanics in Electronic Packaging and Materials, pp. 55–62.

Post, D., Han, B., and Ifju, P., (1994), "*High Sensitivity Moire: Experimental Analysis for Mechanics and Materials*", Springer-Verlag.

Qian, Z., Wang, J., Yang, .J., and Liu, S., (1999), "*Visco-elastic-plastic Properties and Constitutive Modeling of Underfills*," IEEE Trans. Comp., Packag., Manufact. Technol., Vol. 22, pp. 152–157.

Rao, Y., Shi, S.H., and Wong, C.P., (2000), "*An Improved Methodology for Determining Temperature Dependent Moduli of Underfill Encapsulants*," IEEE Transaction on Components and Packaging Technology, Vol. 23, No. 3, pp. 434–439.

Rice, J.R., (1988), "*Elastic Fracture Mechanics Concepts for Interfacial Cracks*," Journal of Applied Mechanics, Vol. 55, pp. 98–103.

Rzepka, S., Korhonen, M.A., Meusel, E., and Li, C.-Y., (1998), "*The Effect of Underfill and Underfill Delamination on the Thermal Stress in Flip-Chip Solder Joints*," Journal of Electronic Packaging, Vol. 120, pp. 342–348.

ATTENTION: The Singapore Copyright Act applies to the use of this document. Nanyang Technological University Library

Sham, M.L. and Kim, J.K., (2003), "*Adhesion Characteristics of Underfill Resins with Flip Chip Package Components,*" Journal of Adhesion Science and Technology, Vol. 17, No. 14, pp. 1923-1944.

Shi, X.Q., Wang, Z.P., Pang , H.L.J., and Zhang, X.R., (2002a), "*Investigation of Effect of Temperature and Strain Rate on Mechanical Properties of Underfill Material by Use of Microtensile Specimens,*" Polymer Testing, Volume 21, Issue 6, pp. 725–733.

Shi, X.Q., Wang, Z.P., Zhou, W., Pang, H.L.J., Yang, Q.J., (2002b), "*A New Creep Model for Eutectic Solder Alloy*," Journal of Electronic Packaging, Vol. 124, pp. 85-90.

Shi, X.Q., Wang, Z.P., and Pickering, J.P., (2003), "*A New Methodology for The Characterization of Fracture Toughness of Filled Epoxy Films Involved in Microelectronics Packages,*" Microelectronics Reliability, Vol. 43, pp. 1105-1115.

Shi, X.Q., Pang, H.L.J., and Zhang, X.R., (2004), "*Investigation of long-term reliability and failure mechanism of solder interconnections with multifunctional micro-moiré interferometry system*", Microelectronics Reliability, Vol. 44, Issue 5, pp. *841-852.*

Shi, X.Q., Pang, H.L.J., Zhang, X.R., Liu, Q.J., and Ming, Y., (2004), "*In-Situ Micro-Digital Image Speckle Correlation Technique for Characterization of Materials' Properties and Verification of Numerical Models*", IEEE Transactions on Components and Packaging Technologies, Vol. 27, No. 4, pp. 659-667.

Stellrecht, E., Han, B. and Pecht, M., (2004), "*Characterization of Hygroscopic Swelling Behavior of Mold Compounds and Plastic Packages*", IEEE Transactions on Components and Packaging Technologies, Vol. 27, No. 3, pp. 499-506.

Su, P., Rzepka, S., Korhonen, M., and Li, C.Y., (1999), "*The Effects of Underfill on the Reliability of Flip Chip Solder Joints*," Journal of Electronic Materials, Vol. 28, Issue 9, Pages 1017–1022.

ATTENTION: The Singapore Copyright Act applies to the use of this document. Nanyang Technological University Library

Sutton, M.A., Mcneill, S.R., Helm, J.D. and Chao, Y.J., (2000), "*Advances in Two-Dimensional and Three-Dimensional Computer Vision,*" Photomechanics for Engineers, Pramod Rastogi, Ed., Springer-Verlag.

Suo, Z.G., (1989), "*Mechanics of Interface Fracture*," Ph.D. thesis, Cambridge: Harvard University.

Suo, Z.G., and Hutchinson, J.W., (1989), "*Sandwich Test Specimens for Measuring Interface Crack Toughness*," Materials Science and Engineering, A107, pp. 135–143.

Suryanarayana, D., Wu, T.W., and Varcoe, J.A., (1993), "*Encapsulants used in Flip-Chip Packages*," IEEE Trans. Comp., Hybrids, Manufact. Technol., Vol. 16, pp. 858–962.

Tay, A.A.O., and Lin, T.Y., (1996), "*Moisture Diffusion and Heat Transfer in Plastic IC Packages*," IEEE Transactions on Components and Packaging Manufacturing Technologies, Vol. 19, pp. 186–193.

Tay, A.A.O., and Lin, T.Y., (1999), "*Influence of Temperature, Humidity, and Defect Location on Delamination in Plastic IC Packages*," IEEE Transactions on Components and Packaging Technologies, Vol. 22, No. 4, pp. 512–518.

Tounsi, A., Bedia, E.A., and Verchery, G., (2002), "*Influence of Anisotropy on the Transient Hygroscopic Stresses in Polymer Matrix Composites with Cyclic Environmental Conditions,*" Composite Structures, Vol. 55, pp. 393–405.

Tuhus, T., and Bjorneklett, A., (1993), "*Thermal Cycling Reliability of Die Bonding Adhesives*," IEEE/IRPS, pp. 204–208.

Uschitsky, M., and Suhir, E., (2001), "*Moisture Diffusion in Epoxy Molding Compounds Filled with Particles*," Journal of Electronic Packaging, Vol. 123, pp. 47–51.

ATTENTION: The Singapore Copyright Act applies to the use of this document. Nanyang Technological University Library

Varelidis, P.C., Kominos, N.P., and Papaspyrides, C.D., (1998), "*Polyamide Coated Glass Fabric in Polyester Resin: Interlaminar Shear Strength versus Moisture Absorption Studies*," Composites–Part A, 29A, pp. 1489–1499.

Varelidis, P.C., Papakostopolos, D.G., Pandazis, C.I., and Papaspyrides, C.D., (2000), "*Polyamide Coated Kevlar^{TM} Fabric in Epoxy Resin: Mechanical Properties and Moisture Absorption Studies*," Composites: Part A: Applied Science and Manufacturing, Vol. 31, pp. 549–558.

Wang, J.–S., and Suo, Z.G., (1990), "*Experimental Determination of Interfacial toughness Curves Using Brazil-Nut-Sandwiches*," Acta Metall. Mater. Vol. 38, No. 7, pp. 1279–1290.

Wang, J., Qian, Z., Zhou, D., and Liu, S., (1998), "*Creep Behaviour of a Flip-chip Package by Both FEM Modeling and Real Time Moire Interferometry*," Journal of Electronic packaging, Vol. 120, pp. 179–185.

Williams, M.L., (1959), "*The Stresses around a Fault of Crack in Dissimilar Media*," Bull Seismol. Soc. Am., Vol. 49, pp. 199–206.

Wong, E.H., Teo, Y.C., and Lim, T.B., (1998), "*Moisture Diffusion and Vapour Pressure Modeling of IC package*," in Proceedings of Electronic Components and Technology Conference, pp. 1372-1378.

Wong, E.H., Chan, K.C., Tee, T.Y., and Rajoo, R., (1999), "*Comprehensive Treatment of Moisture Induced Failure in IC Packaging*," 3rd IEMT, pp. 176–181.

Wong, E.H., Koh, S.W., Lee, K.H., and Rajoo, R., (2002a), "*Comprehensive Treatment of Moisture Induced Failure–Recent Advances*," IEEE Transaction on Electronics Packaging Manufacturing, Vol. 25, No. 3,pp. 223–230.

ATTENTION: The Singapore Copyright Act applies to the use of this document. Nanyang Technological University Library

Wong, E.H., Rajoo, R., Koh, S.W., and Lim, T.B., (2002b), "*The Mechanics and Impact of Hygroscopic Swelling of Polymeric Materials in Electronic Packaging*," Journal of Electronic Packaging, Vol. 124, pp. 122–126.

Wong, E.H., Koh, S.W., Lee, K.H., and Lim, T.B., (2002c), "*Advances in Vapor Pressure Modeling for Electronic Packaging*," in Proc. 3rd Eurosime Conference, Paris France, pp. 347–355.

Wong, E.H., and Rajoo, R., (2003), "*Moisture Absorption and Diffusion Characterisation of Packaging Materials—Advanced Treatment*" Microelectronics Reliability, Vol. 43, Issue 12, pp. 2087–2096.

Wu, T.Y., Tsukada, Y., and Chen, W.T., (1996), "*Materials and Mechanics Issues in Flip–Chip Organic Packaging*," IEEE Electronic Components and Technology Conference, pp. 524–534.

Wylde, J.W., and Spelt, J.K., (1998), "*Measurement of Adhesive Joint Fracture Properties as a Function of Environmental Degradation*," International Journal of Adhesion & Adhesives, Vol. 18, pp. 237–246.

Xiao, G.Z., and Shanahan, W.E.R., (1998), "*Swelling of DGEBA/DDA Epoxy Resin during Hygrothermal Aging*," Polymer, Vol. 39, No. 14, pp. 3253–3260.

Yan, X., and Agarwal, R.K., (1998), "*Two Test Specimens for Determining the Interfacial Fracture Toughness in Flip-Chip Assemblies*," Journal of Electronic Packaging, Vol. 120, pp. 150-155.

Yao, Q.Z., Qu, J.M., Wu, J.L., and Wong, C.P., (1999), "*Characterization of Underfill/Substrate Interfacial Toughness Enhancement by Silane Additives*," International Symposium and Exhibition on Advanced Packaging Materials, pp.264–268.

Yi, S. and Hilton, H.H., (1995), "*Hygrothermal Effects on Viscoelastic Responses of Laminated Composites*," Composites Engineering, Vol. 5, No. 2, pp. 183–193.

ATTENTION: The Singapore Copyright Act applies to the use of this document. Nanyang Technological University Library

Yi, S., Goh, J.S., and Yang, J.C., (1997), "*Residual Stresses in Plastic IC Packages During Surface Mounting Process Preceded by Moisture Soaking Testing*," IEEE Transaction on Components, Packaging, and manufacturing Technology–Part B, Vol. 20, No. 3, pp. 247–254.

Zhang, W.G., Wu, D., Su, B.Z., Hareb, S.A., Lee, Y.C., and Masterson, B.P., (1998),"*The Effect of Underfill Epoxy on Warpage in Flip-Chip Assemblies*," IEEE Transactions on Components, Packaging and Manufacturing Technology–Part A, Vol. 21, No.2, pp.323–328.

Zhang, X.R., Pang, J.H.L., Shi, X.Q., and Wang, Z.P., (2002), "*On the Moduli of Viscoelastic Materials*," Proc. 4th Electronics Packaging Technology Conference, pp. 318–322.

Zhang, Y.L., Shi, X.Q., and Zhou, W., (2004), "*Determination of Fracture Toughness of Underfill/Chip Interface with Digital Image Speckle Correlation Technique*", In Proceedings of ECTC 2004, Vol. 1, pp. 140-147.

Zhu, J., Zou, D., and Liu, S., (1998), "*Real–Time Monitoring and Simulation of Thermal Deformation in Plastic Package*," Journal of Electronic Packaging, Vol. 120, pp. 160–165.